The Canadian Journal of Chemical Engineering

THE UNIVERSITY OF MICHIGAN
DEC 0 1960
ENGINEERING LIBRARY

formerly

CANADIAN JOURNAL OF TECHNOLOGY

CONTENTS

A Study of Aggregative Fluidization	*Geoffrey Davies* *Donald B. Robinson*	175
Heat Transfer to a Surface Reacting Fluid in Turbulent Flow	*Ronald I. Rothenberg* *J. M. Smith*	184
Fundamental Aspects of Solids-Gas Flow Part V: The Effects of Fluid Turbulence on the Particle Drag Coefficient	*L. B. Torobin* *W. H. Gauvin*	189
Temperature Dependence of the Binary Diffusion Coefficient of Gases	*D. S. Scott* *K. E. Cox*	201
Formation and Quenching of Nitric Oxide in a Continuous Flow Furnace	*D. L. Mordell* *A. L. Thompson* *G. Yano*	206
The Efficiency of Fibrous Aerosol Filters: Deposition by Diffusion of Particles of Finite Diameter	*Ralph E. Pasceri* *S. K. Friedlander*	212
Industrial Section		
Design of Steam Tracing Systems for Protection Against Freezing	*W. S. Cotton*	214
The Development of the Alum-Amine Process for the Recovery of Alumina from Shale	*G. Thomas* *T. R. Ingraham*	220
Index of Authors—1960		223
Index of Papers—1960		224

Published by
THE CHEMICAL INSTITUTE OF CANADA
OTTAWA CANADA

Photograph taken at C-I-L Central Research Laboratory, McMasterville, Que.

POLYMERIC PRECISION

This is an ebulliometer—being assembled by the master glass-blower on his own lathe at our Central Research Laboratory.

The ebulliometer uses two vapor lift pumps such as those found in electric coffee percolators. One circulates a polymer solution while the other circulates boiling solvent—each liquid stream is directed over a temperature detector so sensitive that a difference of one-millionth of 1°C. may be sensed. This device allows the measurement of high molecular weights related to the physical properties of polymers.

Such C-I-L research contributes to higher standards of performance in the plastics industry . . . to new and better plastic products . . . and—through better technical service—to greater success in the application of these new materials to modern living.

C-I-L

CANADIAN INDUSTRIES LIMITED

Serving Canadians Through Chemistry

Agricultural Chemicals • Ammunition • Coated Fabrics • Industrial Chemicals • Commercial Explosives • Paints • Plastics • Textile Fibres

The Canadian Journal of Chemical Engineering

formerly

Canadian Journal of Technology

Published by The Chemical Institute of Canada

VOLUME 38 | DECEMBER, 1960 | NUMBER 6

Editor
A. Cholette
Faculty of Science, Laval University
Quebec, Que.

Managing Editor
T. H. G. Michael

Publishing Editor
D. W. Emmerson

Assistant Publishing Editors
R. G. Watson
R. N. Callaghan

Circulation Manager
M. M. Lockey

EDITORIAL BOARD

Chairman
W. M. CAMPBELL, Atomic Energy of Canada Limited, Chalk River, Ont.

P. W. BLAYLOCK, Shawinigan Chemicals Limited, Montreal, Que.

L. D. DOUGAN, Polymer Corp. Limited, Sarnia, Ont.

F. A. FORWARD, University of British Columbia, Vancouver, B.C.

J. W. HODGINS, McMaster University, Hamilton, Ont.

A. I. JOHNSON, University of Toronto, Toronto, Ont.

LEO MARION, National Research Council, Ottawa, Ont.

R. R. McLAUGHLIN, University of Toronto, Toronto, Ont.

G. L. OSBERG, National Research Council, Ottawa, Ont.

A. C. PLEWES, Queen's University, Kingston, Ont.

J. H. SHIPLEY, Canadian Industries Limited, Montreal, Que.

H. R. L. STREIGHT, Du Pont of Canada Limited, Montreal, Que.

EX-OFFICIO

W. N. HALL, President, The Chemical Institute of Canada.

A. A. SHEPPARD, Chairman of the Board of Directors.

B. A. B. CLARK, Director of Publications.

Authorized as second class mail, Post Office Department, Ottawa. Printed in Canada

Manuscripts for publication should be submitted to the Editor: Dr. A. Cholette, Faculty of Science, Laval University, Boulevard de l'Entente, Quebec, Que. (Instructions to authors are on the next page).

Editorial, Production and Circulation Offices: 48 Rideau Street, Ottawa 2, Ont.

Advertising Office: C. N. McCuaig, manager of advertising sales, *The Canadian Journal of Chemical Engineering*, Room 601, 217 Bay Street, Toronto, Ont. Telephone—EMpire 3-3871.

Plates and Advertising Copy: Send to *The Canadian Journal of Chemical Engineering*, 48 Rideau Street, Ottawa 2, Ont.

Subscription Rates: In Canada—$6.00 per year and $1.25 per single copy; U.S. and U.K.—$7.00, Foreign—$7.50.

Change of Address: Advise Circulation Department in advance of change of address, providing old as well as new address. Enclose address label if possible.

The Canadian Journal of Chemical Engineering is published by The Chemical Institute of Canada every two months.

Unless it is specifically stated to the contrary, the Institute assumes no responsibility for the statements and opinions expressed in *The Canadian Journal of Chemical Engineering*. Views expressed in the editorials do not necessarily represent the official position of the Institute.

The Canadian Journal of Chemical Engineering

INSTRUCTIONS TO AUTHORS

Manuscript Requirements for Articles

1. The manuscript should be in English or French.
2. The original and two copies of the manuscript should be supplied. These are to be on 8½ x 11 inch sheets, typewritten, and double spaced. Each page should be numbered.
3. Symbols should conform to American Standards Association. An abridged set of acceptable symbols is found in the third edition of Perry's Chemical Engineers' Handbook. Greek letters and subscripts and superscripts should be carefully made.
4. Abstracts of not more than 200 words in English indicating the scope of the work and the principal findings should accompany all technical papers.
5. References should be listed in the order in which they occur in the paper, after the text, using the form shown here: "Othmer, D. F., Jacobs, Jr., J. J., and Levy, J. F., Ind. Eng. Chem. **34**, 286 (1942). Abbreviations of journal names should conform to the "List of Periodicals Abstracted by Chemical Abstracts". Abbreviations of the common journals are to be found in Perry's Handbook also. All references should be carefully checked with the original article.
6. Tables should be numbered in Arabic numerals. They should have brief descriptive titles and should be appended to the paper. Column headings should be brief. Tables should contain a minimum of descriptive material.
7. All figures should be numbered from 1 up, in Arabic numerals. Drawings should be carefully made with India ink on white drawing paper or tracing linen. All lines should be of sufficient thickness to reproduce well, especially if the figure is to be reduced. Letters and numerals should be carefully and neatly made, with a stencil. Generally speaking, originals should not be more than twice the size of the desired reproduction; final engravings being 3¼ in. or 7 in. wide depending on whether one column or two is used.
8. Photographs should be made on glossy paper with strong contrasts. Photographs or groups of photographs should not be larger than three times the size of the desired reproduction.
9. All tables and figures should be referred to in the text.

Submission of Manuscripts

1. The three copies of the manuscript, including figures and tables, should be sent directly to:
   DR. A. CHOLETTE, editor,
   The Canadian Journal of Chemical Engineering,
   Faculty of Science, Laval University,
   Boulevard de l'Entente,
   Quebec, Que.
2. The authors addresses and titles should be submitted with the manuscript.
3. The author may suggest names of reviewers for his article, but the selection of the reviewers will be the responsibility of the editor. Each paper or article is to be reviewed by two chemical engineers familiar with the topic. Reviewers will remain anonymous.
4. All correspondence regarding reviews should be directed to the editor.

Reprints

1. At least 50 free "tear sheets" of each paper will be supplied.
2. Additional reprints may be purchased at cost. An estimated cost of reprints, with an attached order form, will be sent to the author with the galley proofs.
3. Orders for reprints must be made before the paper has appeared in the Journal.

Communications, Letters and Notes to the Editor

Short papers, as described below, will be considered for publication in this Journal. Their total length should not exceed 600 words, or its equivalent.

Communications

A communication is a prompt preliminary report of observations made which are judged to be sufficiently important to warrant expedited publication. It usually calls for a more expanded paper in which the original matter is republished with more details.

Letters

A letter consists of comments or remarks submitted by readers or authors in connection with previously published material. It may deal with various forms of discussion arising out of a publication or it may simply report and correct inadvertent errors.

Notes

A note is a short paper which describes a piece of work not sufficiently important or complete to make it worth a full article. It may refer to a study or piece of research which, while it is not finished and may not be finished, offers interesting aspects or facts. As in the case of an article a note is a final publication.

* * *

A Study of Aggregative Fluidization[1]

GEOFFREY DAVIES[2] and DONALD B. ROBINSON[3]

The effects of size distribution on the expansion of a gas-solid fluidized system have been studied by the fluidization of glass beads and char particles by air in a 2¼ inch diameter column. Log-probability distributions of 5, 10, 25 and 100-fold size variation, with an average size of 271 microns, were tested, and changes in the average diameter of the bed due to elutriation were obtained. Systematic tests with beds of closely sized particles ranging in size from 74 to 912 microns were also made. The results show that compared with the effect of particle diameter, size distribution has little influence on the shape of the bed expansion curves.

Various correlations, and in particular that suggested by Zenz for particulate fluidization, have been tested using the single size measurements. It is concluded that up to the present time, no really satisfactory correlation for aggregative fluidization has been proposed.

In the preliminary design of any fluidized bed reactor, the extremes of gas velocity within which the bed can exist must be determined, since they define the limits of bed expansion. The lower limit is referred to as the critical or minimum fluidizing velocity, and the many papers on this topic have been reviewed by Sinclair and Robinson[1]. The upper limit of fluidization occurs at the gas velocity at which the bed is destroyed, and for closely sized particles, this has been shown to be the terminal velocity of the particles[2]. The literature contains excellent studies of such terminal velocity data for regular non-spherical particles[3,4] but relatively little is available on irregular particles[5,6], probably due to the difficulties involved in defining particle diameter and shape. When considering the upper limit of fluidization for beds containing a range of particle sizes, the weighted mean size has little significance. If the velocity exceeds the terminal velocity of the smaller particles, they will be entrained at a definite rate depending on the system properties[7,8,9]. Further increases in velocity result in an increase in the average particle size in the bed, until the upper limit is reached when the largest significant particle is removed. This elutriation of fine material constitutes one of the major problems in processes using the fluidized-bed technique, and the work described in this paper was therefore designed to study the fluidization limits and expansion of beds with wide particle size distributions.

Bed expansion between the fluidization limits is conveniently represented as a logarithmic plot of bed porosity versus superficial velocity, and is referred to in this paper as the expansion curve. Generalized correlations of these expansion data for gas-solid (aggregative) fluidization have mostly been attempted on the basis of liquid-solid (particulate) fluidization results, despite observed differences in bed behavior. The literature does, however, contain references to the differences between some experimental results and these published correlations. Friend, in a discussion of the correlation of Wilhelm and Kwauk[2], showed certain discrepancies in the cases of small catalyst particles with wide size distributions, fluidized in air. Lewis et al[10] found that for their experiments with small diameter particles, in which apparently "good" aggregative fluidization was involved, the data did not agree with either their correlation based on the standard drag curve for spheres, or the empirical relationship $(\epsilon - \epsilon_{mf})/(1 - \epsilon_{mf}) = \text{constant}\ (V - V_{mf})/D_p^{0.5}$, based solely on their aggregative fluidization results. Ergun and Orning[11] also developed an approximate relationship of this form from their work on fixed and fluidized beds, but Johnson[12], and Beranek[13], using similar functional groups, found that this type of equation did not correlate their data for aggregative fluidization.

Leva et al[14] analyzed their data for aggregative fluidization according to the modified fixed-bed equation:-

$$G\mu_f l_e/\rho_f = \text{constant}\ [(1 - \epsilon)^2/\epsilon^3]^m$$

and found that m varied from -0.7 to -4.5, as compared with the theoretical value of -1 which was obtained for particulate fluidization. To allow for this discrepancy, they defined a fluidization efficiency, and presented graphs relating this efficiency to bed expansion and gas velocities. However, it should be noted that this whole concept is based on the approximation that the logarithmic plots of $G\mu_f l_e/\rho_f$ versus $(1 - \epsilon)^2/\epsilon^3$ are linear, and as Leva indicates, this is only true for a very small range of bed expansion. Nevertheless, Leva's work on gas-solid fluidization is probably the most extensive presently available, and his correlation the most frequently discussed.

More recently, Zenz[15] has reviewed the effects of variables leading to particulate and aggregative fluidization, and has presented a useful correlation for the particulate fluidization of spherical particles. It is based on the standard drag curve for

[1]*Manuscript received April 15; accepted September 10, 1960.*
[2]*Dow Chemical of Canada Limited, Sarnia, Ont.*
[3]*Department of Chemical and Petroleum Engineering, University of Alberta, Edmonton, Alta.*
Contribution from the Research Council of Alberta and the Department of Chemical and Petroleum Engineering, University of Alberta, Edmonton, Alta.
Based on a paper presented at the C.I.C. Chemical Engineering Conference, Quebec City, November 7-9, 1960.

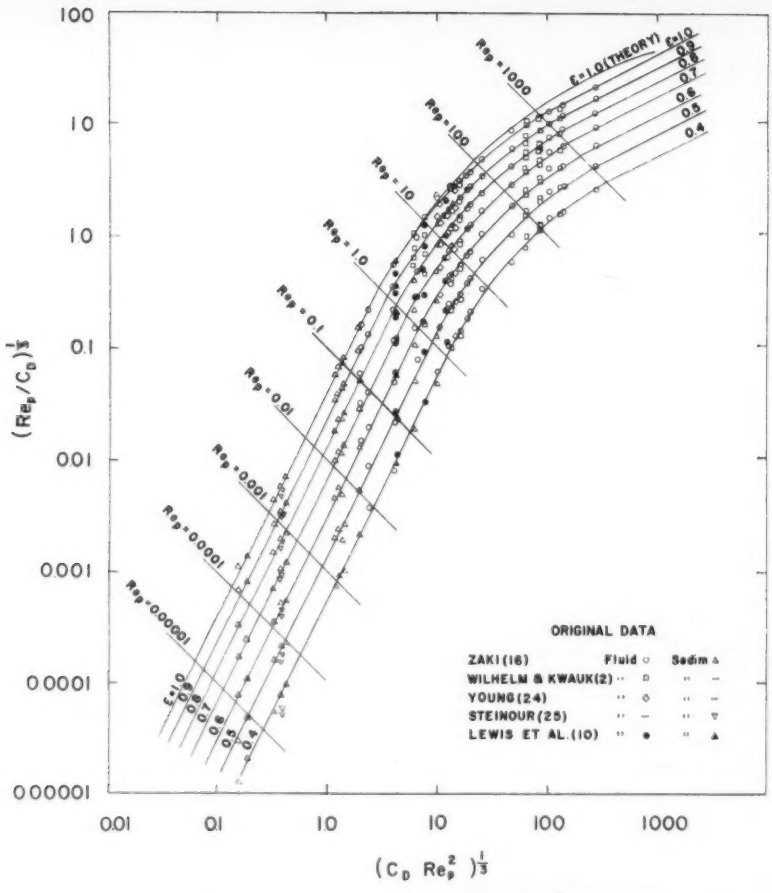

Figure 1—Smoothed correlation for particulate fluidization and sedimentation of spherical particles.

spheres, and consists of a plot of the dimensionless group $(C_D\ Re_p^2)^{1/3}$ versus $(Re_p/C_D)^{1/3}$ where:

$$(C_D\ Re_p^2)^{1/3} = D_p \left/ \left[\frac{3}{4}\ \frac{\mu_f^2}{\rho_f(\rho_s - \rho_f)g}\right]^{1/3}\right.$$

$$(Re_p/C_D)^{1/3} = V \left/ \left[\frac{4}{3}\ \frac{\mu_f(\rho_s - \rho_f)g}{\rho_f^2}\right]^{1/3}\right.$$

and with bed porosity ϵ as a parameter. This correlation, extended to cover the excellent data of Richardson and Zaki[16], is shown in Figure 1. Since the product of the co-ordinates gives the Reynold's number, values of Re_p and C_D can be rapidly obtained for any point on the graph, eliminating the usual trial and error solution. It is also interesting to note that the extension of the correlation into the region of low Reynold's numbers is based on the analogy between the sedimentation of concentrated suspensions and particulate fluidization.

Considering the application of this correlation to the case of the aggregative fluidization of beds of wide size distribution, Zenz showed that the expansion data for a batch of 60 micron cracking catalyst did not agree with his particulate correlation. However, he suggested that in either batchwise or recycle operation, the finer material which was elutriated could be considered as a part of the discontinuous gas phase, and therefore the unelutriable coarser particles constituted the more characteristic size of the fluid-bed. Thus, bed expansion data should be correlated on the basis of this corrected particle diameter. Based on this assumption, and with the introduction of a particle shape factor, his data were apparently correlated by the particulate curves, but Zenz considered that further studies would be necessary to confirm this type of correlation.

The second object of this paper was, therefore, to test the correlation of aggregative fluidization proposed by Zenz. In this connection, it was found necessary to study the fluidization of closely sized particles, and correlations of the expansion data for these single sizes are also discussed.

Experimental

The equipment used in the fluidization tests was of standard design. Constant pressure air at about 5 p.s.i.g. and metered by an orifice plate was used as the fluidizing medium. The humidity of the air, measured on a sensitive diaphram-type hygrometer, was controlled by water or steam injection in a humidifier, and the air temperature was measured on a dial-type thermometer. The column consisted of a 6-in. calming section packed with glass tubing, a porous bronze supporting grid, and a 4 ft. length of 2¼ in. I.D. Lucite tubing. Above the grid, the column was fitted with a scale graduated in inches, and multiple turns of grounded copper wire helped to reduce the static electrical charges built up during the tests. The pressure drop across the bed was measured from a pressure tap opening through the flange over the grid, to one in the upper section of the column; both taps were fitted with glass wool filters to prevent the loss of particles from the bed. Particles elutriated from the bed were removed from the air stream by a cyclone and bag-filter.

TABLE 1

PROPERTIES OF PARTICLES TESTED

Tyler Mesh	10/12	16/20	24/28	35/42	48/60	65/80	100/115	170/200
D_m*	1524	912	645	384	271	192	136	82
Beads:								
D_s	——	930	650	410	276	198	140	83.5
D_z	——	921	652	392	274	195	138	83.5
ρ_s*	——	2.555	2.545	2.465	2.550	2.520	2.470	2.400
ϵ_{mf}	——	0.409	0.401	0.396	0.410	0.404	0.409	0.432
V_{mf}*	——	105.5	62.5	29.5	14.0	6.75	3.63	1.63
V_T	——	1200	906	547	374	239	164	91
Char:								
D_s	1775	1020	725	430	310	220	156	93
D_z	1584	947	670	399	282	199	141	84.5
ρ_s	1.075	1.080	1.075	1.085	1.085	1.085	1.085	1.100
ϵ_{mf}	0.502	0.518	0.509	0.505	0.519	0.517	0.533	0.554
V_{mf}	108	63.5	40.5	15.0	9.3	4.5	2.5	0.8
V_T	830	602	468	258	190	133	100	56

*diameters in microns, velocities in ft./min. (in air at 70°F; 70 cm.Hg.), density in gm./cc.

Materials and Method

Closely sized batches, ranging in size from 14/16 mesh down to −325 mesh, of both char particles and glass beads were prepared using successive Tyler sieves. The char particles were produced by the low-temperature (600°C.) carbonization of a sub-bituminous coal in a fluid-bed, and the glass beads were obtained from Potters Brothers Inc., Carlstadt, N.J.

Some important properties of the particles are listed in Table 1. The sieve diameter, D_m, is taken as the arithmetic mean of the confining sieve openings. The effective particle diameter D_e is defined as the diameter of the sphere with the same number of particles per unit volume of bed (n_m), both counted at the critical porosity ϵ_{mf}, thus $D_e = 1.043/\sqrt[3]{n_m}$ [17]. The spherical diameter D_s is calculated as the diameter of the sphere with the same volume as the particle from the relationship $(\pi/6)D_s^3 = k\,D_m^3$. Both the volumetric shape factor k and the number of particles n_m were obtained by counting and weighing a batch of particles. Because of the internal porosity of the char particles, an apparent density was determined using a mercury displacement method according to Van Heerden et al.[17]. This method of allowing for internal porosity is probably not as rigorous as the method of Ergun [18], but it is considerably simpler when a large number of samples must be considered. The density of the glass beads was measured by a standard water-displacement method. The terminal velocity was determined as the velocity required to elutriate 50% of a given batch of closely-sized particles from the fluidization tube. A shape factor for the char particles was determined from fixed bed experiments, using the correlation of Leva et al[14] as shown in Figure 2. Assuming the glass beads to have a shape factor $\phi = 1.0$, then $\phi_{char} = 0.725$ and $\phi_{coal} = 0.622$. It is interesting to note that the data obtained with beds of beads at their loosest packing, (i.e. after fluidization), agreed with other tests at dense packings, but in the case of char, the results were always some 20-30% lower. It seems likely that this decrease in pressure drop was due to some orientation effect of the irregular particles, since all other variables are accounted for in the correlation used.

Size distributions were represented throughout on log-probability co-ordinates, as shown in Figure 3. This method of plotting gives a straight line for 'skewed' size-frequency distributions, using a logarithmic diameter scale as the ordinate, and a frequency scale graduated according to the probability integral as the abscissa. The 50% point represents the geometric mean particle diameter, and is used as the particle size representative of the mixture, while the size distribution is defined by the slope of the line through the plotted data.

Size distributions of 5, 10, 25 and 100-fold with an average diameter of 271 microns were made up according to Figure 3, and the batches were well mixed in a twin-shell blender. A weighed sample was charged to the column, and the air rate increased until all the bed was fluidized, after which the velocity was reduced in steps to zero, readings being taken at each step. The velocity was then increased, and readings again taken at each step until elutriation of particles became significant. In the case of single sizes, runs were terminated when a disperse phase

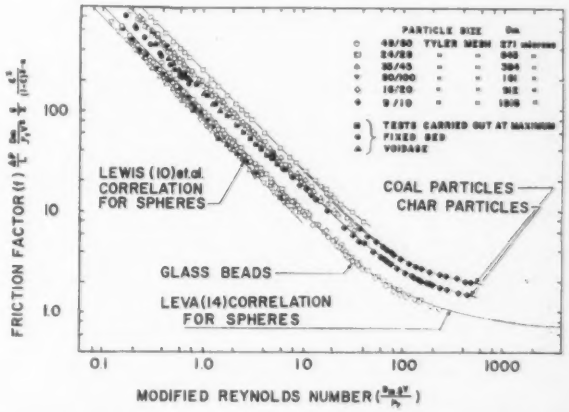

Figure 2—Correlation for the flow of air through packed beds of coal, char and glass beads, according to Leva et al. [14].

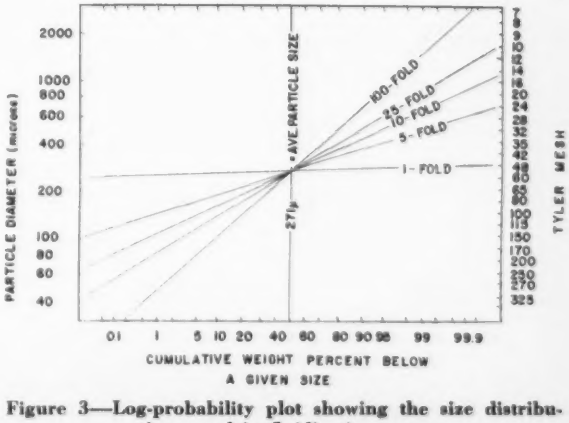

Figure 3—Log-probability plot showing the size distributions used in fluidization tests.

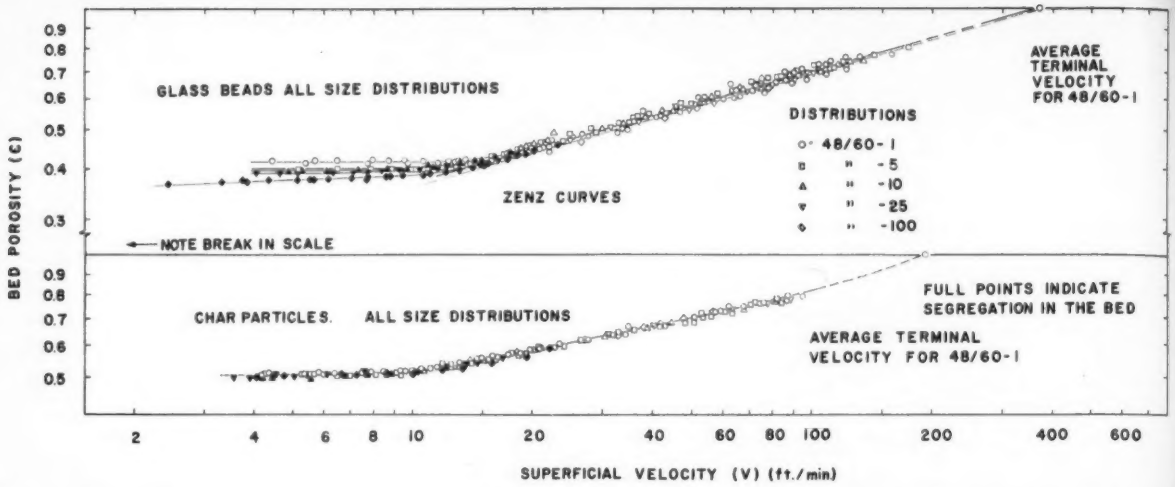

Figure 4—Expansion data for glass beads and char, showing in each case that size distribution has no effect on the shape of the expansion curve for particles of the same average diameter.

formed above the bed. The air rate was then increased to give a desired elutriation velocity, and the test continued until elutriation was completed. The unelutriated part of the bed was further tested as described for the original charge before removal from the column for size analysis. This procedure was repeated using different elutriating velocities, and size changes due to elutriation were calculated. After each stepwise change in velocity, the temperature, static and differential pressures, bed height and appearance were noted. During tests with glass beads the humidity of the air was so controlled that any slight decrease in humidity resulted in particles being attracted to the column wall. This occurred at about 60-70% relative humidity. With the char, electrostatic forces did not seem to be as great, and the air was used at about 20-30% relative humidity.

The height at which the bed settled was carefully noted during tests, extreme caution being exercised since the slightest vibration could cause serious errors. After fluidization, the bed action became increasingly violent with increasing flow rate, and bed height readings were taken as the average of the maximum and minimum readings noted.

Fluidization of Mixed Sizes

The first series of experimental tests were conducted on samples of glass beads and particles of char, each having an average size of 271 microns and covering a size range up to 100-fold. These samples are designated by the Tyler mesh limits (i.e. 48/60) followed by the size distribution as defined by Figure 3. Expansion curves for all the distributions tested are shown in Figure 4. This shows that between the point of fluidization and the onset of elutriation, the results are correlated by the 48/60-1 expansion curve, and size distribution has no effect. The magnitude of these limits, however, depends on the size distribution, and in general the velocity of complete fluidization increases, and the velocity at the onset of elutriation decreases, for the wider distributions. Complete fluidization is defined here as the point at which larger particles segregate from the bed as the velocity is reduced, and is synonymous with the point of segregation. In the case of the 48/60-100 tests, elutriation and fluidization occurred simultaneously.

Segregation velocities for the various tests are listed in Table 2. Segregation was not observed for distributions less than about

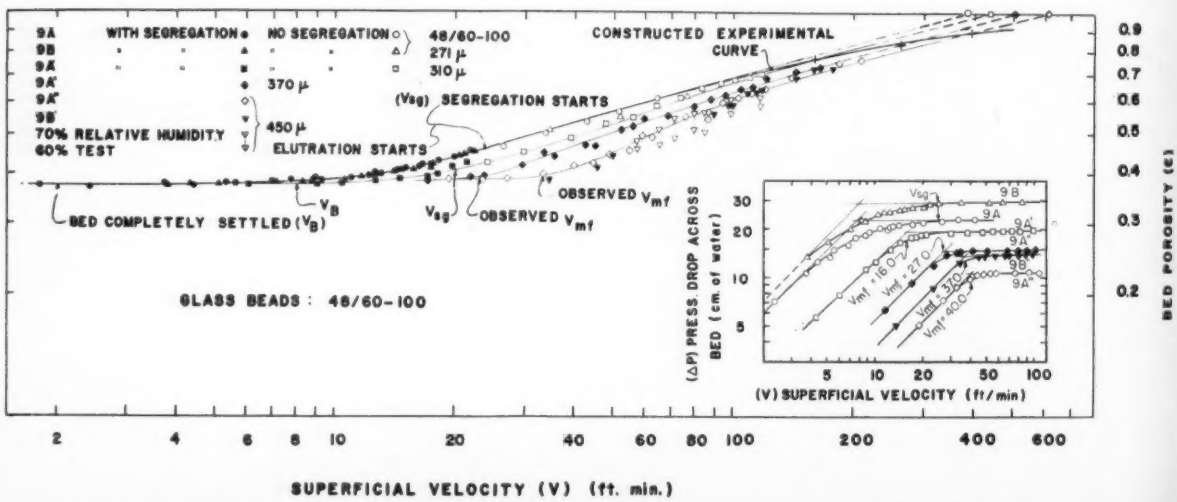

Figure 5—Expansion and pressure drop data for 48/60-100 glass beads, showing the effects of elutriation on bed properties.

TABLE 2

SEGREGATION AND MINIMUM FLUIDIZING VELOCITIES FOR GLASS BEADS AND CHAR.

Distribution	48/60–1	48/60–5	48/60–10	48/60–25	48/60–100
Beads:					
$\epsilon_{v\to\infty}$	0.410	0.392	0.383	0.381	0.350
ϵ_{mf}	0.410	0.400	0.419	0.452	0.453
ϵ_{tf}					
V_{mf}	14.0	12.0	18.0	20.0	23.0
V_{tf}					
Char:					
$\epsilon_{v\to\infty}$	0.510	0.498	0.495	0.498	0.490
ϵ_{mf}	0.519	0.509	0.516	0.565	0.592
ϵ_{tf}					
V_{mf}	9.3	7.8	9.6	17.0	23.0
V_{tf}					

Velocities in ft./min. (in air at 70°F. and 70 cm. Hg.)

5-fold; instead a minimum fluidizing velocity was observed which was less than the corresponding critical velocity for the 48/60-1 size. For wider distributions in which segregation did occur, both the pressure drop and the porosity were dependent on the history of the bed, since the amount of fines trapped in the segregated portion depended on the rate of change of velocity. The influence of segregation on the pressure drop curve is shown in Figure 5 (inset), a more gradual change being obtained instead of the characteristic "break point". Figure 4 shows the effect of segregation on the bed porosity at low velocities ($\epsilon_{v\to\infty}$). For the glass beads, the porosity $\epsilon_{v\to\infty}$ decreases as the size distribution increases, due to the inter-packing of the smaller particles amongst the larger ones. For the char particles, the same trend is evident, but the variation is much smaller.

The expansion curves in Figure 4 show that the tests with char and glass beads gave similar results. Minimum fluidization porosities (ϵ_{mf}) are higher for the char, and the slope V/ϵ also much larger than the corresponding slope for the beads. These differences, together with the smaller variation in $\epsilon_{v\to\infty}$, can be attributed to the irregular shape of the char particles. The greater scatter of the data for the glass beads is probably due to the importance of static and humidity effects in these tests. By careful control of the humidity of the fluidizing air, static effects were minimized, but it is possible that the humidity had a separate effect on bed expansion, as discussed later. Neither of these effects was important in the tests with char particles.

In general, the wider distributions resulted in smoother fluidization, though little difference could be observed between the fluidization of the 10, 25 and 100-fold distributions. This is in accord with the observations of Matheson et al[19], who found that the addition of fines to closely sized beds resulted in better fluidization, and with Zenz[20], who calculated that the maximum improvement of fluidization quality should be obtained with about an 11-fold size distribution.

Some typical expansion curves obtained from elutriation tests on samples of 48/60-100 glass beads are shown in Figure 5. Similar results were obtained for the other distributions, and in each case, the expansion curve for the original distribution is as shown in Figure 4. However, the expansion curves for the distributions obtained by elutriation showed a curvature which increased with increasing average particle diameter. This suggested that bed expansion was a different function of velocity for different average particle sizes, and the tests on single sizes discussed in the next section were designed to study this problem.

The constructed expansion curve in Figure 5 shows the actual change in bed porosity with increasing velocity when elutriation from the bed is also taking place, and it shows that a considerable amount of fine material can be removed from the bed before there is any detectable change in bed properties. These constructed curves were obtained for all the tests by plotting the various elutriation velocities on the expansion curves* obtained for the corresponding unelutriable portions of the original distribution. The results of elutriation tests for glass beads are summarized in Figure 6, which shows the observed changes in average size for the various distributions with

*The expansion curves used in this construction are extrapolated to the terminal velocities of the average sizes of the distributions. This is based on the conclusion that any size distribution can be represented by a single average size, and is discussed in the section on single sizes.

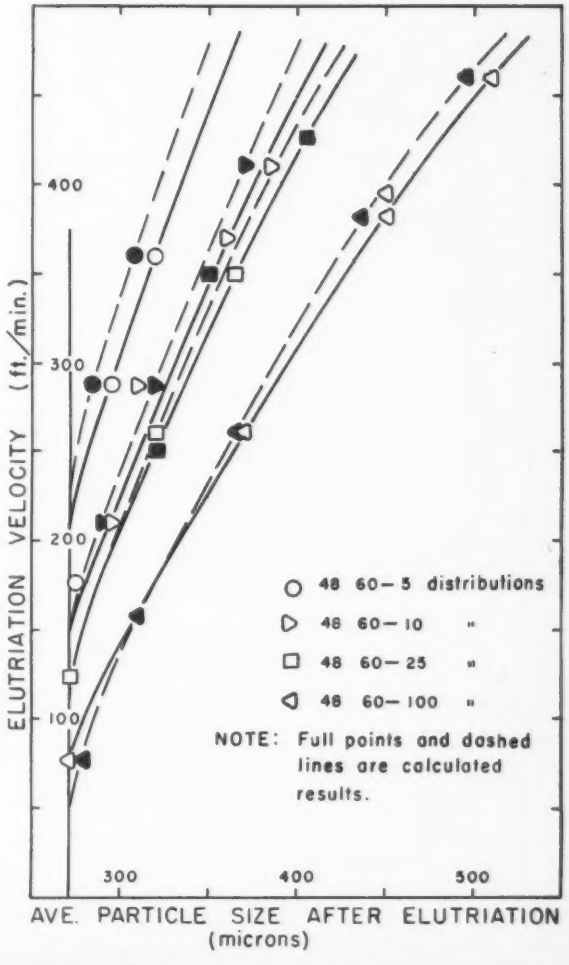

Figure 6—Changes in average particle diameter due to elutriation of fines from beds of widely sized glass beads.

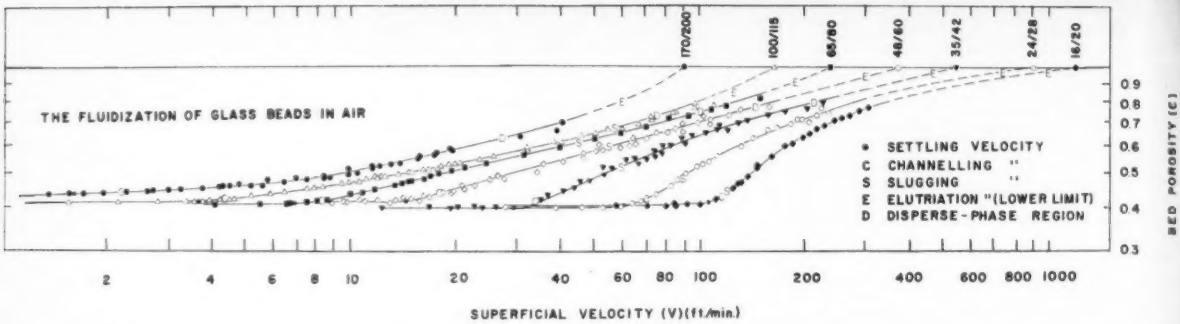

Figure 7—Expansion data for closely sized glass beads, showing the variations in shape of the expansion curve for different particle diameters.

increasing elutriation velocity. The results are compared with calculated values based on terminal velocity data, and good agreement is obtained, with the calculated values being from 1-4% low.

Fluidization of Single Sizes

To investigate the variation in shape of the expansion curves obtained during elutriation experiments, a series of tests were made with glass beads and char particles ranging in size from 1524-81 microns. Bed weight was found to have no significant effect on the expansion data, and the results shown in Figures 7 and 8 are for bed weights of 500 gm. (beads) and 300 gm. (char) respectively. Good fluidization was established at some point *C* (i.e., at the end of the channelling region) and slugging began at point *S*. Channelling tendencies were observed to increase sharply with decreasing particle diameter, and slugging tendencies increased as particle diameter increased. Tests were usually completed at the point *D*, when a disperse phase formed above the bed, and the extrapolated data (dotted) terminate at the measured average terminal velocity of the particles.

The systematic variation in shape of the expansion curves in Figures 7 and 8, is obviously due to the variation in particle diameter. For larger sizes, the bed porosity increases rapidly at low velocities and slowly at high velocities, while for small sizes the opposite is true. Between these extremes, a transitional linear expansion curve is obtained. These results suggest that the variations in bed expansion data published by other workers, (and usually presented as linear expansion curves), are due in most cases to the limited range of bed expansion and particle diameters considered. The relative differences between the curves for the char and the beads are again probably due to the differences in electrostatic effects, particle density and shape.

A comparison of expansion data shows that the curves for the elutriated samples can be represented by the curves for the single sizes of the same average particle diameter, and it is concluded that the average size of *any* continuous distribution, as defined by the log-probability scale, can be used to describe the expansion curve for the bed by reference to the expansion curve for sized particles of this same diameter. Simple mixtures which cannot be represented by a continuous function on log-probability co-ordinates have been considered by other workers[14,17], and a reciprocal mean diameter should be used in these cases.

Comparison with Published Correlations

Since it has been shown that size distribution has little effect on bed expansion between the points of good fluidization and elutriation, the following discussion will be limited to a consideration of single sizes.

The expansion data for the closely sized particles are compared with the appropriate region of Zenz's particulate correlation in Figures 9 and 10, and it can be seen that considerable deviations exist. A study of the expansion curves in Figures 7 and 8 shows that the slope V/ϵ increases with decreasing particle size and sphericity. A very large slope is also obtained, if Zenz's data[18] for the 60 micron catalyst particle are considered, and the spread of this data is clearly due both to the small average diameter and irregular shape of the particles, and to the size distribution (i.e., elutriation). This latter effect is, however, only of secondaty importance, and in general, it may be concluded that Zenz's correlation cannot be used to correlate the data for aggregative fluidization.

If the expansion curves predicted by Zenz's correlation are superimposed on Figure 7, a series of straight lines joining the terminal and minimum fluidization velocities are obtained. For 48/60-1 beads, the experimental data and the Zenz curve coincide; but for smaller and larger sizes, bed porosities are respectively always smaller or greater than the corresponding

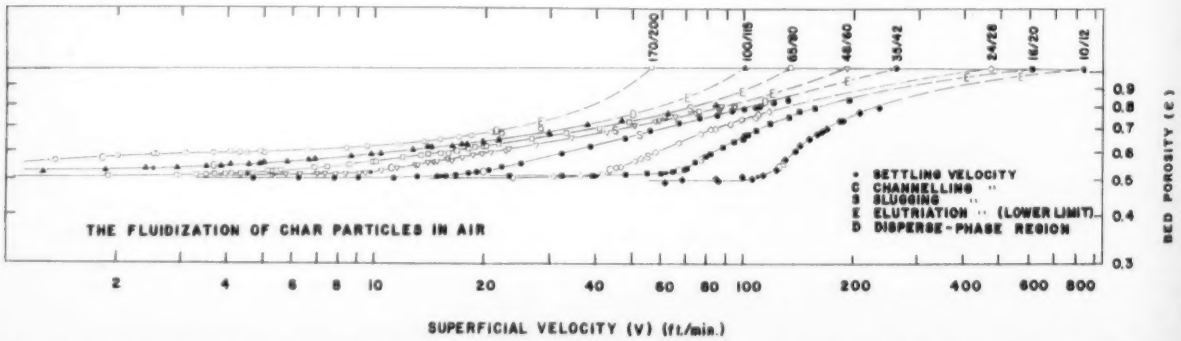

Figure 8—Expansion data for closely sized char particles showing the variations in shape of the expansion curve for different particle diameter.

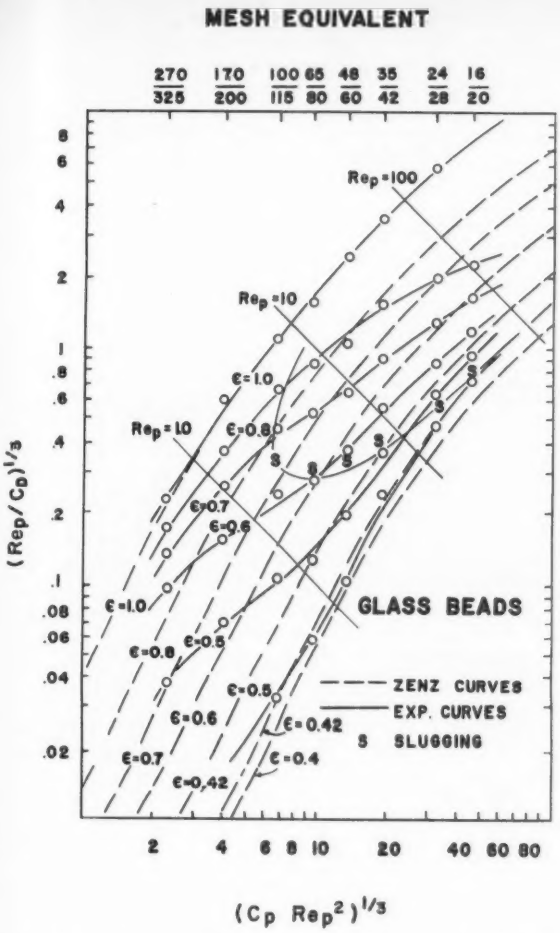

Figure 9—Comparison of aggregative fluidization data for closely sized glass beads with Zenz's particulate correlation.

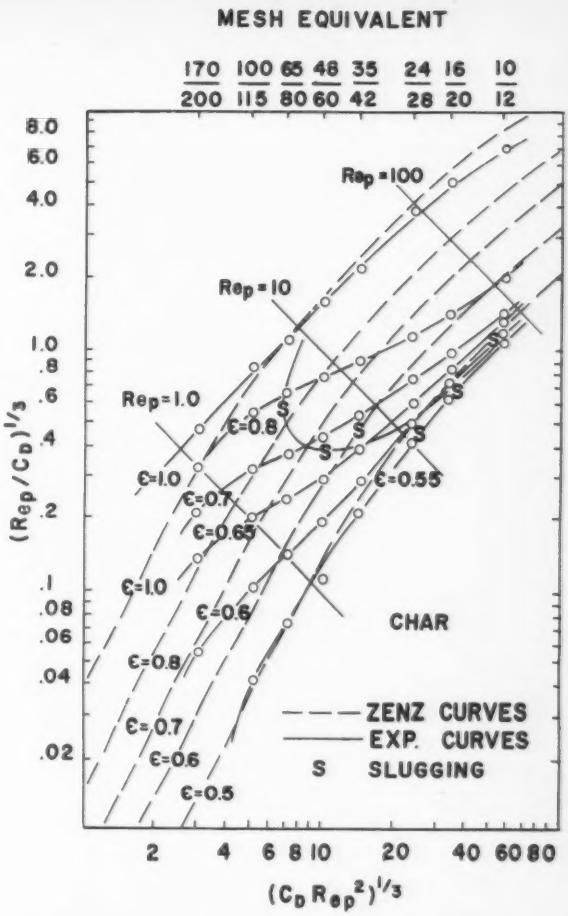

Figure 10 — Comparison of aggregative fluidization data for closely sized char particles with Zenz's particulate correlation.

particulate value. This indicates that at least two effects (dependent on particle diameter) are acting in opposition in the bed, and for 48/60-1 beads, these effects balance out and "pseudo-particulate" expansion is obtained. The forces involved are almost certainly due to inter-particle or particle-wall attractions, and have been mentioned by several authors[2,21,22]. The strong diameter effect indicated in this work supports these assumptions. Some qualitative explanations of bed expansion have been suggested[22] based on the differences in particle motion and energy losses. Beds of small particles show strong turbulence and high energy losses, resulting in less bed expansion, whereas large particles tend to show rapid expansion, with particles aggregating strongly (i.e., slugging) and with little relative motion between the particles, and therefore smaller energy losses. It is also likely that these differences in particle motion affect the formation of electrostatic charges, and that the greater presence of static with smaller sizes is due to this effect. In tests with very small particles, terminal velocities were increased by static, and it is possible that static forces might well be associated with the behaviour of very small particles when fluidized above their true terminal velocity[2].

A common method of reducing static forces is to increase the relative humidity of the fluidizing gas. Experiments with 48/60-1 beads showed that increases in humidity had little effect until static forces were reduced to the point at which particles would no longer stick to the column. At this point, bed expansion increased (as indicated in Figure 5), and stable operation was obtained for a narrow range of humidity. Further increases in humidity increased the aggregating tendencies of the bed, presumably due to moisture adhering to the surface of the particles and causing sticking, and unstable operation resulted. The tests described in this paper were carried out in this minimized-static region, and as such, the data presented are comparable. However, it is obvious that variable electrostatic and moisture effects can cause differences in operation of aggregative fluidized beds[20,22] and a comprehensive study of inter-particle forces is required before a correlation of expansion data can really be satisfactory.

A comparison of Figures 9 and 10 shows that for irregular particles, the slope V/ϵ is larger and that the terminal velocity data show marked deviations from the standard drag curve for spheres. The expansion data of Presler[23] for magnesite and galena fluidized in water were also considered, and the slope V/ϵ was again found to increase with decreasing sphericity. Similarly, Richardson and Zaki[16], working with large particles, found that the volumetric shape factor of Heywood[6] (K) correlated their results as

$$V/\epsilon = 2.7K^{0.16}$$

The effects of particle shape are also shown in Figure 11. The free fall data for mineral particles[5,6] and for isometric particles[3] are plotted on the same co-ordinates as the particulate correlation, and it can be seen that the $\epsilon = 1$ lines for non-spherical particles fall below that for spheres, the deviation increasing with decreasing sphericity and with increasing Reynold's number.

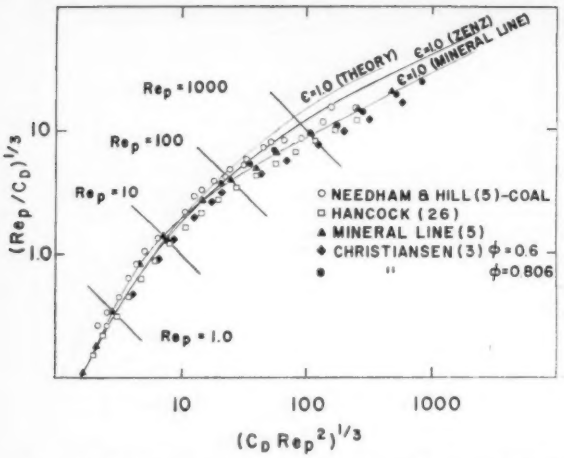

Figure 11—Comparison of free-fall data for non-spherical particles with the Zenz correlation for spheres.

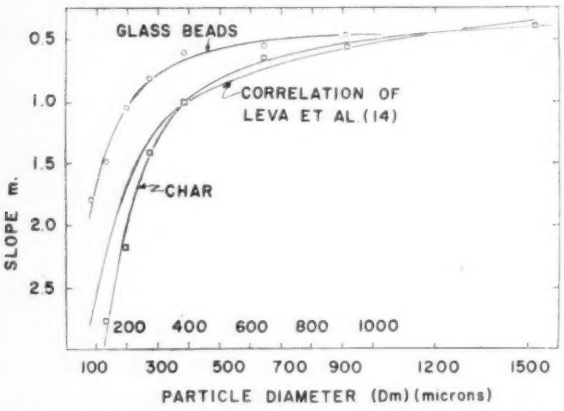

Figure 12—Comparison of the expansion data for char and beads with the correlation of Leva et al. [14].

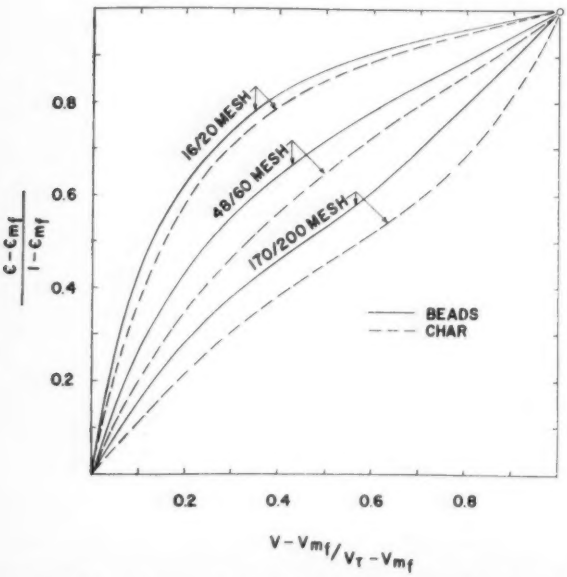

Figure 13 — Aggregative fluidization data for beads and char, plotted on reduced co-ordinates, showing the effects of particle diameter and shape.

From these considerations, it would seem that contrary to Zenz's suggestions, a simple shape factor cannot be used to correlate the particulate fluidization data of non-spherical particles. A separate correlation would be required, giving a shape correction factor versus the group $(C_D Re_p^2)^{1/3}$, with a simple shape factor such as sphericity as a parameter. At the present time, very little reliable information is available, and such a correlation cannot be made from a literature survey.

Correlation of the expansion data for single sizes was also attempted on the basis of the correlations mentioned earlier. Figure 12 shows a comparison with the work of Leva et al.[14]; differences can be attributed to both shape effects and to the approximations inherent in this method. A study of Leva's original data shows that the more irregular particles give a larger negative slope (m), and the Leva correlation represents an average line based mostly on irregular particles. The analysis of the present data showed that the logarithmic plots of $G\mu_f l_e/\rho_f$ versus $(1 - \epsilon)^2/\epsilon^3$ were increasingly curved as the particle diameter decreased, and this type of correlation is severely limited to small expansion ratios.

Methods involving plots of porosity versus velocity on reduced co-ordinates were also considered, but marked diameter and shape effects were evident, and considerably more data are required before a generalized correlation can be attempted. The co-ordinates $(\epsilon - \epsilon_{mf})/(1 - \epsilon_{mf})$ and $(V - V_{mf})/(V_t - V_{mf})$, as used by Beranek[13], were considered since they define the complete range of bed expansion between the limits of O and 1. Figure 13 shows the expansion results for three sizes of char and beads plotted in this form, and it can be seen that there are strong effects of particle diameter and shape and that no simple correlation exists. A plot using the groups $(l_e - 1)$ and $(V/V_{mf}) - 1$ showed similar differences due to particle properties, but gave straight lines within the range of expansion considered (i.e., also within the range of normal dense-phase operation). These latter groups might offer a useful empirical method of correlating shape and diameter effects in the aggregative expansion of a fluidized bed.

Conclusions

(1) Size distribution has no effect on the shape of the expansion curve above the point of good fluidization and below the point of elutriation, for beds of the same average diameter as defined by the log-probability scale. Segregation occurs with distributions greater than about 5-fold, but no means of predicting a segregation velocity are presently available. The change in the average diameter of a bed of particles of wide size distribution due to elutriation can be calculated with better than 5% accuracy from a knowledge of the terminal velocity data for the material involved.

(2) The shape of the expansion curve for aggregative fluidization is dependent on particle diameter, being in general non-linear, and Zenz's particulate correlation cannot be used to correlate the data for gas-solid systems. The Zenz correlation can be used to predict the behavior of spherical particles in liquids, but for non-spherical particles, it must be further modified. It cannot be adapted by the inclusion of a simple shape factor in the co-ordinates, since the shape correction function also varies with the Reynold's number.

(3) There are no satisfactory generalized correlations presently available for aggregative fluidization. Static electricity and excessive moisture in the fluidizing gas have both been found to have a considerable effect on aggregative fluidization, and a better understanding of inter-particle and particle-wall forces, as well as data on shape effects, are required before such a correlation can be obtained.

Acknowledgment

This work was carried out at the Research Council of Alberta, and presented in partial fulfilment of the requirements for a Master of Science degree at the University of Alberta. The helpful discussions of C. Moreland, and the laboratory assistance of E. Kyto are gratefully acknowledged. Permission to publish this paper as Contribution Number 121 from the Research Council of Alberta is also acknowledged.

*Nomenclature**

C_D = drag coefficient = $(4/3)\, gD_p(\rho_s - \rho_f)/(\rho_f V^2)$
D_e = effective diameter of particle[17]
D_m = average sieve diameter of particle
D_p = particle diameter
D_s = spherical diameter of particle
g = gravitational constant
G = superficial mass velocity
K = volumetric shape factor[6]
l_e = bed expansion ratio = (L/L_{mf})
L = bed height
m = slope of correlation proposed by Leva[14]
Re_p = particle Reynold's number = $(D_m\rho_f\, V/\mu_f)$
V = superficial velocity
ϵ = average bed porosity
$\epsilon_{s\to 0}$ = average bed porosity at zero velocity
μ_f = fluid viscosity
ρ_f = fluid density
ρ_s = particle density
ϕ = sphericity = ratio of the surface area of the sphere of the same volume as the particle to the surface area of the particle.

Subscripts

mf = minimum fluidization
sg = segregation
T = terminal (free fall)

References

(1) Sinclair, C. G., and D. B. Robinson, Can. J. Chem. Eng., **36,** 51 (1958).
(2) Wilhelm, R. H., and M. Kwauk, Chem. Eng. Progr., **44,** 201 (1948).
(3) Prettyjohn, E. S., and E. B. Christiansen, **Ibid,** p. 157.
(4) Heiss, J. F., and J. Coull, Ibid, **48,** 133 (1952).
(5) Needham, L. W., and N. W. Hill, Fuel, **26,** 101 (1947).
(6) Heywood, H., Proc. Inst. Mech. Engrs. (London), **140,** 257 (1938).
(7) Leva, M., Chem. Eng. Progr., **47,** 39 (1951).
(8) Osberg, G. L., and D. H. Charlesworth, **Ibid,** p 566.
(9) Lang, P. M., Sc.D. Thesis, Mass. Inst. Tech., Cambridge (1952).
(10) Lewis, W. K., E. R. Gilliland, and W. C. Bauer, Ind. Eng. Chem. **41,** 1104 (1949).
(11) Ergun, S., and A. A. Orning, **Ibid,** 1179.
(12) Johnson, E., Inst. Gas. Engrs. Research Fellowship Report, Pub. 378/179 (1950).
(13) Beranek, I. J., Brit. Chem. Eng., **3,** 358 (1958).
(14) Leva, M., M. Weintraub, M. Grummer, M. Pollchik, and H. H. Storch, U.S. Bur. Mines Bull., **504** (1951).
(15) Zenz, F. A., Petroleum Refiner, **36,** No. 8, 147 (1957).
(16) Richardson, J. F., and W. N. Zaki, Trans. Inst. Chem. Engrs. (London), **32,** 35 (1954).
(17) Van Heerden, C., A. P. P. Nobel, and D. W. Van Krevelen, Chem. Eng. Sci., **1,** 37 (1951).
(18) Ergun, S., Anal. Chem., **23,** 151 (1951).
(19) Matheson, G. L., W. A. Herbst, and P. H. Holt, Ind. Eng. Chem., **41,** 1099 (1949).
(20) Zenz, F. A., Petroleum Refiner, **36,** No. 5, 261 (1957).
(21) Parker, H. W., and W. F. Stevens, A.I.Ch.E. Journal, **5,** 314 (1959).
(22) Othmer, D. F., ed., "Fluidization", p. 14, Reinhold Pub. Corp., New York (1956).
(23) Presler, A. F., Ph.D. Thesis, Iowa State College, Ames (1956).
(24) Young, R. J., J. App. Chem., **2,** S55 (1952).
(25) Steinour, H. H., Ind. Eng. Chem., **36,** 618 (1944).
(26) Hancock, R. T., Mining Magazine, **55,** 90 (1936).

★ ★ ★

*Any consistent set of units may be used.

Heat Transfer to a Surface Reacting Fluid in Turbulent Flow[1]

RONALD I. ROTHENBERG[2] and J. M. SMITH[2]

The effect of chemical reaction on heat transfer has been studied for turbulent flow in tubes of a reacting gas. The analysis is carried out for a heterogeneous, catalytic reaction occurring at the wall surface. Equations are presented for predicting the increase in heat transfer coefficient due to reaction in terms of the rate of reaction, diffusion, and operating conditions. For an exothermic reaction the total heat transfer coefficient is increased when the gas temperature is greater than the wall temperature, and decreased when the gas temperature is less than the wall value. The effect is greatest for rapid reactions; that is, when diffusion of reactants to the tube wall determines the rate of reaction.

The equations are applied to the catalytic hydrogenation of ethylene. The results show that the total heat transfer coefficient can be at least ten fold larger than the coefficient for a non-reacting system at the same flow conditions.

In general, the results of this study suggest that a wall-catalyzed reaction can be an effective means of increasing the heat transfer rate from gases in turbulent flow in tubes. Furthermore, for a porous catalyst applied to the wall, enlarging the thickness of the catalyst layer will increase the effect on the heat transfer rate.

Heat transfer between a fluid and boundary surface can be significantly affected by chemical reaction in the fluid. In experimental studies on the flow of $NO_2-N_2O_4$ in a heated tube, Schotte[1] measured over-all heat transfer rates several times as high as expected in a chemically inert system. In an analytical study[2] for the same mixture, point ratios of the total and inert heat transfer coefficients are predicted to be as high as 15.

In the $NO_2 - N_2O_4$ system the reaction occurs homogeneously within the gas phase, while in the dissociation of such molecules as oxygen and nitrogen reaction probably takes place heterogeneously on the hot solid surface as well as in the fluid phase. This paper is restricted to the case in which: (1) the reaction is entirely heterogeneous, and (2) the fluid is in turbulent flow in a circular pipe. This situation would result when the gas flows through a tube whose inside surface serves as a catalyst for the reaction. There have been a number of investigations[3,4,5,6,7,8] of heat transfer with surface reaction treated from the stand-point of a laminar boundary layer near a solid surface, but none for turbulent flow in pipes. Studies with turbulent flow have been concerned with reaction in the boundary layer[9].

[1]*Manuscript received April 8, 1960; accepted June 28, 1960.*
[2]*Northwestern University, Evanston, Ill.*
Based on a paper presented to the C.I.C. Chemical Engineering Conference, Quebec City, Que., Nov. 7-9, 1960.

The effect of reaction on heat transfer is due to the diffusion of reactants through the fluid to the wall surface where reaction occurs, and energy is evolved or absorbed. Hence, the magnitude of the effect depends upon the rates of diffusion and reaction. Furthermore, if the resistance to diffusion is negligible with respect that for reaction, the effect on the heat transfer will be controlled by the kinetics of the wall reaction. Under these circumstances, the diffusion process does not influence the result. At the other extreme, the reaction resistance is so small that the chemical process occurs at near-equilibrium conditions. Then the kinetics of the reaction are unimportant, and the diffusion rate determines the effect on heat transfer. These points are evident from considering the expression for the total heat transfer rate at the tube wall:

$$q_w = q_c + q_D$$

$$q_w = -k\left(\frac{\partial t}{\partial y}\right)_w + r_A\,(\Delta H)_w \qquad (1)$$

The first term on the right represents the conventional contribution due to the temperature gradient, and the second, the contribution associated with the wall reaction. The quantity r_A is either the rate of diffusion of reactant A to the wall or the rate of reaction of A on the surface. If the total heat transfer coefficient h_T is defined as $q_w/(t_w - t_b)$, and the conventional coefficient h_c as $q_c/(t_w - t_b)$, Equation (1) may be written:

$$\frac{h_T}{h_c} = 1 + \frac{r_A(\Delta H)_w}{h_c(t_w - t_b)}$$

or

$$\frac{h_T - h_c}{h_c} = \frac{q_D}{q_c} = \frac{r_A(\Delta H)_w}{h_c(t_w - t_b)} \qquad (2)$$

Equation (2) presents the relative change in heat transfer coefficient due to reaction in terms of the rate of diffusion (or reaction) and the thermal properties of the system. It should be noted that h_c is the conventional coefficient for a non-reactive fluid with the same physical properties as the reacting system. To use Equation (2) directly for predicting the effect of reaction on heat transfer requires expressing the right side of the equation in terms of the design parameters of the equipment and known properties of the system. This is carried out in general, and for specific reactions, in the following sections.

General Equations for Heat Transfer Coefficients

Equation (2) can be written in terms of an enthalpy ratio H^* as follows:

$$\frac{h_T - h_c}{h_c} = H^*\left(\frac{r_A \bar{C}_p \bar{M}}{h_c}\right) \qquad (3)$$

where

$$H^* = \frac{\Delta H_w}{(t_w - t_b)\,(\bar{C}_p \bar{M})} \qquad (4)$$

The conventional or inert heat transfer coefficient (h_c) for well-developed turbulent flow can be approximated by the Colburn type equation[10].

$$\frac{h_c}{C_p G} = 0.04\,(\mathrm{Re})^{-0.25}\,(\mathrm{Pr})^{-2/3} \quad \ldots\ldots(5)$$

Substitution of this expression in Equation (3) leads to the result

$$\frac{h_T - h_c}{h_c} = (\mathrm{Pr})^{2/3}\,H^*\,F^* \quad \ldots\ldots(6)$$

where

$$F^* = \frac{25\,(\mathrm{Re})^{0.25}\,\overline{M}\,r_A}{G} = \frac{r_A\,\overline{C}_p\overline{M}}{(\mathrm{Pr})^{2/3}\,h_c} \quad \ldots\ldots(7)$$

Equation (6) expresses the effect of reaction on heat transfer in terms of the Prandtl number and two dimensionless quantities: (1) the enthalpy ratio H^*, and (2), a transport group F^* containing the ratio of the rate of diffusion and conventional heat transfer coefficient. The evaluation of F^* requires a knowledge of r_A, which in turn depends upon the chemical reaction involved.

For a general reaction

$$aA + bB + iI \rightleftharpoons rR + sS + iI$$

r_A may be expressed by the double equation:

$$r_A = k_f\left(p^a_{Aw}\,p^b_{Bw} - \frac{p^r_{Rw}\,p^s_{Sw}}{K_e}\right) = k_A\,(p_{A_b} - p_{A_w}) \quad \ldots\ldots(8)$$

The mass transfer rates of the other reactant and the two products of the reaction can be related to diffusion of A by the equations:

$$k_A\,(p_{A_b} - p_{A_w}) = a/b\;k_B\,(p_{B_b} - p_{B_w}) \quad \ldots\ldots(9)$$

$$= -\,a/r\;k_R\,(p_{R_b} - p_{R_w}) \quad \ldots\ldots(10)$$

$$= -\,a/s\;k_S\,(p_{S_b} - p_{S_w}) \quad \ldots\ldots(11)$$

Equations (8-11) are sufficient to determine the partial pressures at the wall, p_{Aw}, p_{Bw}, p_{Rw} and p_{Sw}, and then r_A from Equation (8). To do this necessitates estimating the several mass-transfer coefficients k_A, k_B, k_R and k_S. Supposing that the Colburn analogy is applicable for mass transfer as it was used for heat transfer, Equation (5), the mass transfer coefficients are given by expressions similar to the following one for reactant A:

$$\left(\frac{\overline{M}\,k_A\,p_{f-A}}{G}\right) = 0.04\,(Re)^{-0.25}\,(Sc_A)^{-2/3} \quad \ldots\ldots(12)$$

In applying Equation (12) the Schmidt number depends upon the multi-component diffusion coefficient D_{AM}. This can be estimated from the binary coefficients D_{AB}, D_{AS}, etc. according to the procedure proposed by Wilke[11]. The film pressure factor p_{f-A} depends upon the total pressure p and the stoichiometric coefficients a, b, r, s, as explained by Hougen and Watson[12]. Solution of Equations (8-11) for the partial pressures at the wall conditions is a trial and error procedure, since the evaluation of k_A, p_{f-A}, and similar quantities for the other components, depends upon the desired partial pressures. Approximate results for first estimates can be obtained by utilizing bulk properties to evaluate k_A and p_{f-A}.

The procedure just outlined can be used to determine r_A, and the effect of reaction on heat transfer from known properties of the system. Explicit expressions for r_A and F^* can be achieved only when simplications are possible in the reaction system or the relationship between diffusion and reaction rate.

If the resistance to reaction is much greater than the diffusion resistance, k_f/k_A approaches zero and $p_b = p_w$ for component A. Thus, under reaction-controlling circumstances, Equation (8) becomes

$$r_A = k_f\left(p^a_{A_b}\,p^b_{B_b} - \frac{p^r_{R_b}\,p^s_{S_b}}{K_e}\right) \quad \ldots\ldots(13)$$

On the other hand, if k_A/k_f approaches zero, diffusion is controlling and chemical equilibrium is approached at the wall conditions. Then

$$r_A = k_A\,(p_{A_b} - p_{A_{w-eq.}}) \quad \ldots\ldots(14)$$

and the equilibrium value of p_A at the wall temperature, $p_{A_{w-eq.}}$ is determined by the equation

$$K_e = \left(\frac{p^r_R\;p^s_S}{p^a_A\;p^b_B}\right)_w \quad \ldots\ldots(15)$$

The evaluation of F^* for several simple types of reactions is considered in the following section.

Applications to Specific Types of Reactions

For an isomerization-type of reaction

$$A \rightleftharpoons R$$

Equation (8) reduces to the form:

$$r_A = k_f\left(p_{A_w} - \frac{p - p_{Aw}}{K_e}\right) = k_A\,(p_{A_b} - p_{A_w}) \quad \ldots\ldots(16)$$

Using the latter equality in this equation to eliminate p_{A_w} leads to the following expressions for r_A and F^*:

$$r_A = \frac{p_{A_b}\left[1 + \frac{1}{K_e}\left(1 - \frac{p}{p_{A_b}}\right)\right]}{\frac{1}{k_A}\left(1 + \frac{1}{K_e}\right) + \frac{1}{k_f}} \quad \ldots\ldots(17)$$

$$F^* = \frac{25\;Re^{0.25}\,\frac{p_{A_b}\overline{M}}{G}\left[1 + \frac{1}{K_e}\left(1 - \frac{p}{p_{A_b}}\right)\right]}{\frac{1}{k_A}\left(1 + \frac{1}{K_e}\right) + \frac{1}{k_f}} \quad \ldots\ldots(18)$$

where k_A is determined by Equation (12). For this reaction type, $p_{f-A} = p$. This expression for F^* can be used in Equation (6) to evaluate the effect of reaction on heat transfer.

If reaction controls (k_f/k_A approaches zero), Equation (18) reduces to the form

$$F^* = 25\;Re^{0.25}\,\frac{p_{A_b}\overline{M}\,k_f}{G}\left[1 + \frac{1}{K_e}\left(1 - \frac{p}{p_{A_b}}\right)\right] \quad \ldots\ldots(19)$$

in which the mass-transfer coefficient is not involved. If diffusion controls, the expression does not involve the reaction rate constant k_f; i.e.

$$F^* = (Sc_A)^{-2/3}\left[\frac{p_{A_b}}{p} - \frac{1}{K_e + 1}\right] \quad \ldots\ldots(20)$$

If the reaction is irreversible, still further simplication is possible. The resulting expressions for F^* are shown in Table 1 under the column for the reaction $A \rightleftharpoons R$.

The forms of the F^* function for other types of 2 and 3 component reactions are also presented in Table 1. Blanks in the table occur when explicit equations for F^* are not possible. However, Equations (7-11) can be solved numerically for any reaction system and for the intermediate case of neither reaction nor diffusion controlling the process. The results for a system of this type are developed next for the hydrogenation of ethylene.

Catalytic Hydrogenation of Ethylene

The heat of reaction for the gas-phase hydrogenation of ethylene at 298°K. and 1 atmosphere pressure is −58,920 B.t.u./lb. mole. For this relatively high ΔH, the effect of reaction

TABLE 1

F* FOR SEVERAL CHEMICAL SYSTEMS

↓ Conditions \ System →	$A \rightleftharpoons R$	$A \rightleftharpoons 2R$
Reversible reaction	$\dfrac{25\ Re^{0.25}\ (p_{A_b}\ \overline{M}/G)\left[1+\dfrac{1}{K_e}\left(1-\dfrac{p}{p_{A_b}}\right)\right]}{\dfrac{1}{k_{gA}}\ (1+1/K_e)+\dfrac{1}{k_f}}$	
Reversible reaction; Reaction controlling	$25\ Re^{0.25}\ (p_{A_b}\ \overline{M}\ k_f/G)\left[1+\dfrac{1}{K_e}\left(1-\dfrac{p}{p_{A_b}}\right)\right]$	$25\ Re^{0.25}\ \dfrac{\overline{M}\ k_f}{G}\left[p_{A_b}-\dfrac{(p-p_{A_b})^2}{K_e}\right]$
Reversible reaction; Diffusion controlling	$(Sc_A)^{-2/3}\left[\dfrac{p_{A_b}}{p}-\dfrac{1}{K_e+1}\right]$	$(Sc_A)^{-2/3}\ Ln\ \dfrac{p+p_{A_b}}{p-\left[\dfrac{K_e^2}{4}+p\ K_e\right]^{1/2}+\left[\dfrac{K_e}{2}+p\right]}$
Irreversible reaction	$\dfrac{25\ Re^{0.25}\ (p_{A_b}\ \overline{M}/G)}{(1/k_{gA}+1/k_f)}$	
Irreversible reaction; Reaction controlling	$25\ Re^{0.25}\ (p_{A_b}\ \overline{M}\ k_f/G)$	$25\ Re^{0.25}\ (\overline{M}\ p_{A_b}\ k_f/G)$
Irreversible reaction; Diffusion controlling	$(Sc_A)^{-2/3}\ (p_{A_b}/p)$	$(Sc_A)^{-2/3}\ Ln\ \dfrac{p+p_{A_b}}{p}$

↓ Conditions \ System →	$2A \rightleftharpoons R$	$A+B \rightleftharpoons R$
Reversible reaction		
Reversible reaction; Reaction controlling	$25\ Re^{0.25}\ \dfrac{\overline{M}\ k_f}{G}\left[(p_{A_b})^2-\dfrac{p-p_{A_b}}{K_e}\right]$	$25\ Re^{0.25}\ \dfrac{k_f\ \overline{M}}{G}\left[p_{A_b}\ p_{B_b}-\dfrac{p_{R_b}}{K_e}\right]$
Reversible reaction; Diffusion controlling	$-\ 2\ (Sc_A)^{-2/3}\ Ln\ \dfrac{p-p_{A_b}/2}{p-1/2\left\{+\left[\dfrac{1}{K_e}\left(p+\dfrac{1}{4K_e}\right)\right]^{1/2}-\dfrac{1}{2K_e}\right\}}$	
Irreversible reaction		
Irreversible reaction; Reaction controlling	$25\ Re^{0.25}\ (\overline{M}\ k_f/G)\ (p_{A_b})^2$	$25\ Re^{0.25}\ \dfrac{k_f\ \overline{M}}{G}\ (p_{A_b}\ p_{B_b})$
Irreversible reaction; Diffusion controlling	$-\ 2\ (Sc_A)^{-2/3}\ Ln\ \dfrac{p-p_{A_b}/2}{p}$	$Sc_A^{-2/3}\ Ln\ \dfrac{p}{p-p_{A_b}}$; for $p_{A_w}=0$ $Sc_B^{-2/3}\ Ln\ \dfrac{p}{p-p_{B_b}}$; for $p_{B_w}=0$

on heat transfer at the wall is potentially significant. To illustrate the calculations for this system, Wynkoop and Wilhelm's[13] kinetic measurements on a packed-bed reactor containing particles of porous catalyst will be employed. The rate of reaction for this system, expressed as pound moles of hydrogen reacting/(atm) (hr.) (cu. ft. of porous catalyst) is

$$r'_{H2} = 13.1 \times 10^5\ [e^{-13,220(1.8)/RT}]\ p_{H2} \qquad (21)$$

$$k' = 13.1 \times 10^5\ e^{-13,220(1.8)/RT} \qquad (22)$$

Suppose that this catalyst is applied to the interior surface of a tube through which mixtures of hydrogen and ethlene are passed. To determine the rate constant, k_f, based upon a unit area of tube wall, the thickness of the porous catalyst deposit must be known. If this quantity is designated as ϵ,

$$k_f = k'\epsilon \qquad (23)$$

Whynkoop and Wilhelm found that internal thermal and diffusion resistances in the pores of the catalyst were zero. The same situation will be supposed here. This amounts to assuming an effectiveness factor of unity for the porous catalyst, or that all the catalyst area is at the same temperature and partial pressures as the surface area. For relatively thin catalyst thicknesses this is a valid assumption.

Since the hydrogenation reaction is essentially irreversible, Equation (8) becomes

$$r_{H_2} = (k'\epsilon)\ p_{H_{2_w}} = k_{H_2}\ (p_{H_{2_b}} - p_{H_{2_w}}) \qquad (24)$$

It is not possible to obtain an explicit expression for F^* for this system, in general. However, for a set of operating conditions,

TABLE 1 (Cont'd)

System → / ↓ Conditions	$A \rightleftharpoons R + S$	
Reversible reaction		
Reversible reaction; Reaction controlling	$25\ Re^{0.25}\ \frac{k_f\ \overline{M}}{G}\left[p_{A_b} - \frac{p_{R_b}\ p_{S_b}}{K_e}\right]$	
Reversible reaction; Diffusion controlling		
Irreversible reaction		
Irreversible reaction; Reaction controlling	$25\ Re^{0.25}\ \frac{k_f\ \overline{M}\ p_{A_b}}{G}$	
Irreversible reaction; Diffusion controlling	$Sc_A^{-2/3}\ Ln\ \frac{p + p_{A_b}}{p}$; for $p_{A_w} = 0$ $Sc_B^{-2/3}\ Ln\ \frac{p + p_{B_b}}{p}$; for $p_{B_w} = 0$	

including the flow rate, bulk composition and temperatures, pressure, and wall temperature, $p_{H_{2_w}}$ can be obtained by trial from Equations (24) and (9-11). Then the rate of reaction and F^* follow immediately from Equations (24) and (7). To illustrate the results computions have been carried out for the following fixed conditions:

1. Tube diameter = 3″
2. Catalyst thickness, ϵ = 1/16″
3. Pressure, p = 1 atm.
4. Conversion of hydrogen = 50%, with an inlet mixture of 40 mole % hydrogen and 60 mole % ethylene. Under these conditions

$$(p_{H_2})_b = 0.25 \text{ atm}$$

$$(p_{C_2H_4})_b = 0.50 \text{ atm}$$

$$(p_{C_2H_6})_b = 0.25 \text{ atm}$$

Figure 1 shows the variation of F^* with the reaction temperature at the wall and the flow rate, for a bulk gas temperature of 120°F. Explicit expressions are available for F^* for the special cases of diffusion and reaction controlling, as shown in the next to the last column of Table 1. As $p_{H_{2_w}}$ approaches $p_{H_{2_b}}$, the reaction controlling case is approximated. The lower, horizontal line drawn dotted in Figure 1 corresponds to $p_{H_{2_w}} = 0.98\ p_{H_{2_b}}$. Thus the use of the reaction controlling equation from Table 1 will yield an error in F^* of less than 2% in the region below the lower, horizontal line in Figure 1. The diffusion-controlling case gives an upper limit to F^* as shown by the upper line in Figure 1. From Equation (6) it is seen that this also corresponds to the maximum values of $(h_T - h_c)/h_c$.

To provide direct information on the effect of reaction on the heat transfer rate, h_T/h_c has been computed for the conditions of Figure 1, except the wall temperature is fixed at 250°F. and the bulk temperature is a variable. The results are shown in Figure 2. Since the hydrogenation of ethylene is exothermic, the reaction contribution to the heat transfer rate will always be in the direction away from the fluid and through the tube wall. When the bulk temperature is greater than t_w, the inert, or conventional heat transfer will be in the same direction. For this situation h_T is greater than h_c, as indicated in Figure 2 by the curves for bulk temperatures greater than 250°F. It is evident that reaction can increase the heat transfer coefficient by over ten-fold at the lower mass velocities. In general, the effect of reaction is less at higher mass velocities and higher gas temperatures (larger $t_b - t_w$ values), and approaches the limit of $h_T/h_c = 1.0$. Although not shown in Figure 2, F^* and hence h_T/h_c, is smaller the lower the wall temperature (see Figure 1) and the lower the value of k_f.

For bulk gas temperatures less than t_w, the reaction and conventional heat transfer rates are in opposite directions. Taking the direction of q_c as positive, this situation results in the curves on Figure 2 in the region where t_b is less than 250°F. Here q_w/q_c is negative.

As already mentioned, any factors which decrease the rate of reaction at the wall result in a decrease in F^*, and a decreased effect on the total heat transfer rate. Hence, a smaller amount of porous catalyst on the wall (lower value of ϵ), or a less effective catalyst, will decrease the significance of the reaction

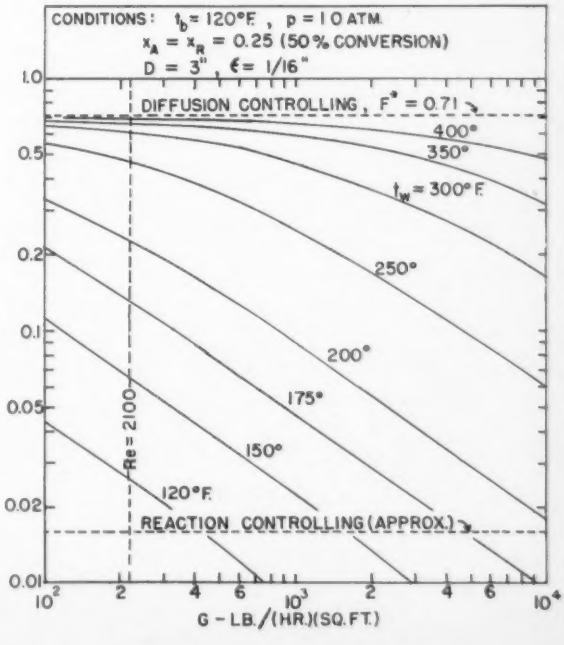

Figure 1—F^* vs mass velocity.

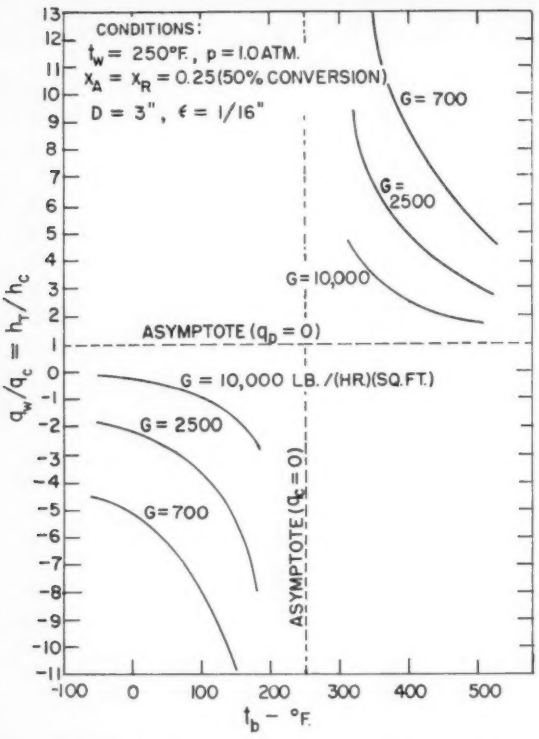

Figure 2—q_w/q_c vs bulk temperature, t_b − °F.

contribution to the heat transfer. For the same reason, the importance of reaction is less the higher the conversion of the reacting gas mixture. For example, q_w/q_c will decrease along the length of the tube as the reactants are converted to products and the rate of reaction becomes progressively less. The magnitude of these effects can be ascertained by solving Equations (6-11) for any particular case.

Heat transfer rates from gases are relatively low. To the conventional methods of increasing this rate, such as filling the tube with solid packing units, should be added the possibility of a wall-catalyzed reaction. The increase in heat transfer can be regulated by the amount of catalyst added to the wall. The pressure drop would not be affected significantly by this procedure. However, other problems such as catalyst poisoning and regeneration may be introduced.

Acknowledgement

This project was carried out with the financial assistance of a Rayonier Incorporated Fellowship.

Nomenclature

A,B,R,S,I = Chemical species involved in a reaction (I is an inert component)
$\overline{C}_p$ = mean specific heat, B.t.u./lb. °F.
D_{AB} = diffusivity of A in a binary mixture of A and B, ft.²/hr.
D_{AM} = diffusivity of A in a multicomponent mixture, ft.₂/hr.
D = diameter of tube, ft.
F^* = transport parameter defined by Equation (7), dimensionless
G = mass velocity, lbs./(hr. ft.²)
h_c = conventional heat transfer coefficient, B.t.u./(hr. sq. ft. °F.)
h_T = total heat transfer coefficient in a reacting system, B.t.u./(hr. sq. ft. °F.)
ΔH_w = heat of reaction evaluated at the wall temperature, B.t.u./lb. mole
H^* = enthalpy ratio defined by Equation (4), dimensionless
k = thermal conductivity of reaction mixture, B.t.u./(hr. ft. °F.)
k_f = specific reaction rate in the forward direction; k' is based upon a unit volume of catalyst material, k_f upon a unit area.
k_A = mass transfer coefficient of component A, lb. mole/(hr. sq. ft. atm.);
K_e = chemical equilibrium constant
$\overline{M}$ = mean molecular weight of reaction mixture
p_A = partial pressure of component A, atm.
p_{f-A} = film pressure factor for component A, atm.
p = total pressure, atm.
Pr = Prandtl number, $\overline{C}_p\mu/k$ dimensionless
q_c = conventional, or inert, heat transfer rate due to a temperature difference, B.t.u /(hr. sq. ft.)
q_D = heat transfer rate due to diffusion and reaction, B.t.u./(hr. sq. ft.)
q_w = total heat transfer rate at the wall, B.t.u./(hr. sq. ft.)
r_A = rate of diffusion or reaction of reactant A, lb. mole per hour per sq. ft. of tube wall area; r'_A is based upon a unit volume of catalyst material
Re = Reynolds' number, DG/μ dimensionless
Sc = Schmidt number, $\mu/\rho D$; $Sc_A = \mu/\rho D_{AM}$, dimensionless
t = temperature °F.
T = temperature, °R
y = distance measured perpendicularly from tube wall, ft.
ϵ = thickness of porous catalyst on the tube wall, ft.
μ = viscosity of reaction mixture, lb./hr. ft.
ρ = density of reaction mixture, lb./ft.³

Subscripts

b = bulk mean conditions in the reaction mixture
w = wall conditions

References

(1) Schotte, W., Ind. and Eng. Chem., **50,** 683 (1958).

(2) Irving, J. P. and Smith, J. M., "Heat Transfer in a Chemically Reacting System". To be published in A.I.Ch.E. Journal.

(3) Acrivos, A. and Chambre, P., Ind. and Eng. Chem. **49,** 1025 (1957).

(4) Fay, J. A. and Riddell, F. R., J. of Aeronaut. Sciences **25,** 73 (1958).

(5) Goulard, R., Jet Propulsion, **28,** 737 (1958).

(6) Lees, L., Jet Propulsion, **26,** 259 (1956).

(7) Rosner, D. E., Princeton Univ. Aeronaut. Engineering Report No. 419, March, 1958.

(8) Rossberg, M. and Wicke, E., Chem.-Ing.-Tech. **28,** 181 (1956) (R.A.E. Library Translation 603, October 1956).

(9) Altman, D. and Wise, H., Jet Propulsion **26,** 256 (1956).

(10) Bird, R. B., Steward, W. E., and Lightfoot, E. N., "Notes on Transport Phenomena", John Wiley and Sons, New York, 1958.

(11) Wilke, C. R., Chem. Eng. Prog., **46,** 95 (1950).

(12) Hougen, O. A. and Watson, K. M., "Chemical Process Principles, Part 3, Kinetics", John Wiley and Sons, New York, 1955.

(13) Wynkoop, R. and Wilhelm, R. H., Chem. Eng. Prog., **46,** 300 (1950).

★ ★ ★

Fundamental Aspects of Solids-Gas Flow

Part V: The Effects of Fluid Turbulence on the Particle Drag Coefficient[1]

L. B. TOROBIN[2] and W. H. GAUVIN[2]

This article presents an analysis of the experimental evidence presently available on the effects of the free-stream turbulence on particulate momentum transfer, obtained from both wind-tunnel tests with stationary bodies and from single-particle systems in which the solid is moving freely with the stream. Original experimental measurements recently obtained with a radio-tracer technique are also included. The drag coefficient appears to depend primarily on the magnitude of the relative turbulence intensity and on the particle Reynolds Number, while acceleration has negligible effects. Increasing intensities cause a systematic regression of the transition region of the drag coefficient curve towards lower Reynolds Numbers, together with a moderate increase of the drag coefficients for both the subcritical and supercritical Reynolds Numbers. The momentum transfer behavior suggests the occurrence of a laminar-turbulent transition in the attached boundary layer at a critical value of the Reynolds Number for a given relative intensity. Indirect evidence involving heat and mass transfer phenomena appears to support this hypothesis.

Parts I to IV[1,2,3,4] of this series have dealt with the dynamics of single particles in fluids which were free from turbulent motion. In Part I, it was shown that the turbulence intensity in a particle-free duct would vary from about 3% in the core to about 60% at the wall. The presence in the system of particles whose Reynolds Numbers are sufficiently high for them to have turbulent wakes would be expected to augment the general intensity level, acting like a three-dimensional grid. Also, the boundary layer and wake structure of an entrained particle can be subjected to very high relative turbulence intensities even if the free stream level is a moderate one. Consider a particle moving at 90 ft./sec. cocurrently with a stream which has a velocity of 100 ft./sec. and an intensity of turbulence of 5%. Assuming that its inertia is such that it does not have a fluctuating motion, the boundary layer and wake of the particle will be generated by a relative movement of 10 ft./sec., and the relative disturbance to this flow will amount to an intensity of 50%. In fact because of the large amount of kinetic energy associated with this fluctuating component, compared with the kinetic energy of the mean relative motion, it would no longer be proper to consider the former as being merely a disturbance which is superimposed on the latter. These remarks underline the necessity of considering the effect of large turbulence intensities on the momentum transfer coefficients, if they are to be applied to cocurrent multiparticle systems.

[1]*Manuscript received June 20; accepted September 26, 1960.*
[2]*McGill University and Pulp and Paper Research Institute of Canada.*

The discussion which follows deals at first with drag data obtained with single stationary bodies in wind-tunnel trials, and then with single particle systems in which the solid is moving freely with the stream. This will be followed by a theoretical and experimental elaboration of the effects of free-stream turbulence on boundary layer transition phenomena.

IX—THE EFFECT OF FREE STREAM TURBULENCE ON MOMENTUM TRANSFER

The early wind-tunnel measurements on aeroplane models were plagued with a lack of reproducibility between studies carried out in different testing establishments. Furthermore, the tunnels often failed to predict the actual behavior of a body in free flight. It was gradually realized that in addition to the effects of the wall and support mechanisms, the fluid turbulence could exert a profound influence on the ambient flow structure. At the time, there were no quantitative methods of measuring the fluid turbulence, and the criterion for good tunnel design was the extent to which contractions and damping screens would damp out the large and small scale velocity fluctuations. Accumulating evidence showed that there were very large discrepancies in the drag coefficient of spheres in the region of the upper critical Reynolds Number[5,6,7,8,9] and that increasing turbulence levels were associated in some way with decreasing critical Reynolds Numbers. Typical results given by Hoerner[10] are shown in Figure 1 for flows having different turbulence levels. Although these results are not directly quantitatively applicable since the turbulence parameters were not evaluated, several qualitative features are noteworthy. In general, the curves retreat with increasing turbulence levels, while the supercritical drag increases with increasing turbulence and therefore with decreasing critical Reynolds Numbers. The critical Reynolds Number, Re_c, is *by convention* the point at which the characteristic steeply-sloped curve intersects the C_D value of 0.3. Oddly enough the curves are not all parallel or even similar in shape and slope. This may reflect differences in the scales, spectra and degree of isotropy of the turbulence at the position of the test bodies, while in addition the surface characteristics of the sphere may be expected to exert a considerable influence on the phenomenon. It may very well be that the transition process is not well fixed and that there is some randomness associated with the phenomenon which would make reproduction possible on an average basis only. It should also be noted that the very low minimum drag values do not appear in an orderly manner, i.e., they do not decrease steadily with increasing Re_c values. Minimum values below those shown in Figure 1 have been reported[11] and an extremely low C_D of 0.05 has been measured by Wiselius[12].

The transition curves in some ways resemble the family of curves obtained for transition with increasing relative roughness (shown in Part IV, Figure 4). Although both processes can

cause premature transition, nevertheless, they cannot be considered identical. Body roughness may trigger a transition in the boundary layer by introducing some small-scale vorticity in the region of the solid surface, and this eventually contaminates the entire boundary layer flow. The wake structure would also react in some manner since the percentage of random vorticity it receives from the separation would be increased. In the case of free-stream vorticity, on the other hand, the boundary layer is attacked from without, and the wake, in addition to its reaction to the increased vorticity from the separated boundary layer, is similarly attacked by the free-stream.

The development of hot wire anemometry initiated some systematic studies of the influence of turbulence on the critical values. The most systematic stationary wind-tunnel investigation of the effects of the intensity and scale of turbulence on Re_c has been performed by Dryden and co-workers[13,14,15,16]. The results are plotted in Figure 2 as a function of the longitudinal intensity, and they show a regular decrease of Re_c with increasing turbulence levels. Even closer grouping of the results was obtained when they were plotted as a function of $(\sqrt{\overline{u'^2}}/U_v)\ (d/L)^{1/5}$, where d is the particle diameter, and L is the Eulerian scale of turbulence in the y direction. The significance of this parameter will be amplified in the section dealing with boundary layer stability. The results are complicated in that Re_c was determined not from direct drag coefficient determinations, but from measurements of the pressure coefficient C_p defined as:

$$C_p = 2(P_1 - P_2)/\rho U_r^2 \quad \ldots\ldots\ldots\ldots\ldots\ldots (1)$$

where U_r is the velocity of the fluid relative to the body, P_1 is the fluid pressure taken at the front stagnation point, and P_2 is the pressure taken through a hole at the rear sphere surface. In the critical region, curves of C_p versus Re bear some resemblance to the C_D curves and Platt[17] found that a C_p value of 1.22 approximated a C_D of 0.3. The method, while being far easier to use than the actual determination of the net force on the sphere surface, suffers somewhat in that the positioning and number of holes used to obtain P_2 is arbitrary, and this will result in different curve characteristics, as shown in Figure 3. Furthermore, Dryden cautions that "the relations between the values of the critical Reynolds Number as determined by pressure measurements with different locations of the pressure openings are only approximate, and sufficient work has not been done to determine the influence of turbulence, sphere diameter, and exact location of the rear holes".

Although this work was concluded in 1937, there does not seem to have been any further investigation of these complicating factors. A direct approach to the problem would be very difficult, since it would call for a point-by-point survey of the base pressure of the sphere as a function of the free stream turbulence. Nevertheless, there are indications that these factors are important. For example, Roshko[18], working with cylinders, found a marked influence on the pressure profile when the interplay of the wake vortices was interrupted by the insertion of splitter plates. Dryden's investigations did not extend to turbulence levels in excess of 4.5%, since increased values could only be obtained by coming very close to the turbulence generating grids and in this region the fluctuations would not be completely random. The inability to extend the turbulence is regrettable, particularly since Figure 2 does not suggest an asymptotic behavior, and in fact the extrapolation of the Re_c curve intersects the zero Reynolds Number intercept at a value of approximately 13% (an asymptotic behavior would, of course, be expected to occur at some finite Reynolds Number since Re_c is arbitrarily linked to a constant drag coefficient value). The effect of higher turbulence levels on the sphere transition has not been investigated in stationary wind-tunnel tests because of the inability to create the required intensities and still preserve a random energy spectrum.

A graphic insight into what would occur at higher levels of free stream vorticity has been provided by Ahlborn[19] who qualitatively studied the effects of large disturbances on the boundary layer and wake of a fixed cylinder by making use of the commonly employed particle tracer photography technique. Figure 4 shows the flow around a cylinder with a laminar incident stream. Relating the wake dimensions to the results obtained by Taneda[20], the Reynolds Number for the flow about the cylinder would be of the order of 30. Figure 5 shows the flow for the same system at the same velocity but with a strip grid placed upstream to introduce what is obviously an

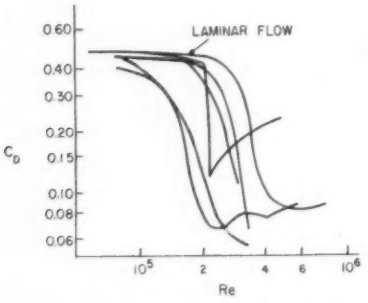

Figure 1—Typical drag coefficients of spheres obtained in the upper critical Reynolds Number region in flows having different turbulence levels (Hoerner).

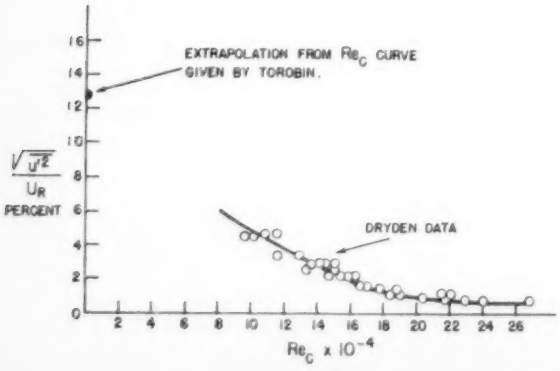

Figure 2—Re_c as a function of the intensity $\sqrt{\overline{u'^2}}/U_r$ (Dryden).

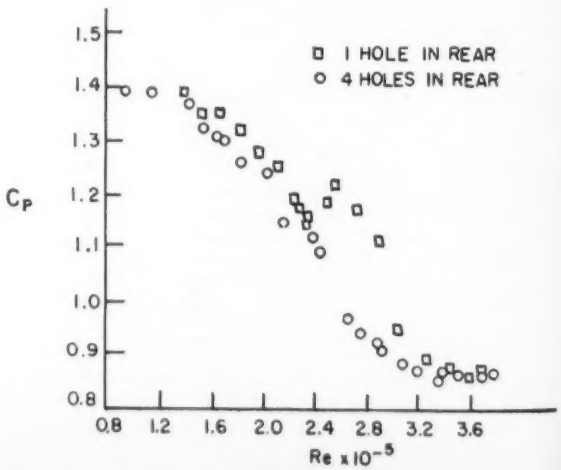

Figure 3—Variation of C_p results with location of pressure taps (Dryden)

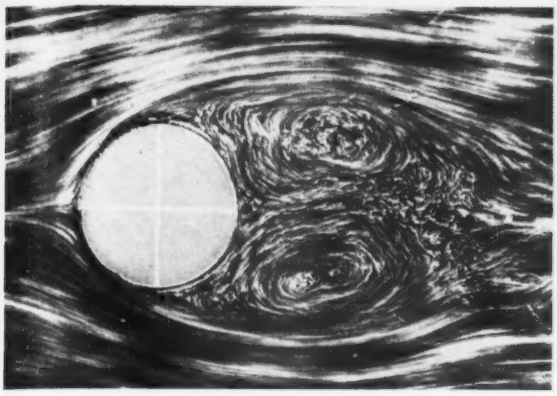

Figure 4—Cylinder flow with laminar incident stream.

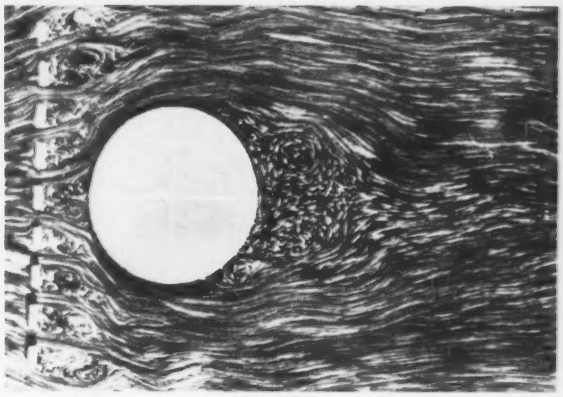

Figure 5—Cylinder flow with free-stream vorticity.

intense free stream vorticity. The result is startling. The boundary layer separation point has been shifted far downstream and it has the separation characteristics of a turbulent boundary layer, i.e., the turbulent flow can make a deeper penetration into the downstream adverse pressure gradient. Even more dramatic is the stunting action of the vorticity on the cylinder wake. It would seem to be even smaller than the wake characteristic of the super-critical region and only faint suggestions of the two standing vortices can be seen. It is obvious from the photograph that the flow fluctuations are definitely periodic and the energy transfer or interaction with a random field of equal intensity would be different. However, similar results can be expected to occur with a turbulent field of the proper severity.

Pressure distributions have been taken over the surface of cylinders placed in turbulent flows in the course of experiments which were primarily concerned with heat transfer considerations. The results of Geidt[21] and van der Hegge Zijnen[22] both show that in the subcritical region, increases of the turbulence level will cause a moderate increase in the form drag component of the drag coefficient, confirming some of the tendencies noted by extrapolation of the critical Reynolds Number experiments. It is interesting to note that the levels used in these experiments fall below the value required for transition as indicated by the extension of Dryden's data.

Schiller and Linke[23] have provided a possible explanation for the increased subcritical drag in experiments conducted on the sensitive separated boundary layer of a cylinder. By artificially stimulating it with a very fine wire, they caused the laminar-turbulent transition point of the separated layer to shift back towards the separation point, and this in turn caused an increase in the form drag. Free-stream turbulence would be expected to have a similar effect, but in addition, it may also affect the vorticity transfer and dissipation in the wake. Roshko[18] felt that the rate of energy transfer from the Strouhal Number peaks to the rest of the spectrum would be accelerated by frequencies feeding in from the free stream to fill in the spectral density valleys.

Komeda[24] has actually compared the turbulence in the wake of a cylinder placed first in a laminar and then a turbulent stream. In the second case, Komeda generated a scale of turbulence approximately equal to the width of the wake by inserting an appropriate grid, and found that the effect of the free stream turbulence was to increase the turbulence intensity in the wake. This demonstrated that even relatively large scale vorticities will produce changes in the smaller scales, contrary to the intuitive contention sometimes expressed that if a particle's diameter is equal to the turbulence scale, it will behave as if it were in a laminar fluid.

The direct effect of increasing intensities on the wake is available from the studies of Schubauer and Dryden[25] on flat plates set normal to the flow. In this system the separation point is fixed, so that shifts in the separation point which would cause changes in the wake dimensions do not complicate the drag variations as they do in the sphere case. The drag results are shown in Figure 6 to increase linearly with increasing intensities. The same increase would be expected to occur with a sphere, but only up to the level required to trigger the attached layer. Any subsequent increase would be more than cancelled by the characteristic drastic drag reduction.

Just as the flat plate study avoided the complications of the attached boundary layer, the work of Speidel[26] minimized the wake contribution to the drag by using a streamlined profile shape. The disturbance to the flow was not random, but was created by a wire mounted upstream of the shape and set oscillating perpendicular to the flow. By varying the frequency of the oscillation, he could in effect change the incident fluctuating energy, and Speidel then measured the changes that this would produce in the drag force on the body. The fluctuations were characterized by a Strouhal Number here defined as:

$$Sr = 2\pi fl/U, \quad \ldots\ldots\ldots\ldots\ldots\ldots\ldots\ldots (2)$$

where f is the fluctuation frequency and l is the body length in the down-stream direction. At low Sr values, the drag coincided with that calculated by assuming a laminar boundary layer. As the Strouhal Number was increased, the drag gradually increased until it reached the level predicted by the assumption of a

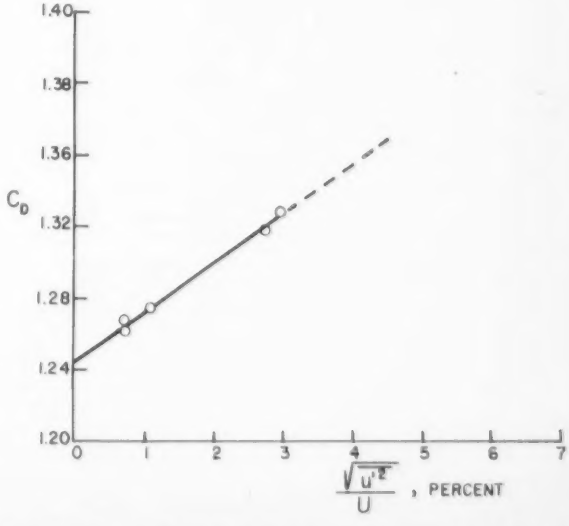

Figure 6—The effect of free-stream turbulence on the drag of normal flat plates (Schubauer and Dryden).

turbulent boundary layer. Very noteworthy was the observed increase in the drag beyond this level at still higher Strouhal Numbers. This showed that in addition to promoting transition, free-stream vorticity acted to change the characteristic properties of the laminar or turbulent boundary layer itself.

It is unfortunate that in all of these experiments no further specification was made of the fluid vorticity. Although this is difficult to measure, it is necessary if the contribution is to yield quantitative results. The turbulence intensity in the upstream direction is only one of the factors, and the degree of homogeneity and isotropy as well as the spectrum characteristics and scales must be established if reproducible information is to be obtained from turbulent momentum transfer studies.

Measurements With Freely Entrained Bodies

In parallel with the early wind-tunnel studies, researches into the drag coefficients of freely moving spheres were subject at first to a wide scattering effect which was eventually traced to departures from laminar motion in the free stream. Lunnon[27] noted that the drag coefficients obtained from tests performed in a mine shaft would be consistently low when very slight and barely perceptible disturbances were present in the air, and he felt that these must have been the cause of similar discrepancies obtained by Shakespear[28]. Oddly enough, the discrepancies were not all negative.

In 1928 Burke and Plummer[29] published a paper in which they argued against the application of momentum transfer coefficients obtained in laminar fluids to turbulent solids-gas systems. They supported their argument with measurements of the loss of weight of various solids in a vertical pipe flow of air. Lead and glass spheres up to 25 mm. in diameter were suspended but not rigidly held in 8 and 16-cm. diameter tubes by fine silk threads attached to a balance. They corrected for the threads by extrapolation and their data fell accurately on logarithmic plots of the loss in weight versus the square of the air velocity. These results, which were obtained at particle Reynolds Numbers all in excess of 500, showed resistances approximately 60% higher than those given by the standard curve. Burke and Plummer consider their curve as well established because of the narrow range traversed, and they urged that this work be extended. Their results may be complicated by the presence of the suspending threads and also by the proximity of the tube wall since this would interfere with the complete development of the wake in the rear of the sphere.

Increases in the drag coefficient averaging about 40% have been noted by Wilhelm and Valentine[30] for spherical particles freely suspended in an upward current of air. Their results covered an approximate Reynolds Number range from 1,500 to 30,000, and in one case a drag value of 0.75 was recorded, in marked contrast with a standard curve value of 0.42. Increased drag coefficients would be expected for this region, since the turbulence was probably not sufficiently high to trigger transition. It was not possible, however, to measure the actual fluid velocity immediately upstream from the particle, so that the actual drag values may be subject to some revision.

Results showing decreased rather than increased drag in the presence of fluid turbulence have been reported by Miller and McInally[31] who found that in an upward current of water, the suspension velocity in a tube would be as much as 47% higher than the terminal settling velocity for particles in the vicinity of $Re = 20$. They do not give the dimensions of their tube, but they note that in all tests the upward suspension velocity for a particle was increased as its location was moved towards the water inlet where the maximum disturbance occurred.

A systematic investigation of the "floating velocity", i.e., the upward fluid velocity required to suspend a single particle, is extremely difficult to perform. Whetton and Broadhurst[32,33,34] attempted some measurement in a vertical 6-in. diameter tube, and they found that the test particles would remain stationary for only a fraction of a second before moving to the pipe wall. Garner and Kendrick[35] found it necessary to construct a carefully designed wind-tunnel to float single droplets for any length of time. Results obtained from the restrained suspension of spheres or from their "floating velocity", even if available on a quantitative basis, could not be directly applied to particles moving cocurrently with the stream. In the former case, the velocity of the fluid with respect to the particle surface would coincide with the fluid velocity relative to the pipe wall, and the particle relative intensity would be restricted to the comparatively low absolute free-stream intensity. In addition, it would be almost impossible to obtain conditions in which the fluid would be turbulent, and yet have the particle Reynolds Number in the Stokes Law region.

Workers dealing with multiparticle solids-gas flow systems have at times been unaware of the possible turbulence effect on the momentum transfer from the gas phase, and some have been surprised to find that the drag curve could not correlate their results. Others, like Pinkus[36], have pointed out that the extension of streamline flow characteristics to turbulent flow would have doubtful validity since the latter implies the destruction of the parallel shearing forces occurring in the Stokes solution. On the other hand, Dalla Valle[37] instinctively assumed that in a turbulent fluid the drag coefficient had a constant value of 0.44 for all particle Reynolds Numbers from zero up to the upper critical region. This feeling may be prompted by the confusion of the so-called "turbulent region" of the standard drag curve, with the presence of turbulence in the fluid. Whether or not a particle will exhibit Stokesian behavior at very low Reynolds Numbers will depend on its size relative to the dimension of the small domains of viscous motion in the turbulent field. This will be discussed in greater detail in a subsequent article.

Consideration will now be given to drag coefficients measured with particles moving in a turbulent fluid. Published drag coefficients for cocurrent flow must be treated with caution. They are complicated by variables - to be discussed in the subsequent section on multiparticle flow - which can at times obscure even qualitative interpretation. The crux of the difficulty is that for proper measurement, the particle velocity, the drag forces and the fluid turbulence must be accurately defined. These quantities are often obtained from indirect measurements and are inaccurate. In addition, the results are expressed in many cases as graphical functions of parameters, such as the air velocity and tube diameter, which are not fundamental but are specific to the particular experimental system involved. Two significant works by Fledderman and Hanson[38,39] and by Ingebo[40] have been referred to in Part III of this series[3] and only a brief recapitulation of the findings will be made here.

Fledderman and Hanson used a photographic method to observe droplets cocurrently entrained in an air stream, and they found that the drag values were very much less than those given for particles in a laminar fluid. The results are reported in the form of a family of curves of C_D versus Re for Reynolds Numbers of 20 to 100. The shape of liquid droplets depends on the Weber Number or the viscosity group, but small droplets may be considered as spheres at Reynolds Numbers less than 300. The absolute air velocity varied from 50 to 70 ft./sec. and was used as the third variable. The curves are hyperbolic, and give C_D values of approximately 0.03, 0.02 and 0.01 at $Re = 80$ for air velocities of 70, 60 and 50 ft./sec. respectively, representing a decrease from the standard values of approximately a thousand percent. The air velocity effect at constant Reynolds Numbers may reflect changes in the relative intensities.

Ingebo[40] investigated a similar system using both solid and liquid spheres, and he confirmed that in the low Reynolds Number region there were no differences in the aerodynamic behavior of solids and liquid droplets, even when the latter were evaporating. A second very important finding, from the point of view of multiparticle behavior, is that a tenfold increase in the particle concentration produced no noticeable alteration on the single particle drag, so the drag coefficients obtained with single particle systems can presumably be applied to the multi-

particle case. Although Ingebo attributed his decreased drag values to the effects of acceleration, other acceleration findings suggest that they may be due to the ambient fluid turbulence. Ingebo's original drag data (rather than those recalculated by Mercier as discussed in Part III), as well as the others discussed in this section have been graphically compiled for the sake of comparison in the form of the single plot shown in Figure 7.

Foeking[41] in an investigation of solids-gas flow in horizontal and vertical tubes of ½, 1 and 2-in. diameter calculated drag coefficients values which appeared to vary with the particle Reynolds Number, the pipe diameter, and also the air velocity. His results for horizontal flow are as low as 0.09 at $Re = 5$; they then go through a maximum of approximately 1 at $Re = 100$ and finally drop to minimums of $C_D = 0.03$ in the post-wake shedding region. The values of C_D obtained from vertical flow trials increased steadily with the Reynolds Number from lows of approximately 0.06 at $Re = 4$ to highs in the vicinity of 5 at $Re = 1{,}000$. Separate curves are given for each air velocity and pipe diameter employed.

A more extensive discussion of the work of Foeking and others dealing with cocurrent solids-gas flow in ducts will be given with relation to the overall momentum transfer considerations in a later section. However, the general method used to derive the drag coefficients in these cases should be explained here. The practice is to determine an average force per particle from the overall pressure drop due to the solids movement and the number of particles contained in the system. The velocity term in the drag equation is obtained by subtracting the average measured particle velocity from the mean fluid velocity. The studies have been confined to systems in which the particles are identical, thus avoiding averaging of their physical properties. Some major weaknesses of this method are immediately apparent: since both the fluid and solids have velocities which vary with the cross-section of the duct, the difference of the local velocities should be measured, and the mean of the squares of these values should be used, rather than the square of the mean values which they actually employed. In addition, since the drag coefficient is a function of the relative velocity at the particle, there will be a wide range of drag coefficients acting in the system at the same time. In spite of these serious oversimplifications, the results can still be useful in indicating the order of magnitude of the drag coefficients calculated by this method.

Mehta[42] calculated values of C_D for 0.097-mm. glass spheres entrained in horizontal and vertical flows of air in a steel pipe. These show the drag coefficient to decrease from a value of 30 at $Re = 4$ to a value of 0.025 at $Re = 300$. On the other hand, his data for 0.036 mm. spheres, which were too disordered for correlation, showed a general tendency for C_D to increase with increasing Re in approximately the same range, but the area of the vertical results is in the lower drag region although it occurs at a higher Reynolds Number. Mehta also calculated some C_D values from Hinkle's investigations[43]. These are very scattered, but again there seems to be a general tendency for the drag coefficient to increase with the Reynolds Number. Typical values go from $C_D = 0.36$ at $Re = 102$, to $C_D = 1.19$ at $Re = 10{,}200$.

Khudiakow[44,45] obtained the velocity of motion of particles in a vertical gaseous stream flowing downwards through the use of high speed cinematography at shutter speeds of up to 4,000 frames per second. The tube was 150 cm. in length and had a diameter of 3.2 cm. Photographs indicated that particles entering the stream at the top of the tube would invariably be "pressed out" towards the periphery of the stream and would then move down the column in the immediate vicinity of the wall. Khudiakow attributed this mainly to the non-uniform velocity distribution over the cross-section of the tube. The results, which show considerable variation, were presented as C_D-versus-Re plots and they have been reproduced in Figure 8. An interesting characteristic is apparent in that the points form erratic curves for each particle for individual air velocities. For example, a 845-micron particle in an air stream of 20 metres per second gave C_D values varying continuously from 1.3 at $Re = 180$ down to a minimum of 0.2 at $Re = 270$ and back up to 1.4 at $Re = 390$. A 70-micron particle at the same air velocity followed a continual increase from $C_D = 0.4$ at $Re = 10$ to a value of 2.2 at $Re = 45$. Khudiakow attempted to draw an average overall curve through his data and found that it was

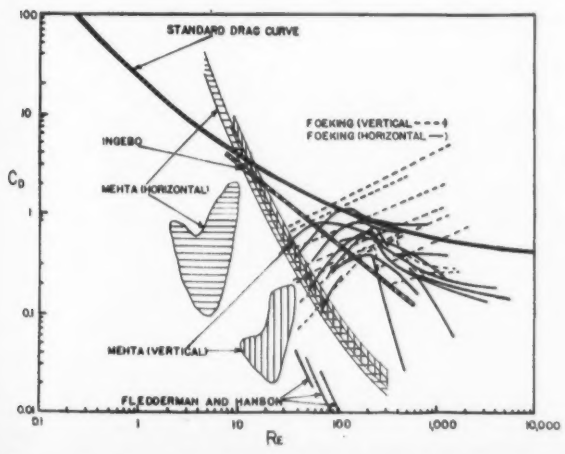

Figure 7—Accumulated drag data obtained in cocurrent solids-gas systems.

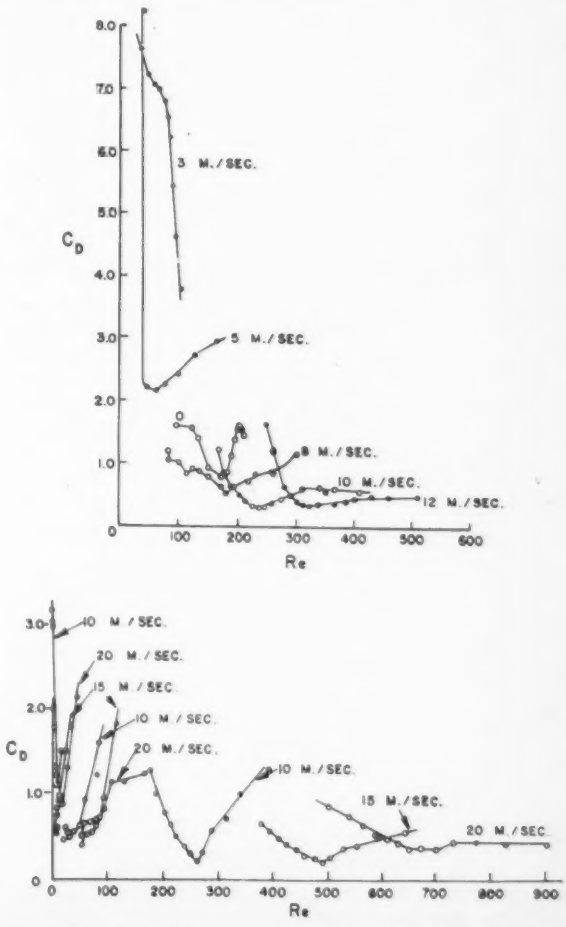

Figure 8—Drag data obtained by Khudiakow.

given by $C_D = 1.4\ Re^{-0.18}$. This averaging does not appear to be justified because many values would deviate from the curve by as much as 4,000%, and the standard deviation is too high. It also fails to account for the continuous curves obtained with each particle at a given air speed. Nowhere in his column did the solids attain an equilibrium velocity, and his data may have been complicated by acceleration phenomena if they were operative. The condition of the fluid in the test section would be expected to be unstable, since according to the sketch of his apparatus it was located immediately after a sharp ninety-degree bend. This instability may account for the strong pulsations of the particles which were recorded at high air velocities. Khudiakow also noted that large electrostatic forces were generated in some of the trials and this complication, as well as the collisions of the particles with the tube wall would invalidate a force balance based on the gravitational attraction alone.

Chernov[46] has cast further doubt on Khudiakow's results by challenging his method of calculating the particle velocities and acceleration from the time-distance data on the basis of the very large amplification of error which accompanies the process of double differentiation.

Lewis, Gilliland and Bauer[47] investigated the flow of glass spheres in a vertical air stream in a 1.25-in. i.d. brass pipe at different solids concentrations. They extrapolated their results back to zero solids concentration, and they found that the relative velocity of the solids to the fluid (referred to as the *slip velocity*) did not correspond to the free-fall velocities indicated by the standard curve. A logarithmic plot of the ratio of the slip velocity to the free-fall velocity as the ordinate against the particle diameter as the abscissa resulted in a smooth curve with the ratio equal to 10 at a particle diameter of 0.001 inch. It decreased to a much lower value of 0.7 at a particle diameter of 0.05 inch. This offers a rough indication that the flow disturbances in some cases increased and in others decreased the drag coefficients.

A study of the effects of turbulence on the drag coefficients of spheres moving in both steady and accelerated motion has recently been completed by the authors[48]. The experiments were conducted in a specially designed 8-in. diameter upward cocurrent turbulent flow wind-tunnel incorporating a vertical 20-ft. particle or ballistics range. Single aerodynamically-smooth spheres of different densities and diameters were injected into the central core of the flow by means of a particle accelerator located at the tunnel entrance which enabled complete control of the particle entrance velocity. The firings were accomplished in a manner which did not impart any initial rotation to the particle, while no significant contribution was made to the momentum of the moving fluid. A hot-wire anemometer facility was incorporated into the tunnel design and the intensities, scales and energy spectra were measured throughout the test section. A novel arrangement of orifice grids in series was employed to create a flow with a flat central mean velocity profile and a truly random energy spectrum for the entire particle trajectory. Although the actual intensities of the flow were low, very high relative intensities could be attained because of the cocurrent effect. In order to obtain the accuracy needed for the drag determination, a radioactive tracer technique, which was sensitive to intervals of 10^{-3} second, was developed with the collaboration of I.S. Pasternak and L. Yaffe[49]. This allowed a continuous record to be made of the particle flight, as compared with the single velocity determinations used by previous investigators, and the time-distance data were processed by a special I.B.M. 650 program. The results are summarized in Figure 9, as a function of the relative turbulence intensity $\sqrt{\overline{u'^2}}/U_r$ and the curves bear a strong resemblance to the transition curves obtained in the wind-tunnel tests at lower intensities. At the low intensities, the results coincide with those obtained in laminar fluids, whereas moderate intensities cause a relatively small increase in the drag values. At sufficiently high disturbances there is a characteristic sharp drop in the momentum transfer, and then a gradual increase to values which lie below the standard curve.

Conspicuous by its absence is any effect due to acceleration. Results with particles having varying degrees of negative or positive accelerations agreed very closely, and there was no association of the results with the time elapsed from the introduction of the particle into the flow. This seems to correspond with the acceleration data presented in Part III where the acceleration effect was shown to diminish with increased turbulence in the particle wake. The lack of a time dependency is supported by the theoretical boundary layer solutions, which indicate that such dependency should be limited to a few particle diameters at the most.

The particle Reynolds Numbers corresponding to a drag coefficient of 0.3, obtained during the characteristic transition stage, were designated as the critical Reynolds Numbers Re_c in accordance with the convention employed by Dryden. The results are shown in Figure 10, and they form a smooth curve, although they were obtained with varying particle diameters, densities and accelerations. Two regions are indicated: at the higher Reynolds Numbers, the curve extrapolates to the results given by Dryden and Re_c decreases rapidly with increasing intensities. When the Reynolds Number falls below 800, there is a sharp upswing in the curve, and large increases in intensity are required to precipitate the characteristic reduction of the drag coefficient. At a Reynolds Number of 400, for example, intensities in excess of 40% are required, and the curve would be asymptotic to the zero Reynolds Number. This second region coincides with the change from the stationary

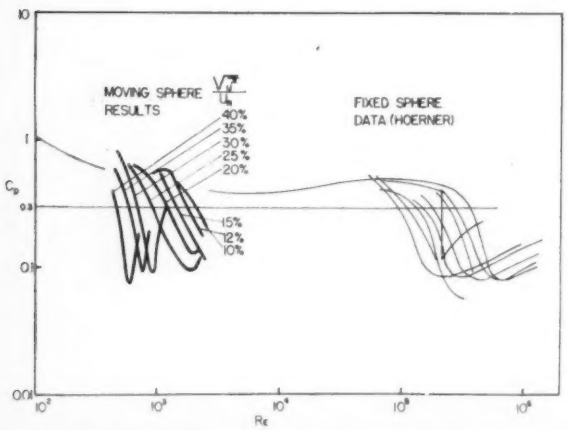

Figure 9—Drag coefficients of single spheres moving in a turbulent field, as a function of the intensity relative to the particle.

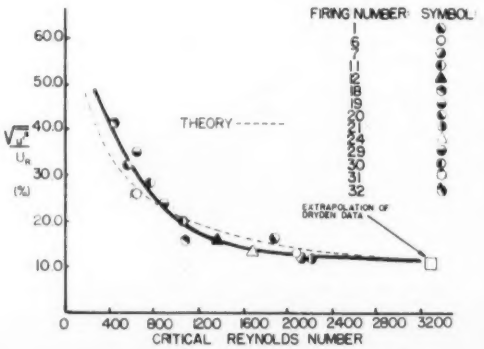

Figure 10—Re_c as a function of the relative intensity $\sqrt{\overline{u'^2}}/U_r$.

to the shedding behaviour of the wake cited in Part II. On the basis of Figure 10, it appears highly unlikely that the steeply sloped transition curves will exist at Reynolds Numbers much below 100, although Ahlborn's photograph (Figure 5) shows that non-random vorticities of a suitable type may cause this to occur as low as $Re = 30$. Very high relative intensities will introduce a new complication, because their action would cause particles of small inertia to have a fluctuating motion of their own. Results obtained with low-density spheres showed that small diameter particles, below Reynolds Numbers of 400, would not reliably follow a truly axial path and the data were not directly useable. At Reynolds Numbers below 1, the system must be dealt with by stochastic methods, and the relative intensity would result from a complex subtraction of the fluid and particle intensities. At very low Reynolds Numbers the skin friction component of the drag would predominate and the relative turbulence effects would probably always cause a drag increase.

Estimation of the drag coefficient to two significant figures for a given situation in the transition region would not be warranted since the phenomenon is not well fixed, and a variation in results does not necessarily reflect an error in observation. Even the use of the standard drag curve for drag estimation to the second figure for bodies moving freely and at steady state in a laminar fluid outside of the Stokesian region is not valid. The most recent measurements taken for these conditions by Barker[50] have shown that there is as much as 30% scattering about the average curve which cannot be attributed to instrumentation errors.

The significance of the rough data presented in Figures 7 and 8 will now be discussed in the light of the direct drag coefficient determinations. In a cocurrent solids-gas system, the relative turbulent intensity will be affected by changes in the relative particle velocity, the absolute fluid velocity and possibly the solids concentration in the stream. In the case of a spray, the system is further complicated in that the fluid intensity would be expected to decrease as the distance of the particle from the nozzle is increased. Owing to the characteristics of the drag coefficient curves as a function of the intensity, systems operating in the region of the critical Reynolds Number curve should be subjected to wide variations in the momentum transfer coefficients. On the other hand, relatively moderate departures from the laminar fluid behavior will occur in the regions away from the critical Reynolds Number curve.

In general, the multiparticle results show a general tendency to be lower than the standard curve and this could be due to the intensity effect noted. Separate curves were given by Focking and Hanson for each air velocity and this would be expected since at a constant particle Reynolds Number, the intensity would vary with the velocity of the fluid. Most of Focking's data fall within the area of the present authors measured drag coefficients, except for some of the results with the vertical system. The latter are too high to be explained as a turbulence effect, and are probably due to the assumptions made in their calculation. Some of Mehta's results are plausible, but the low drag values in the range $1 < Re < 10$ would be difficult to explain, although there is a general upward tendency with decreasing Reynolds Numbers.

Sharp minima have resulted in the intensity curves, but values as low as those given by Fledderman and Hanson have not been observed. There is the possibility however that very low minima have been overlooked, since they occur in a very narrow Reynolds Number range and would require a close grouping of determinations. Data from the fixed sphere experiments have sometimes shown very narrow and sharp depressions which seem to have been overlooked in the adjacent curves.

Khudiakow's results are both above and below the standard curve, but an interpretation of his results is made difficult among other things by his use of the mean air velocity over the duct cross-section, rather than the one occurring at the particle. In a cocurrent system, this can cause very large drag errors since a 20% uncertainty with the fluid velocity can mean errors in excess of 100% in the particle relative velocity, and this error would be doubled in the drag calculation.

Ingebo's data are perhaps the most reliable of the group, and they fall within the area included by the intensity curves. In Ingebo's experimental system, the particle Reynolds Numbers decrease with increasing downstream distance, and the intersection of his results with the intensity curves indicates increasing relative intensities with downstream distance. This would be expected from the decreasing relative velocity as the particle decelerates relative to the stream.

The grouping of the drag coefficient curves for different intensities offers an explanation for the completely divergent tendencies noted by different investigators who in some cases found increasing and in other cases decreasing drags with increasing Reynolds Numbers. Drag coefficients plotted on the basis of the Reynolds Number alone could form curves of almost any slope or shape, depending on the variation of relative intensities with the Reynolds Number specific to the particular system.

The data required to extend the intensity curves below $Re = 400$ could not be obtained in the ballistics wind-tunnel, since the very small high-density spheres which would be required could not be retrieved with the present particle-arresting mechanism. Extension of the data to much above $Re = 3{,}000$ would be of little interest in solids-gas investigations, since the particle Reynolds Numbers seldom exceed this value in most systems. The intensity versus drag curves were obtained with spherical particles whose surfaces appeared smooth under microscopic examination. The results obtained by Ingebo indicated no difference in behavior between smooth and roughened particles, but differences in particle shape will impose differences on the drag coefficient characteristics. A program has been started by Marchildon in these laboratories to assess the effect of particle shape.

Theories Governing Transition to Turbulence

An explanation of the effects of the free-stream turbulence on the momentum transfer from the fluid to the solids phase requires an understanding of the reasons and conditions for instability of laminar flows and its transition to turbulence; conversely, evidence from the momentum transfer investigations can often help to shed light on the perplexing phenomenon of transition. This aid is sorely needed since a satisfactory transition theory has yet to be attained.

Lord Rayleigh[51] was one of the first to search for instability in laminar flows by superimposing an infinitesimal disturbance on the Navier-Stokes equations for steady laminar motion, and then seeing whether the disturbance will grow or be damped out with time. The possibility of an instability developing was shown to be a function of the frequency or wave length of the disturbance. Rayleigh assumed a flat velocity profile and the resulting analysis showed that for this case all flows were stable. Tollmien[52] obtained a solution to the Blasius boundary layer velocity profile for the semi-infinite flat plate, and this was subsequently refined by Schlichting[53] and then Lin[54]. This work led to the development of *neutral stability* curves, which have a disturbance frequency group as the ordinate and a boundary layer Reynolds Number as the abcissa as shown in Figure 11. The frequency group generally employed is the ratio $(2\pi fv/U_\infty)$, where f is the frequency, v is the kinematic viscosity and U_∞ is the free-stream velocity. The characteristic length used in the Reynolds Number is the boundary layer *displacement thickness*, which is a measure of the height of influence of the boundary layer flow. According to the solutions, infinitesimal disturbances falling within the region bounded by the curve will be amplified at their associated Reynolds Numbers, whereas the frequencies falling outside of the bounded region will be damped with time. The lowest Reynolds Number which will give an intersection with the curve would then be a critical

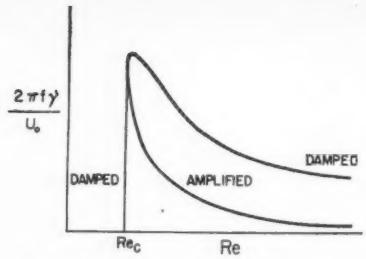

Figure 11—Neutral stability curve.

one, since all disturbances would be ineffectual with a further Reynolds Number reduction. The important inference of this analysis is that developing laminar shear flows have an inherent instability to infinitesimal disturbances of the proper frequency, and these will gain energy from the mean flow and amplify with time. (It is assumed that the laminar fluctuations will eventually break down into turbulent motion, but the mechanism by which this occurs is still in doubt).

Similar stability curves for the sphere boundary layer have been calculated by Pretsch[55]. If the stability curves were applicable to the case of a sphere moving in a turbulent fluid, it would be a relatively simple matter to predict what turbulent frequencies would be expected to affect the momentum transfer, and in addition a minimum Reynolds Number, Re_c, would be obtained, below which laminar behavior could be assumed for any type of free-stream turbulence. The analysis also predicts that the magnitude of the intensity would have no effect on the drag, and the disturbance frequency would be the predominating influence. Unfortunately, the physical model and the mathematical simplifications employed in the solutions invalidate them for such a purpose.

The solutions for the stability curves employed a linearization on the assumption that the disturbance was infinitesimal and that it exerted no influence on the mean motion. Meskyn and Stuart[56], however, have shown that finite disturbances, when incorporated into the solution, decrease the value of Re_c, and the extent of the decrease is proportional to the disturbance amplitude. Stuart[57] also pointed out that the Reynolds stresses due to the disturbance can become sufficiently large to alter the nature of the flow, so that the mean motion would no longer correspond to the original laminar motion.

The oscillations predicted by the Tollmien-Schlichting theory could at first not be detected experimentally. When they were finally discovered by Schubauer and Skramstad[58], it was found that they could only be observed in the pure state in streams having intensities which were less than 0.2%. It has recently been found that increases in the free-stream turbulence from the vanishingly small values necessary to observe them will cause the Tollmien-Schlichting oscillations not to appear as a part of the transition process. A detailed insight into how this comes about has been provided by Bennett and Lee[59]. They subjected the boundary layer on a smooth flat plate to free-stream intensities varying from 0.1 to 0.5 percent, and the energy spectra of the resulting laminar oscillations were monitored continuously. A dramatic sequence of events was noted. As the free-stream turbulence increased, the Tollmien-Schlichting waves became less pure, and the surrounding frequencies began to draw momentum energy away from the laminar oscillation. The feeding rate increased with increasing free-stream intensities, so that progressively smaller energies were concentrated in the amplified frequency predicted by the stability curve. The extrapolation of these trends to intensities above 0.5% showed that eventually the laminar oscillations played no part in the transition process, and Bennett and Lee felt that a different model was required for its description. It was also found that the critical Reynolds Numbers specifying the appearance of the laminar oscillations, the start of transition and the end of transition all decreased and converged with increasing turbulence levels.

There is an interesting analogy between the mode of spectral energy transfer shown by these results and the transfer from the Strouhal Number peaks in the wake of the cylinder described in Part II of this series. The peaks melted into the adjacent frequencies as they moved downstream, resembling the downstream movement of the laminar instability waves. The free-stream turbulence very likely accelerates the absorption of the Strouhal Number peaks as it did in the study of Bennett and Lee, and this in turn would cause the stunted type of vortices shown in Figure 5. It should be stressed at this point that knowledge of the instability-transition process is still in development[68].

The most significant theory dealing with the effects of large free-stream turbulence levels on transition has been given by Taylor[60] and it is based on an entirely different model than the one which produced the neutral stability curves. Because of its importance, and the need to confine its application to situations which are compatible with the assumptions it incorporates, it will now be discussed in some detail. The crux of the Taylor Theory is that instead of the frequency-sensitive laminar oscillations being the causative factor in transition, the latter is instead ascribed to the magnitude of the fluctuating pressure gradients which accompany the velocity fluctuations of the free-stream turbulence. In isotropic turbulence, these pressure gradients are related to the intensity by the equation:

$$[\overline{(\partial p'/\partial x)^2}]^{1/2} = 2(2)^{1/2}\,\rho_o\overline{u'^2}/\lambda \qquad (3)$$

where $(\partial p'/\partial x)$ is the instantaneous pressure fluctuation gradient in the x direction and λ is the "microscale" of turbulence which is obtained from the curvature of the Eulerian correlation curve (Equation (20), Part I) at $x = 0$. In isotropic turbulence, the microscale can more easily be calculated from the Eulerian scale L, using:

$$\lambda/(L)^{1/2} = [B(\nu)/\sqrt{\overline{u'^2}}]^{1/2} \qquad (4)$$

where B is a constant which depends on the system used to generate the turbulence. Now according to the Karman-Pohlhausen boundary layer theory - which incorporates some rather drastic approximations - the velocity distribution in the boundary layer is dictated by the *instantaneous* pressure gradient at the point in question and the boundary layer thickness δ. The latter is characterized by a dimensionless shape factor:

$$\Lambda = (\delta^2/\nu)\,(dU_1/dx) \qquad (5)$$

where U_1 is the velocity at the outer edge of the boundary layer. For steady flows, dU_1/dx can be calculated from the mean pressure gradient dp/dx using:

$$dU_1/dx = -\frac{1}{\rho U_1}\left(\frac{dp}{dx}\right) \qquad (6)$$

Hence:

$$\Lambda = -\frac{\delta^2}{\nu\rho U_1}\left(\frac{dp}{dx}\right) \qquad (7)$$

It has been found that laminar boundary layers will separate when Λ exceeds a critical value, and Taylor suggested that the same might occur if the boundary layer is subjected to sufficiently large fluctuating pressures. In the course of a fluctuation, there would be a corresponding separation and reattachment, and this would supposedly bring about a laminar-turbulent transition. As an approximation, Equation (7) would be modified for a turbulent free-stream to give:

$$\Lambda + \Lambda' = \frac{-\delta^2}{\nu\rho U_1}\left(\frac{d\sqrt{\overline{(p+p')^2}}}{dx}\right) \qquad (8)$$

where Λ' is the addition to the overall shape factor governing the velocity distribution which was introduced by the free-stream turbulence. The problem then remains to relate a critical value of $(\Lambda + \Lambda')$ to the free-stream turbulence, the dimensions of

the sphere, and its Reynolds Number. Combining Equations (3), (4), (7) and (8), Λ' will be given by:

$$\Lambda' = -B(\sqrt{\overline{u'^2}}/U_o)^{5/2}(v/U_o d)^{1/2}(d/L)^{1/2}(U_o/U_1)^2(U_1\delta/v)^2 \ldots (9)$$

In order to proceed, several additional assumptions were now introduced by Taylor. If it is assumed that the drag coefficient is a unique function of the angle α which the separation point makes with the front stagnation point, then α will have a constant value at transition, since C_D, corresponding to Re_c, is fixed by arbitrary convention at 0.3. At high Reynolds Numbers, the boundary layer theory predicts that for steady laminar flow, Λ will be independent of Re, and will be a function of α only. This means that at transition α will be a constant so that U_o/U_1 is a constant, and $U_1\delta/v$ will be a function of the Reynolds Number $U_o d/v$. Now since Re_c is a function of Λ', then Equation (9) leads to the conclusion that Re_c is a function of $[(u'^2)^{1/2}/U_o]\ (d/L)^{1/5}$. If the sphere is in motion, U_o should be replaced by U_r. Dryden replotted his drag results as a function of this Taylor parameter, and with the exception of a few points, the scatter was noticeably reduced. The shape of the curve which resulted is probably general but the ordinate and other constants would have to be shifted to account for changes in the constant B. It has also successfully been applied to the data of Schubauer[61], who studied the effect of turbulence on transition in the boundary layer of an elliptic cylinder. In view of the approximations made in the derivation of the parameter, it cannot be applied to the commonly occurring non-isotropic flows, and its validity at higher turbulence levels and at lower Reynolds Numbers cannot be assumed.

The results obtained by the present authors at lower Reynolds Numbers did not show any particle diameter dependency, although a very wide diameter range would have to be investigated to detect a variation to the 1/5 power. They do, however, confirm that Re_c is strongly dependent on the turbulence intensity. All the results at intensities above 1% have also confirmed that it is the *magnitude* of the turbulence disturbance that is the important causative factor for transition rather than its frequency.

The present authors would like to suggest an alternative transition criterion for high turbulent levels. Before proceeding it may be helpful to cite several characteristics of the system considered. The turbulent flow in a duct is in a state of dynamic equilibrium in which there is a production, diffusion and dissipation of turbulent energies. A spherical particle entering this system may, by virtue of its relative motion and the viscous damping forces which are produced at its surface interface, create an isolated region of quasi-laminar flow in its immediate vicinity, as a laminar boundary layer and wake. Throughout its entire length this fluid system will be subjected to the disturbances from the free-stream turbulence. The nature of the disturbances may be such that they would soon die out if introduced only at a given region of the boundary layer, but since they occur all along the sphere system, their effect will be governed by the extent and depth to which they can penetrate the laminar flow.

A volume element upstream from the sphere which, by definition eventually becomes part of the laminar motion on the sphere, must have all of its turbulent energy damped out by the viscous damping forces in the sphere environment before it enters the laminar flow. The turbulent energy E_T of the incident fluid element will be given in Cartesian tensor notation by:

$$E_T = 1/2\rho \int\int\int dx_1\, dx_2\, dx_3\, \overline{u'_i u'_i} \ldots\ldots\ldots (10)$$

and the depth within the boundary layer to which the volume element will penetrate before losing "all" of its turbulent energy will be a function of E_T. E_T in turn will be a function Φ_1 of $(\rho u'^2_1)$ per unit volume. The distance penetrated will also be a function of the viscous damping forces set up by the velocity gradients at the sphere surface. These viscous damping forces F_V per unit volume may be expected to follow the functional relationship:

$$F_V = \Phi_2 \mu \partial\,(\partial U_1/\partial x_2)/\partial x_2 \ldots\ldots\ldots\ldots (11)$$

$$\simeq \Phi_3 \mu \bar{U}_1/x_1^2 \ldots\ldots\ldots\ldots\ldots\ldots (12)$$

If it is further assumed that the characteristic length over which the damping forces act is a function of the sphere diameter, then the viscous damping energy E_V associated with the damping action will be:

$$E_V = \Phi_4 \mu U_1/d \ldots\ldots\ldots\ldots\ldots\ldots (13)$$

The ratio (E_T/E_V) will therefore specify the extent of penetration of the turbulent energy towards the sphere surface, and it will be given by:

$$\left(\frac{E_T}{E_V}\right) = \Phi_5\left(\frac{\rho\overline{u'^2_1}d}{\mu\bar{U}_1}\right)\left(\frac{\bar{U}_1}{\bar{U}_1}\right) = \Phi_5\,(Re)\left(\frac{\sqrt{\overline{u'^2_1}}}{\bar{U}_1}\right)^2 \ldots\ldots\ldots (14)$$

If a disturbance penetrates to the sphere surface, Lin[62] has shown that viscosity effects acting at the wall will lead to a phase shift between its axial velocity component u'_1 and its normal velocity component u'_2 so that the turbulence shear stress $(-\rho\overline{u'_1 u'_2})$ will have a positive value. Hinze[63] points out that since $(\partial\bar{U}_1/\partial x_2)$ at the wall must be greater than zero, the turbulence production term $-(\partial U_1/\partial x_2)\ (\rho\overline{u'_1 u'_2})$ will be positive, and there will be a generation of turbulence in the boundary layer flow. Hinze feels that this analytic result is supported by the experimental conclusions reached by Lindgren[64] who found that at transition "....turbulence should originate from wall effects acting on disturbed flow in the immediate vicinity of - or in contact with - the boundary walls".

The present authors suggest that at transition, (E_T/E_V) will have reached a critical value $(E_T/E_V)_c$ which will allow sufficient penetration for the production of turbulence in the boundary layer flow. If this is correct, then at transition:

$$(E_T/E_V)_c = \Phi_5\,(Re)_c\,(\sqrt{\overline{u'^2_1}}/\bar{U}_1)^2 \ldots\ldots\ldots\ldots (15)$$

so that (reverting to the original notation)

$$(Re)_c\,(\sqrt{\overline{u'^2}}/U_r)^2 = \text{Constant} \ldots\ldots\ldots\ldots (16)$$

Equation (16) has been superimposed on the experimental results shown in Figure 10, using the value 45 as the experimental value of the constant. In view of the assumptions made, and the expected accuracy of the results, the agreement is surprisingly good. At the low Reynolds Number values, the theoretical curve indicates a lower intensity than was found experimentally. This trend would be expected, since the definition of Re_c used in the plot (i.e., the value at which a transition curve intersects the $C_D = 0.3$ line) does not correspond to the one used in the proposed theory, in that it is not directly linked to the onset of turbulent motion. As the Reynolds Numbers decrease, transition must occur at a higher drag coefficient, particularly where the skin fraction component of the drag becomes significant.

The effects of turbulence levels of up to 3% on boundary layer transition on a flat plate have been studied by numerous workers and some of the results are summarized in Figure 12. There is an obvious decrease in the critical Reynolds Number as the free-stream intensity is increased, but there is also considerable scattering in the data. Oddly enough, Adelberg[65], whose results are the most recent of those shown, has put forth an hypothesis that there will be no further decrease of the critical Reynolds Number if the intensity is increased beyond 3%. He did not substantiate this statement by actual measurements at values above 3%, but based it only on the extrapolation of his results. It is obvious from Figure 12 that this contention is not well founded. Adelberg has by his own admission made no attempt to consult many of the pertinent transition and heat transfer studies which leave no doubt that the transition phenomenon is not insensitive to intensity changes above 3%.

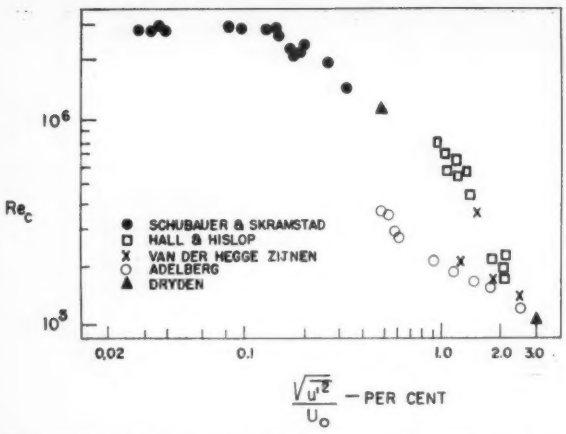

Figure 12—Re_c for a flat plate as a function of the free-stream intensity.

In addition to the Tollmien-Schlichting and Taylor theories for transition, attempts have recently been made to solve the boundary layer equations, replacing $U = U_o$ as the free-stream condition with an arbitrary vorticity. Duffy and Li[66] have shown that for the cylinder even small free-stream vorticity will cause alterations in the pressure field which in turn produce pronounced effects on the boundary layer separation, boundary layer growth and shear stress. The solutions showed that if the free-stream vorticity is characterized by a positive downstream velocity gradient, the separation point is moved downstream, the boundary layer thickness is decreased and the skin friction is increased. If the gradient is negative, the reverse trends will occur. The authors indicate that they expect to extend their work to large free-stream vorticities. In any event, these results show that even when the particles are "small" compared to the characteristic scale length, it may not be valid to consider them as being embedded in a steady laminar flow.

Further discussion of boundary-layer transition phenomena can be found in references 67, 68 and 69.

Additional Experimental Indications

There have been very few momentum transfer investigations at high turbulence levels, but there have been some others, particularly studies involving heat and mass transfer phenomena, which are of direct interest. At the outset, it must be emphasized that there is no direct relationship between heat and mass transfer rates on the one hand and momentum transfer on the other. Nevertheless, the heat or mass transfer observations will reflect changes in the flow system around the test body as affected by the free-stream turbulence levels.

Maisel and Sherwood[70] have studied the effects of large free-stream intensities on the evaporation rate of water from a sphere, for a Reynolds Number range of from 1,000 to 20,000 and for turbulence intensities up to 24%. The high intensities are suspect because they were obtained close to a grid, and the velocity fluctuations may have been periodic. Increasing intensities caused a continual increase in the ratio of the actual mass transfer coefficient to the value of the coefficient at zero turbulence. Instead of the rate of increase decreasing with the higher turbulence levels—as would be the case if Adelberg's contention were correct—it was actually steeper in the region above 15-20%. An extremely interesting tendency can be observed in the data, indicated by an upward break in the curve for the results in the vicinity of $Re = 5{,}000$, which occurs at an intensity of approximately 12%. Up to this level, the mass transfer coefficient ratio had remained approximately constant, and in the region above 15% the rise is a very gradual one. The combination of intensity and Reynolds Number for this break falls on the extension of the critical Reynolds Number curve given by the present authors, and the discontinuity may very well have resulted from a boundary layer transition on the sphere surface. Maisel and Sherwood also measured the scales of their turbulence, and found that their results were unaffected by a twofold variation of the scale.

More recently, Brown, Sato and Sage[71] have studied the effects of the turbulence intensity on mass transfer from the surface of a sphere to turbulence levels of 15%. Unfortunately, the turbulence levels were not measured directly, but were obtained from measurements made previously in a somewhat similar system. At Reynolds Numbers below 1,000, the turbulence intensity had little effect on the transfer rate, but at high Reynolds Numbers there was a marked upswing at the higher intensities. Here again the increases are compatible with the Re_c-intensity curves and it would seem that, as an approximation, systems in which the sphere Reynolds Number-intensity combinations fall below the curve will not show sharp increases in mass transfer resulting from the free-stream turbulence. Similar tendencies are also noticeable in the results for mass transfer from spheres obtained by Schnautz[72]. Edwards and Furber[73] have found that heat transfer will not be markedly changed by turbulence if the boundary layer is completely laminar or turbulent, but it will be strongly affected if transition occurs.

Van der Hegge Zijnen[22] has systematically studied the rate of heat transfer from cylinders to a turbulent air flow for a Reynolds Number range of 600 to 25,800, with an intensity range from 2 to 13% and with ratios of the Eulerian scale to the cylinder diameter varing from 0.31 to 240. However, results were also taken at Reynolds Numbers of 60 and 580, and these showed no turbulence effect up to levels of 13%. It may be that since these values fall far below the Re_c curve obtained for spheres by the present authors, they may also fall below the corresponding curve which would be obtained for cylinders, so that no effect would be expected. For the higher Reynolds Number data, Van der Hegge Zijnen found that the rate of heat transfer was affected, and the increase was a function of Re, $(\sqrt{\overline{u'^2}}/U_r)$ and (L/d). He then proposed that the first two parameters be combined into their product, $(\rho d\sqrt{\overline{u'^2}}/\mu)$. This reasoning may not be correct since it pre-supposes that the functional form of both parameters will be identical, which is not the case at least with momentum transfer, since the critical behavior is very definitely a function of the Reynolds Number. Van der Hegge Zijnen has correlated his data as a function of $(d\sqrt{\overline{u'^2}}/\mu)$ and (L/d), but the measure of success which he does have may be due to the ranges of intensities and Reynolds Numbers which characterize his system. His results are however quite interesting, in that they show a scale sensitivity which is contrary to that predicted by the Taylor parameter. At a Reynolds Number of 10,000 he obtained by interpolation the family of curves which is shown in Figure 13, in which Nu^* is the ratio of the heat transfer coefficient to its value at zero turbulence. Although his actual data are scattered about the curves, the effect of the Eulerian scale is significant. Below a (L/d) ratio of 2, the effect of *increasing* the scale would be to *increase* the effectiveness of the turbulence, whereas the Taylor theory predicts the opposite, and the Dryden data seem to confirm this at (L/d) ratios all below 1. Furthermore, the intensity still has an effect even at (L/d) ratios in excess of 10.

Valid heat and mass transfer information for spheres in a turbulent fluid is unfortunately still limited, but the results from work now in progress will be extremely helpful for a fuller understanding of the effects of the free-stream vorticity on the boundary layer and wake flow.

Schwarz[74] has studied the transverse oscillations of a sphere suspended by a thread in an upward flow of turbulent air as part of an eventual investigation of particle dispersion due to fluid turbulence. In the particle Reynolds Number range concerned ($3{,}000 < Re < 20{,}000$) and in a laminar fluid, the processes occurring during the wake shedding (see Part II) will cause a sideways oscillation which correspond to the trans-

verse motion of the sphere during its fall as noted by Barker[50]. The root mean square values of the displacement could not be measured at zero turbulence because of the residual wind-tunnel turbulence; however, measurements were taken with the intensity being varied to 4%, with varying particle densities and relative scales. The results showed conclusively that the particle oscillations were not directly caused by the variations in the local velocity but were instead affected indirectly because of the disturbance to the sphere flow structure. The experimental system did not permit measurement of the effects of the turbulence on the drag but rather on the scale of the oscillations. It is difficult to relate this effect to the drag, since either the wake or the separation point may first increase and then decrease their large scale fluctuations with increasing free-stream disturbances. The decreasing scale could be caused by increased spectral transfer which would accompany the increase of free-stream vorticity. In some cases, particularly at the low turbulence levels, it was found that a maximum oscillation increase occurred when the free-stream spectrum peak occurred in the vicinity of the sensitive frequencies indicated by the neutral stability curves. The largest oscillation increases, however, occurred at a spectrum peak which was *farthest* removed from the frequency indicated by the stability curves, and Schwarz concluded that this was a result of the intensity level.

CONCLUSIONS

The extent to which the free-stream turbulence exerts an influence on the particulate momentum transfer depends on the magnitude of the relative turbulence parameters and the Reynolds Number. The intensity value would seem to be the predominating turbulence parameter with the scale lengths occupying a secondary position. Increasing intensities cause a systematic regression of the transition region of the drag coefficient curve towards lower Reynolds Numbers, together with a moderate increase of the drag coefficients for both the subcritical and supercritical Reynolds Numbers. The free-stream turbulence also diminishes the drag coefficient dependency on the acceleration which had been previously noted in laminar systems and this probably results from a decreased orderliness in the wake structure as a result of the turbulence. Extended research is needed to study the effects of high free-stream vorticities on the boundary layer and wake, and these in turn will contribute to the eventual theoretical description of the transition and turbulence phenomena.

Acknowledgements

The authors wish to express their appreciation for the continued assistance given to them by Librarians A. Finnemore and L. Lefebvre of the Pulp and Paper Research Institute of Canada, and P. Keir of McGill University, in obtaining the many papers reviewed in this series. L. B. Torobin is indebted to the Scientific Research Bureau, Trade and Commerce Department, Province of Quebec for three consecutive fellowships in support of his research program.

Nomenclature

Any consistent set of units may be employed. Those listed are merely illustrative.

B	=	empirical constant, dimensionless, Equation (4).
C_D	=	drag coefficient, dimensionless.
C_p	=	pressure cofficient, dimensionless, Equation (1).
d	=	body diameter, ft.
E_V	=	energy of viscous damping, ft.-poundals/ft.^{3}
E_T	=	total turbulent energy, ft.-poundals.
f	=	frequency, cycles/sec.
F_V	=	viscous damping force, poundals/ft.^{3}
K_T	=	ratio of turbulent energy to viscous energy, dimensionless.
l	=	characteristic length, ft.
L	=	Eulerian macroscale, ft.
Nu^*	=	ratio of heat transfer coefficient in turbulent flow to value in laminar flow, dimensionless.
P_1	=	fluid pressure at front of sphere, poundal/ft.^{2}
P_2	=	fluid pressure at rear of sphere, poundal/ft.^{2}
$\partial p/\partial x$	=	mean pressure gradient in x direction, poundal/ft.^{3}
$\partial p'/\partial x$	=	instantaneous pressure fluctuation gradient in x direction, poundal/ft.^{3}
Re	=	Reynolds Number, dimensionless.
Re_s	=	upper critical Reynolds Number, dimensionless.

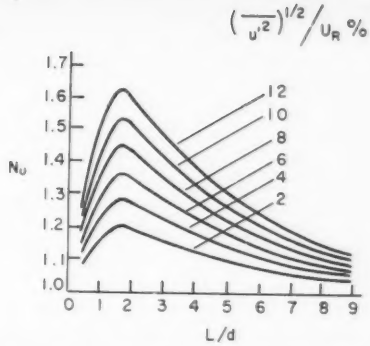

Figure 13—The effect of free-stream turbulence on the heat transfer from cylinders (van der Hegge Zijnen).

Sr	=	Strouhal Number, dimensionless.
u'	=	fluctuating component of velocity in x direction, ft./sec.
U_1	=	fluid velocity at edge of boundary layer, ft./sec.
U_o	=	mean fluid velocity, ft./sec.
U_r	=	mean fluid velocity relative to particle surface, ft./sec.
x	=	length scale in direction of mean flow, ft.
α	=	angle between separation point and front stagnation point, degrees.
δ	=	boundary layer thickness, ft.
λ	=	Eulerian microscale, ft.
Λ	=	Pohlhausen shape factor, dimensionless, Equation (5).
Λ'	=	increase of Pohlhausen factor due to free-stream turbulence, dimensionless.
μ	=	absolute viscosity, lb./(ft.) (sec.).
ν	=	kinematic viscosity, ft.^{2}/sec.
ρ	=	fluid density, lb./ft.^{3}

References

(1) Torobin, L. B., and Gauvin, W. H., Can. J. Chem. Eng., **37:** 129 (1959).
(2) Torobin, L. B., and Gauvin, W. H., Can. J. Chem. Eng., **37:** 167 (1959).
(3) Torobin, L. B., and Gauvin, W. H., Can. J. Chem. Eng., **37:** 224 (1959).
(4) Torobin, L. B., and Gauvin, W. H., Can. J. Chem. Eng., **38:** 142 (1960).
(5) Flachsbart, O., Physik. Z., **28:** 461 (1927).
(6) Jacobs, E. N., N.A.C.A. T.N., 312 (1929).
(7) Fage, A., and Warsap, I., A.R.C. R. and M. No. 1283 (1929).
(8) Millikan, C. B., and Klein, A. L., Aircraft Eng., 169 (1933).
(9) Goldstein, S., "Modern Developments in Fluid Dynamics", Oxford Univ. Press, London (1938).
(10) Hoerner, S., Luftfahrtforschung, **12:** 42 (1935).
(11) Luthander, S., and Rydberg, A., Physik. Z., **36:** 552 (1935).
(12) Wiselius, S. I., N.A.R.I., Rep. A 950, Amsterdam (1947).
(13) Dryden, H. L., J. Washington Acad. Sci., **25:** 101 (1935).
(14) Dryden, H. L., N.A.C.A. T.R., 342 (1929).
(15) Dryden, H. L., and Kuethe, E., N.A.C.A. T.R., 342 (1929).
(16) Dryden, H. L., Schubauer, G. B., Mock, W. C., and Skramstad, H. K., N.A.C.A. T.R., 581 (1937).
(17) Platt, R. C., N.A.C.A. T.R., 558 (1936).
(18) Roshko, A., N.A.C.A. T.R., 1194 (1954).
(19) Ahlborn, F., Zt. fur Technische Physik., **12:** 10 (1931).
(20) Taneda, S., Phys. Soc. Japan, **11:** 302 (1956).
(21) Geidt, W. A., J. Aeronaut. Sci., **18:** 11 (1951).
(22) van der Hegge Zijnen, B. G., Appl. Sci. Res., **A7:** 205 (1958).
(23) Schiller, L., and Linke, W., N.A.C.A. T.M., 715 (1933).
(24) Komeda, H., Japan Soc. Aero. Eng. J., Oct., 6 (1957).
(25) Schubauer, G. B., and Dryden, H. L., N.A.C.A. T.R., 546 (1935).
(26) Speidel, L., Zeit, fuer Flugwissenschaften, **5:** 270 (1957).
(27) Lunnon, R. G., Proc. Roy. Soc. (London), **118A:** 680 (1928).

(28) Shakespear, G. A., Phil. Mag. (6) **28:** 728 (1914).
(29) Burke, S. P., and Plummer, W. S., Ind. Eng. Chem. **20:** 1200 (1928).
(30) Wilhelm, R. H., and Valentine, S., Ind. Eng. Chem. **43:** 1199 (1951).
(31) Miller, W., and McInally, T. W., J. Royal Tech. College Glasgow, **3,** Part 4: 682 (1936).
(32) Whetton, J. T., and Broadhurst, P. H., Trans. Inst. Min. Engrs., **111:** 906 (1951-52).
(33) Whetton, J. T., and Broadhurst, P. H., Trans. Inst. Min. Engrs. (London), **111:** 920 (1951-52).
(34) Whetton, J. T., and Broadhurst, P. H., Trans. Inst. Min. Engrs. (London), **112,** Part 4: 351, 354 (1953).
(35) Garner, F. H., and Kendrick, P., Trans. Inst. Chem. Eng. **37:** 155 (1959).
(36) Pinkus, O., J. Appl. Mech., **19:** 425 (1952).
(37) Dalla Valle, J. M., Heating and Ventilating, **39:** 28 (1942).
(38) Fledderman, R. G., and Hanson, A. R., U. of Michigan Eng. Res. Inst. Rep. No. CM 667 (1951).
(39) Hanson, A. R., Proc. 2nd Midwestern Conf. on Fluid Mech., 415 (1952).
(40) Ingebo, R. D., N.A.C.A. T.N., 3762 (1956).
(41) Foeking, N. L., Ph.D. Thesis, Cornell University (1951).
(42) Mehta, N.G., Ph.D. Thesis, Purdue University (1955).
(43) Hinkle, M., Ph.D. Thesis, Georgia Institute of Technology (1953).
(44) Khudiakow, G. N., and Chukhanov, Z. F., Doklady Akad. Nauk. S.S.S.R. **78:** 681 (1951).
(45) Khudiakow, G. N., Izvest. Akad. Nauk. S.S.S.R. Otdel. Tekh. Nauk. **7:** 1022 (1953).
(46) Chernov, A. P., Izv. Akad. Nauk. Kaz. S.S.S.R., Ser. Energ., **9:** 160 (1955).
(47) Lewis, W. K., Gilliland, E. R., and Bauer, W. C., Ind. Eng. Chem., **41:** 1104 (1949).
(48) Torobin, L. B., and Gauvin, W. H., A.I.Ch.E. Journal (In press).
(49) Gauvin, W. H., Pasternak, I. S., Torobin, L. B., and Yaffe, L., Can. J. Chem. Eng. **37:** 95 (1959).
(50) Barker, D. H., Ph.D. Thesis, University of Utah (1951).
(51) Rayleigh, Lord, Proc. London Math. Soc., **19:** 67 (1887).
(52) Tollmien, W., Mitteilung, Nachr. Ges. Wiss. Gottingen, Math. Phys. Klasse, **22:** (1929).
(53) Schlichting, H., Nachr. Ges. Wiss. Gottingen, Math. Phys. Klasse, **181:** (1933).
(54) Lin, C. C., Quart. Appl. Math., **3:** 117 (1945).
(55) Pretsch, J., N.A.C.A. T.M., 1017 (1942).
(56) Meskyn, D., and Stuart, J. T., Proc. Roy. Soc., **208A:** 517 (1951).
(57) Stuart, J. T., J. Fluid Mech., **4:** 1 (1958).
(58) Schubauer, G. B., and Skramstad, H. K., N.A.C.A. T.R. 909 (1948).
(59) Bennett, H. W., and Lee, C. A., Proc. Amer. Civ. Engrs., **81:** 796 (1955).
(60) Taylor, G. I., Proc. Roy. Soc., **156A:** 307 (1936).
(61) Schubauer, G. B., Proc. 5th Internat. Conf. Fluid Mech. (1937).
(62) Lin, C. C., Proc. Nat. Acad. Sci., Wash., **40:** 741 (1954).
(63) Hinze, J. O., "Turbulence", McGraw-Hill Book Co., New York (1959).
(64) Lindgren, E. R., Arkiv. Fysik., **12:** 1 (1957).
(65) Adelberg, M., Ph.D. Thesis, Purdue University (1958).
(66) Duffy, R., and Li, T. Y., T.R. A.E. 5707, (A.F.S.O.R. T.N., 715) (1957).
(67) Schubauer, G. B., Boundary Layer Research Symposium, Freiburg, 1957, ed. by H. Goertler (Springer, Berlin, Germany, 1958) p. 85.
(68) Klebanoff, P. S. and Tidstrom, K. D., N.A.S.A. TND-195 (1959).
(69) Hama, F. R., Inst. Fluid Dyn. and Applied Math., Univ. of Maryland, Tech. Note BN-195 (1960).
(70) Maisel, D. S., and Sherwood, T. K., Chem. Eng. Prog., **46:** 172 (1950).
(71) Brown, R. A. S., Sato, K., and Sage, B. H., Ind. Eng. Chem., Chem. and Eng. Data Series, **3:** 263 (1958).
(72) Schnautz, J. A., Ph.D. Thesis, Oregon State College, Oregon (1958).
(73) Edwards, A., and Furber, B.N., Proc. Instn. Mech. Engineers, **170:** 941 (1956).
(74) Schwarz, H. W., Dr. Eng. Thesis, Johns Hopkins University, Baltimore (1957).

★ ★ ★

Temperature Dependence of the Binary Diffusion Coefficient of Gases[1]

D. S. SCOTT[2] and K. E. COX[3]

The variation with temperature of the binary gas diffusion coefficient for the gas pairs N_2 - H_2 and NH_3 - H_2 is reported for the temperature range of 0°-300°C. The data were obtained using a steady state flow method, and the apparatus and experimental conditions relative to this technique are discussed. Although this method does not give absolute values of the diffusion coefficient, it is relatively simple and accurate.

The extent of agreement of the data with equations for the prediction of gas diffusion coefficients is shown. Better results are obtained when these equations are applied to nearly ideal systems, such as the N_2 - H_2 pair, rather than to gases which have highly polar molecules such as NH_3.

It is becoming increasingly important in many engineering operations to have, or to be able to predict, reliable values of the diffusion coefficient of gases. A number of correlations[1,2,3,4] have been presented in the literature, and appear to give adequate agreement with experiment at ordinary temperatures and moderate pressures. In general, the most rigorous and satisfactory equation is one of the type given by Hirschfelder et al[1], but even this relationship is reliable over fairly wide ranges of temperature and pressure only for non-polar, nearly spherical molecules. At ordinary temperatures and pressures this equation has also been applied in a modified form, with apparently useful accuracy, for the prediction of coefficients in systems involving one polar or non-spherical type of molecule. However, data for such systems at varying temperatures or pressures are not plentiful and are frequently contradictory. There is a need for reliable experimental values for diffusion coefficients, particularly over a reasonable range of temperatures. In the last few years, some good data have been presented, particularly for the more ideal gas systems. The recent work of Walker and Westenberg[5,6,7,8], using a novel "point source" technique, especially covers a wider range of temperature with greater accuracy than has been previously obtained. Most of this work confirms the fact that the diffusion coefficient varies as $T^{1.5}$ – $T^{2.0}$. However, the temperature variation of different gas pairs between these limits can cause substantial errors in the value of the diffusion coefficient if an exponent for the temperature is arbitrarily selected, or fixed by assumptions made regarding the nature of molecular interactions without experimental confirmation.

In this work, the diffusion coefficients for two systems, one nearly ideal (N_2 – H_2) and one involving a highly polar component (H_2 – NH_3) were measured by a steady state flow technique over the temperature range from 0°C.—300°C.

[1]*Manuscript received June 8; accepted September 26, 1960.*
[2]*Department of Chemical Engineering, The University of British Columbia, Vancouver, B.C.*
[3]*Montana State College, Bozeman, Montana, U.S.A.*

Apparatus and Procedure

The steady state flow technique for the measurement of gas diffusion rates was first used by Wicke and Kallenbach[9] in their studies of ordinary and surface diffusion in porous solids. Later, a modified apparatus of the same type was adapted by Weisz[10] for measuring the effective diffusivities of porous catalytic particles.

A very similar procedure was developed simultaneously in this work for the measurement of gas diffusion coefficients which made use of a carefully selected porous solid as a diffusion path. The solid so selected had a definite and reasonably uniform pore size so that the likelihood of any Knudsen diffusion, or of appreciable forced flow due to small, total pressure differentials was minimized. It can be shown that a pore size of about 1-3 microns diameter should be close to an optimum for these experimental requirements. With the majority of pore space in this size range, and a uniform structure, only ordinary diffusion should occur through such a solid in the absence of total pressure gradients. Further, by using two solids of differing pore diameter and porosity, one can demonstrate the absence of any effect through the void spaces of the solid, except that of ordinary diffusion.

A sketch of the apparatus is shown in Figure 1. Essentially, it consisted of two gas trains, one for hydrogen and one for nitrogen or ammonia. Both gases were passed through fine capillaries to give a smoother flow and then through driers containing Drierite to remove moisture. The flows were metered in float type flowmeters (Matheson Co. Type 203) under a constant pressure of 6 inches of mercury. This pressure was measured by a mercury manometer and maintained at the correct value by adjustment of a needle valve. This allowed a single calibration to be used for the flowmeters even though the pressure drop through the heating coils (50 ft. of 1/8 inch O.D. copper or aluminum tubing) varied widely as the temperature was varied.

The diffusion cell consisted of identical glass halves of the same outside diameter as the cylindrical solid porous sample, which was held between them by a rubber sleeve, or by an

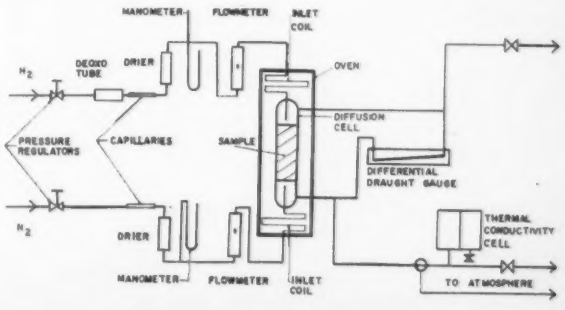

Figure 1—Diffusion apparatus.

epoxy cement. The inlet line came to within about 1 cm. of the sample face in order to minimize end effects. The gases leaving the diffusion cell passed through a section of 1/4 in. O.D. metal tubing which cooled the gases to room temperature. Analysis of hydrogen was by thermal conductivity cell, as was the analysis of nitrogen, when required. Ammonia concentrations were determined by titration after absorption from a gas sample.

Gas lines from the cell through the cooler and analysis system were oversized, and had a very small pressure drop, so that the diffusion cell operated at atmospheric pressure. The diffusion cell itself was mounted inside an electrically heated thermostatically controlled oven equipped with an air circulating fan. The temperature of the oven could be held constant to within ±0.2°C.

The total pressure on both sides of the cell was maintained at the same value by means of an oil-filled draft gauge and flow adjustment valves. The differential pressure could be measured with an accuracy of ±0.002 inches of water pressure.

Two porous samples were used in this work. Both of these materials were microporous porcelain solid rod manufactured by the Selas Corp., and classed as porosity grades 03 and 015. The 03 grade had a porosity of 28.6%, and an average pore diameter of 1.52 microns, while the 015 type had a porosity of 65.9% and an average pore size of 2.33 microns. Pore diameters were determined by the mercury penetration method.

The sample was mounted by cementing it at each end to the glass end piece using an epoxy resin, Araldite AN130, and then coating the entire porous sample with the same resin. When properly applied, this mounting method allowed temperatures up to 250° – 300°C. to be used for short times. Metal to glass joints were made with Kovar seals.

Flowmeters were calibrated against wet test meters and soap bubble flow meters, or by absorption and titration in the case of ammonia. Thermal conductivity cells (Gow Mac Model NIS Diffusion Type Cells) were calibrated by making up streams of known composition, and using a pure gas as the reference. Temperatures in the oven were measured with both shielded thermocouples, and thermometers. The fact that the pre-heating coils actually brought the gas to the oven temperature was verified by the use of a temperature measuring capillary flowmeter described elsewhere[11,12]. It was estimated that the maximum experimental error due to measurements in a value of the diffusion coefficient obtained should be of the order of ±3%.

Theory

In a constant pressure flow system, in which steady-state counter-diffusion of two ideal gases is occurring, the integration of the Maxwell diffusion equation leads to the following relationship,

$$DP = \frac{N_A\,(1 - N_B/N_A)RTL}{A\,ln\,\dfrac{1 - (1 - N_B/N_A)Y_{A2}}{1 - (1 - N_B/N_A)Y_{A1}}} \qquad (1)$$

In this equation N_A and N_B are the molar rates of diffusion of the two gas components, A and B, with Y_{A2} and Y_{A1}, representing the mole fractions of A at each end of the diffusion path of length L and cross sectional area A. When A and L are the geometric area and length of a porous sample, then the binary diffusion coefficient, D_{AB} becomes De, the effective diffusion coefficient through that particular solid. If it is assumed that the geometry of the porous solid is not affected appreciably by moderate temperature changes, then De and D_{AB} are related by a constant which is independent of temperature, pressure, or the particular binary gas pair used, and is affected only by the nature and dimensions of the porous solid, as long as only ordinary molecular diffusion is the major transport mechanism.

Therefore, if measurements of the rates of diffusion are carried out for a gas system under conditions such that its true diffusion coefficient, D_{AB}, is known, then the diffusion ratio, D_{AB}/De, can be determined, and used at other conditions, or for other binary pairs of gases. This makes it possible to determine true diffusion coefficients with an accuracy dependent on the original value used for the known diffusion coefficient. In this work, nitrogen and hydrogen were employed as the initial gas pair, partly because they might be expected to behave closely as ideal spherical molecules, and partly because reliable data were available for this system at 1 atm. and ordinary temperatures. The diffusion ratio for both porous solids used was determined at room temperature, using this system.

The possibility exists that when a fine-pored solid is used as a diffusion path, transport mechanisms, other than ordinary diffusion, may occur. Forced flow due to total pressure differences can be reduced to a negligible factor by maintaining equal pressure on each face of a solid sample, and by using a sample with sufficiently small pores. Surface or two dimensional flow due to molecular adsorption can be eliminated by a careful choice of the solid and gases used, and the operating conditions. In general, Knudsen flow can be made negligible by using pore sizes greater by a factor of 10 than the molecular mean free paths.

A clear indication that Knudsen diffusion is not occurring to a significant extent can be obtained by experimentally measuring diffusion rates at varying total pressures. If ordinary diffusion is the major transfer process, then the DP product from such experiments will have a constant value. Measurements of this nature on the two solids used showed that at 1 atm. the DP product had the same value as that obtained for higher pressures.

The use of Equation (1) depends on a knowledge of the ratio of the two diffusion rates, N_A and N_B. It has been shown by Hoogschagen[13], that for the constant pressure steady state case, the following relationship appears to hold for ordinary diffusion:

$$N_B/N_A = \sqrt{M_A/M_B} \qquad (2)$$

where M_B and M_A are the molecular weights of B and A, respectively.

The behavior with temperature of the binary gas diffusion coefficient in simple correlations has usually been assumed to show a dependence from $T^{1.5} - T^{2.0}$. More rigorous equations have more complex temperature functions. Two of the better known equations of this type are given by Arnold[2] (Equation (3)), and by Chapman and Cowling, given in Equation (4) as presented by Hirschfelder, Curtiss and Bird[1]. The former equation makes use of the Sutherland potential model, while the latter equation has been used with a variety of potential functions.

$$D = \frac{0.00837\ T^{5/2}\,(M_1 + M_2)/M_1M_2^{1/2}}{P\,(V_1^{1/3} + V_2^{1/3})^2\,(T + S_{12})} \qquad (3)$$

In Equation (3) V_1 and V_2 are the molar volumes of the pure substances at their normal boiling points, and S_{12} is the Sutherland constant for the pair of gases. Reid and Sherwood[14] have discussed this equation, as well as the methods suggested by Arnold for obtaining values of the above quantities.

$$D = \frac{0.002628\ T^{3/2}\,(M_1 + M_2)/{}_2M_1M_2}{P\,\sigma^2_{12}\,\Omega_D} \qquad (4)$$

The term σ_{12} is a force constant interpreted as the closest distance of separation of the two species, and Ω_D is the appropriate collision integral (in this work the integrals based on the Lennard-Jones potential model were used).

The form of Equation (4) is rigorous for non-polar, approximately spherical molecules, and, in theory, the success of the equation rests on the validity of the potential function chosen. The Lennard-Jones 6-12 potential function has been widely used, for this and for similar equations describing the transport properties of dilute, ideal gases. Although this function may be oversimplified, it does allow the prediction of diffusion coefficients over wide ranges of temperature for non-polar molecules. The force constants required for Equation (4) are usually

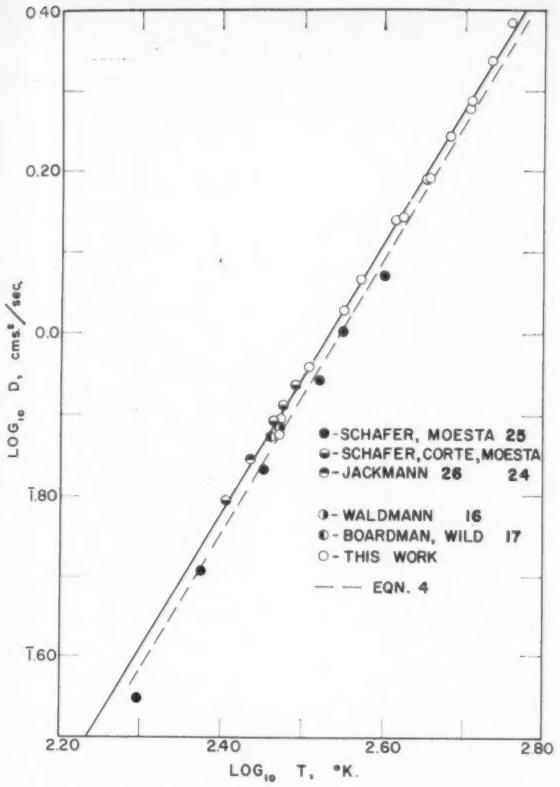

Figure 2—Diffusion coefficients for hydrogen-nitrogen.

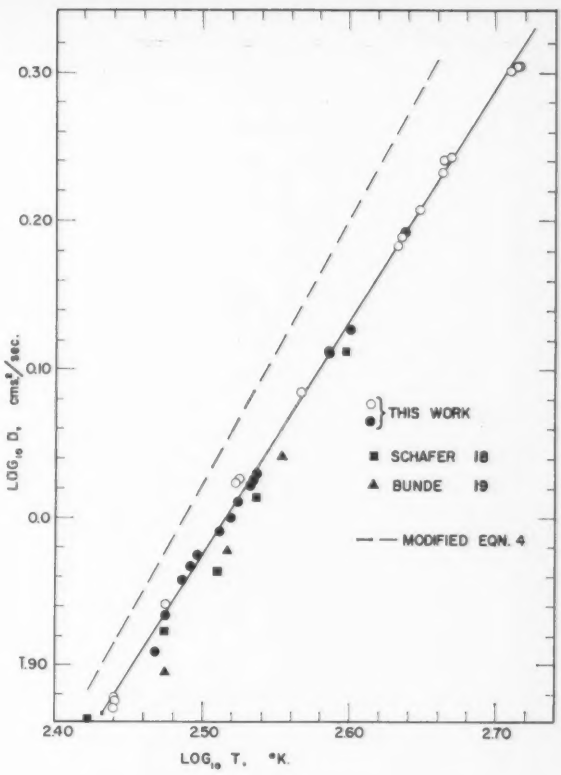

Figure 3—Diffusion coefficients for hydrogen-ammonia.

obtained from values calculated from pure component viscosity measurements, and from simple empirical combining rules. The data of Walker and Westenberg, Amdur and Schatzki[15] and others, show that the accuracy of prediction is sufficiently good for engineering purposes over wide temperature ranges for several nearly ideal gas pairs. However, data over the same ranges of temperature for gas pairs where one or both of the components are polar, or non-symmetrical molecules, are still scarce. The data that does exist, particularly that of Walker and Westenberg[8], indicate that Equation (4) used as described, may be considerably less accurate in these cases, even if an attempt is made to allow for polarity effects in the approximate manner suggested by Hirschfelder (i.e., by use of the Stockmayer potential parameters).

Results

All measurements were done using pure gases on each side of the diffusion cell, and allowing only small changes in concentration of the flowing streams to occur. Therefore, all diffusion coefficients calculated are averaged over essentially 100% of the concentration range. For most pairs, the concentration dependence varies from less than 1% to about 5%, depending on the relative molecular weights, and other properties of the gases.

The variation of the diffusion coefficient with absolute temperature is shown for the nitrogen-hydrogen system, and for the ammonia-hydrogen system in Figures 2 and 3, respectively. Data of other workers for both pairs are also given. In Figure 2, the line drawn through the data points represents the least squares fit. The dashed line gives values calculated from Equation (4), based on use of the Lennard-Jones potential function, with molecular force constants derived by the use of simple combining rules from those for the pure components, which in turn were obtained from viscosity measurements. The necessary calibration factor for the apparatus was obtained using diffusion measurements for the $N_2 - H_2$ system at room temperature, and comparing these to the diffusion coefficient values which were judged to be the most reliable, particularly those of Waldmann[16], and Boardman and Wild[17].

The same cell with the same solid (03) was then used to obtain the data shown as open circles in Figure 3. The same calibration factor was applied in this case. At the time these measurements were carried out, no genuine experimental data for the $NH_3 - H_2$ system had been reported in the literature, to the best of the authors' knowledge. (Some data have appeared recently[18]). The data on this system were checked by cementing in a different solid sample (015) of much greater porosity, and larger mean pore size, and obtaining fresh data after calibrating the new solid with $N_2 - H_2$ diffusion measurements at room temperature. These points are shown as solid circles. A least squares straight line has been fitted through these two sets of data and is shown as the solid line in Figure 3. The dashed line represents Equation (4) calculated, as suggested by Hirschfelder, by the use of the Stockmayer potential parameters, and using values for the molecular parameters and properties of hydrogen and ammonia from[1].

The use of Equation (1) to calculate values of D from diffusion rate measurements implies that the ratio N_A/N_B is either known or conforms to Equation (2). In both cases, measurements were made of the ratio of the rates of the counter-diffusing gases. Although the precision of the results is not high because of difficulties of analysis, the values obtained, as shown in Table 1, confirm the fact that Equation (2) holds for both of these systems. Some experimental values of the diffusion coefficient for the two systems measured are given in Table 2, for convenience.

Discussion

Nitrogen-hydrogen system — The least squares straight line drawn through the data shown in Figure 2 has a slope of 1.682,

TABLE 1

System	Ratio of Diffusion Rates	
	Experimental	Calc. (Eqn. (2))
$H_2 - N_2$	3.44	
	4.03	
	3.75	
	Ave. 3.77	3.742
$H_2 - NH_3$	3.00	
	2.88	
	2.99	
	Ave. 2.95	2.907

and gives a standard deviation of the data of 1.91%. This result is very satisfactory in view of the possible maximum errors in the experiments. Equation (4) over the same temperature range indicates a slope of 1.681, in excellent agreement with the data. Although this equation is not strictly linear on a plot such as that in Figure 2, the deviation from linearity is less than the experimental error over this range. In general, all data points agree with the value predicted by this equation within 3%. It can be concluded from these results that this method presents an accurate and convenient way of determining binary gas diffusion coefficients. The assumption that the diffusion cell calibration is not seriously affected by fairly large temperature changes is justified by the results obtained. It is apparent also that Equation (4) represents this system in a satisfactory manner from 0° − 300°C. Apparently, a simpler potential function — e.g., the point center of repulsion model, would represent the nitrogen-hydrogen system equally well. This fact has also been pointed out by Walker and Westenberg for similar systems. However, for engineering purposes it is more convenient to use a single potential function of the widest possible applicability. For calculations from kinetic equations describing the transport properties of dilute gases, the Lennard-Jones potential seems to be the most generally used of the many potential functions which have been proposed, and the necessary collision integrals are readily available. The values of the potential parameters, σ and ϵ/k, for the nitrogen-hydrogen system are given with adequate accuracy (i.e., about 3%) by use of the simple combining rules employing the pure component values as obtained from viscosity measurements.

The temperature dependence found might be compared to that for the helium-nitrogen system over the range 20°−900°C. reported by Walker and Westenberg[6]. Their value of the temperature exponent was 1.69 compared to the value of 1.682 found in this work for the hydrogen-nitrogen system.

Hydrogen-ammonia system — The results given in Figure 3 may be compared with the various correlations which have been suggested for the prediction of the binary diffusion coefficient. The solid line through the experimental data representing the least squares fit suggests that the diffusion coefficient varies as $T^{1.583}$.

Results predicted by Equation (4) using the Stockmayer parameters for NH_3 show errors of from +9% to +23%. Use of this equation in the usual form, that is without the Stockmayer correction for dipole effects, gives values with a slightly greater error. These equations predict that D should vary as $T^{1.74}$ over the temperature range investigated here. Table 2 also compares some of the calculated and experimental values.

The Arnold Equation (2) gives improved accuracy, and predicts the experimental values with an error of from −3.2% to +5.2%. Both the Gilliland and Slattery correlations are approximately 25%–35% low (see[14], Table 8.3, P.274).

When the results obtained are compared to those reported by Bunde[19], and Schafer[18], it can be seen that the present

TABLE 2

COMPARISON OF EXPERIMENTAL AND CALCULATED DIFFUSION COEFFICIENTS.

Temp. °K.	Exp.	Diffusion Coefficient		
		Calculated from Hirschfelder Eqn.		Arnold, Eqn. (c)
		(a)	(b)	
$N_2 - H_2$				
294	0.763	0.739	0.762	0.831
322	0.903	0.863	0.891	0.965
398	1.289	1.234	1.273	1.374
450	1.541	1.516	1.542	1.673
506	1.883	1.860	1.906	2.020
573	2.417	2.265	2.346	2.465
$NH_3 - H_2$				
273	0.7454	0.811	0.722	0.721
293	0.8337	0.921	0.805	0.819
333	1.021	1.150	1.009	1.021
413	1.435	1.702	1.449	1.475
493	1.899	2.310	1.947	2.00
533	2.149	2.640	2.210	2.26

(a) Using force constants from Hirschfelder, Curtiss and Bird, "Molecular Theory of Gases and Liquids"
(b) Using Lennard-Jones potential function and force constants calculated from experimental data (Table 3)
(c) Calculated according to method given by Reid and Sherwood "Properties of Gases and Liquids".

experimental values are 5%–10% higher. Both Bunde and Schafer used diffusion cells of the Loschmidt type, and in both cases the initial concentration difference was 100%. A survey of the results obtained by various workers who have made use of the Loschmidt technique over significant ranges of temperature shows many discrepancies. It must be concluded that diffusion measurements at different temperatures done by this method must be very carefully controlled to avoid significant errors. The flow method used in this work is free from many of the sources of error encountered in unsteady state, static experiments.

Prediction of Binary Gas Diffusion Coefficients

The most comprehensive comparisons of semi-theoretical correlations have been done by Wilke and Lee[3] and by Reid and Sherwood[14]. An experimental value for the $H_2 - NH_3$ system is given by Wilke and Lee, taken from a paper by Trautz and Muller[20]. Reference to the original article shows that this value, as well as 18 others given by Wilke and Lee as experimental data are, in fact, calculated by Trautz from the theory of Chapman and Cowling, by a less exact approach than that of Hirschfelder et al. Unfortunately, most of these "experimental" values have also been included by Reid and Sherwood in their text. Inclusion of these data probably do not affect the conclusions reached in either case, although the improvement claimed for a modified form of Equation (4) presented by Wilke and Lee may be open to question.

Primarily, it should be realized that a number of systems for which "experimental" data have been tabulated, have, in fact, never been measured. If these systems involve polar or long chain molecules, prediction methods cannot be expected to be too accurate. Improved correlations must depend on more data for these types of systems becoming available.

Because Equation (4) is now commonly used in predicting values of the binary diffusion coefficient, it seems worthwhile to discuss its further applications. A number of potential functions have been proposed, and equations of this type can be used with any potential function for which the collision integrals are available. At ordinary temperatures it is generally conceded that the Lennard-Jones 12-6, Buckingham exponential - 6, or

square well potentials are at least reasonable approximations of the potential energy function. The simpler point-center-of repulsion, and exponential repulsion potentials may be realistic at higher temperatures when attractive forces are of lesser importance.

In a recent paper, Walker and Westenberg[8] have shown that any of these intermolecular potential functions can be made to fit experimental diffusion data within the usual experimental error. Further, there is a range of values which can be assigned to the particular molecular force constants of any one function, and still obtain a good fit for experimental data over wide ranges of temperature. This aspect has been recognized by others[21,22], as has the fact that it may not be possible to assign a single value to the force constants which reproduces experimental results at both low and high temperatures with equal accuracy.

If diffusion values are then to be fitted by a correlation of the type employing collision integrals, it does not matter in practice, within fairly wide limits, which potential function is employed as long as the force constants are evaluated from the diffusion data. Inasmuch as the Lennard-Jones potential function is used in many correlations for transport properties, involves only two constants, and tabulations of collision integrals for this function are available, it is convenient to make use of it to the maximum extent.

The two constants of the Lennard-Jones potential function, ϵ, the maximum potential energy of attraction and, σ, the distance of closest approach, can be obtained in various ways. They may be predicted from boiling point or critical properties by empirical rules, or from pure component values (usually obtained from viscosity measurements) and simple combining rules. For simple, non-polar molecules this latter method leads to a prediction of the absolute value of the diffusion coefficient with acceptable accuracy over wide ranges of temperature (about $\pm 5\%$). However, if the binary gas pair contains one polar molecule, or an unsymmetrical molecule, the prediction accuracy will not be so satisfactory and may be in considerable error at higher temperatures. On the other hand, if the force constants are derived from diffusion measurements, then Equation (4) can generally be made to fit the data over ranges of up to 1000°K. with an error of only about $\pm 3\%$. Whether or not this equation can also be made to fit systems involving two polar molecules is not known at present because of a lack of suitable diffusion data.

Ideally, a tabulation* of Lennard-Jones force constants determined from direct diffusional measurements would make possible a very satisfactory way of allowing prediction of diffusion coefficients. The vindication for this approach lies in the fact that if the constants so determined fit the data well over a range of about 200°C., then extrapolation for a further 300°C. or even more on either side of the experimental range would probably not introduce errors which were too large for engineering calculations. This procedure would not apply if a considerable degree of association or disassociation occurred in the gas as the temperature changed. Apparently, force constants obtained from self-diffusion measurements can be combined also through the usual combining laws to give workable values of the parameters for unlike pairs of gases.

*Table 3 of this paper has been deposited as Document No. 6436 with the ADI Auxiliary Publications Project, Photoduplication Service, Library of Congress, Washington 25, D.C. A copy may be obtained by citing the Document No. and by remitting $1.25 for photoprints, or $1.25 for 35 mm. microfilm. Advance payment is required. Make cheques or money orders payable to: Chief, Photoduplication Service, Library of Congress.

Acknowledgements

The careful work of M. Kiss and Miss J. Young in performing the measurements of the H_2 - NH_3 system is gratefully acknowledged. The work described here was part of a project supported by Imperial Oil Limited, and made possible by their financial assistance.

Nomenclature

A = cross-sectional area of diffusion path, cm.².
D_{AB} = mutual diffusion coefficient of gases A and B, cm.²/sec.
De = effective diffusion coefficient, cm.²/sec.
L = length of diffusing path, cms.
M_A, M_B = molecular weights
N_A, N_B = rates of diffusion, moles/sec.
P = total pressure, atm.
T = absolute temperature, °K.
Y_A = mole fraction of gas A.

$\epsilon/k, \sigma$ = molecular parameters in the Lennard-Jones potential function.

References

(1) Hirschfelder, J. O., C. F. Curtiss and R. B. Bird: "Molecular Theory of Gases and Liquids", John Wiley & Sons Inc., New York, 1954.
(2) Arnold, J. H., "Ind. Eng. Chem., **22,** 1091 (1930).
(3) Wilke, C. R., and Lee, C. Y., Ind. Eng. Chem., **47,** 1253 (1955).
(4) Gilliland, E. R., Ind. Eng. Chem., **26,** 681 (1934).
(5) Walker, R. E., and Westenberg, A. A., J. Chem. Phys., **29,** 1139 (1958).
(6) Walker, R. E., and Westenberg, A. A., J. Chem. Phys., **29,** 1147 (1958).
(7) Walker, R. E., and Westenberg, A. A., J. Chem. Phys., **31,** 519 (1959).
(8) Walker, R. E., and Westenberg, A. A., J. Chem. Phys., **32,** 436 (1960).
(9) Wicke, E., and Kallenback, R., Kolloid Z., **97,** 135 (1941).
(10) Weisz, P. B., Z. Physik. Chem., **11,** 1 (1957).
(11) Scott, D. S., Chem. Eng., **65,** 161, No. 23 (1958).
(12) Scott, D. S., Chem. Eng. Sci. **12,** 127 (1960).
(13) Hoogschagen, J., Ind. Eng. Chem., **47,** 906 (1955).
(14) Reid, R. C., and T. K. Sherwood, "The Properties of Gases and Liquids", McGraw-Hill Co., New York, 1958.
(15) Amdur, I., and Schatzki, T. F., J. Chem. Phys., **27,** 1049 (1957).
(16) Waldmann, L., Naturwissenschaften, **32,** 223 (1944).
(17) Boardman, L. E., and Wild, N. E., Proc. Roy. Soc. (London), **A162,** 511 (1937).
(18) Schafer, K., Z. Electrochem., **63,** 111 (1959).
(19) Bunde, R., Ph.D. Thesis in Chemistry, University of Wisconsin.
(20) Trautz, M., and Muller, W., Ann. Physik, **414,** 333 (1935).
(21) Strehlow, R. A., J. Chem. Phys., **21,** 2101 (1953).
(22) Amdur, I., Irvine, J. W., Mason, E. A., and Ross, J., J. Chem. Phys., **30,** 436 (1952).
(23) Amdur, I., Ross, J., and Mason, E. A., J. Chem. Phys., **20,** 1620 (1952). (Table 3).
(24) Schafer, K., Corte, H., and Moesta, H., Z. Electrochem. **55,** 662 (1951). (Figure 2).
(25) Schafer, K., and Moesta, H., Z. Electrochem., **58,** 743 (1954). (Figure 2).
(26) Jackman, W., International Critical Tables Vol. 5, p. 62 (Figure 2).

★ ★ ★

Formation and Quenching of Nitric Oxide in a Continuous Flow Furnace[1]

D. L. MORDELL[2], A. L. THOMPSON[2] and G. YANO[3]

A pre-pilot plant facility for the thermal fixation of atmospheric nitrogen has been successfully built and operated.

Gas temperatures exceeding 3000°K. have been reached but the quenching rates available to fix the nitric oxide were found to be inadequate for the gases at these high temperatures. However, yields of 3.7% nitric oxide by volume have been realized experimentally.

A separate water cooled sampling probe inserted at the top of the furnace gave quenching rates of the order of 10^6°C./sec. This also permitted the study of the effect of variation in the quenching rate while maintaining other conditions constant. The oxygen concentration appeared to have less effect than previous results indicated, but this may have been due to uncertainties in estimating gas temperatures near 3000°K.

Early experiments on a small scale[1,2] had shown that useful concentrations of nitric oxide could be obtained thermally in a continuous flow process where propane was burned with preheated air. Moreover, a study of methods to recover nitric oxide from a gas containing dilute concentration of nitric oxide showed that two methods, the silica gel adsorption process[3,4,5] and the freeze-out process, commercially known as the Fauser process[6], can be utilized to yield recovery efficiencies over 90%. The scientific and patent literature has been reviewed and some of the most pertinent work is listed[7–15].

It was realized that the process would operate most efficiently with the maximum air preheat temperatures (of the order of 1500°C.) which could be obtained with a counter flow or regenerative ceramic heat exchanger. However, because of the additional cost and uncertainty in operation it was decided to proceed with a pre-pilot plant apparatus based on a stainless steel heat exchanger which would provide some useful information on the influence of oxygen concentration, temperature and necessary quenching rates.

While most of the quenching was achieved by rapid flow of the hot gases through a water-cooled tube, or quick cooler, other methods were attempted: rapid admixture of cold air and/or water spray, and kinetic nozzle quenching.

[1]*Manuscript received February 10, 1959; accepted September 17, 1960.*
[2]*Gas Dynamics Laboratory, McGill University, Montreal, Que.*
[3]*Cyanamid of Canada Limited, Niagara Falls, Ont.*
Contribution from the Gas Dynamics Laboratory, McGill University, supported under Defence Research Board Grant No. 5001-01.
Based on a paper presented at the C.I.C. Chemical Engineering Conference, Hamilton, Ont., Nov. 6-11, 1959.

Experimental Apparatus

A brief sketch of the experimental facility is shown in Figure 1.. The air is preheated to 1000°K. in the air preheater and burns propane to achieve flame temperatures of the order of 3000°K. The hot combustion gases leave the furnace through the "quick cooler" where they are chilled rapidly to fix the nitric oxide at close to its equilibrium concentrations. The gases leave the quick cooler at approximately 1300°K. and are used to preheat the incoming air in the air preheater. From the preheater, the gases enter the gas cooler where they are cooled to about 300°K. and the water condensate from the combustion of the hydrocarbon fuel is removed in the condensate trap.

Zirconia Brick Furnace. A sketch of the furnace in Figure 2, shows also the materials of construction used.

The furnace is designed to provide sufficient reaction time to form 90% of the equilibrium concentration of nitric oxide at the minimum furnace temperature of 2400°K. for a combustion gas flow rate of 0.1 lb./sec. and a furnace pressure of 40 p.s.i.a. This furnace of interlocking zirconia bricks is enclosed by a refractory shell constructed from standard Magnorite bricks ($1\frac{1}{2} \times 4 \times 9$ inches) with an intervening space of about $\frac{1}{2}$ inch where the preheated air passes through to the combustion chamber. Small Magnorite refractory pieces are used as spacers between the zirconia furnace and the Magnorite shell to ensure that the zirconia bricks are jammed together. The Magnorite brick shell is supported in turn by a high temperature resistant 310 stainless steel shell. A smaller stainless steel shell supports the three top plates when they inevitably crack into smaller pieces as a result of thermal shock. The space between the inner stainless steel shell and the outer shell of 24″ standard pipe is packed with Fiberfrax insulation.

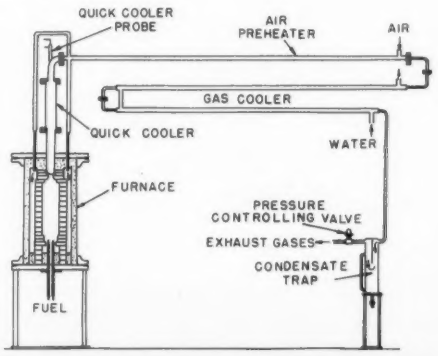

Figure 1—Nitrogen fixation equipment.

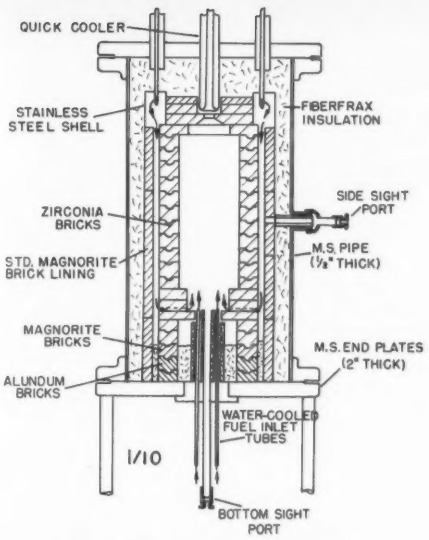

Figure 2—Nitric oxide furnace.

The preheated air enters at the top of the furnace shell and passes down through the annulus between the zirconia furnace and the Magnorite brick shell and enters the combustion chamber through the "spiral plate". The spiral plate has four grooves through which the incoming air is directed into a spiral motion, counter-current to the spiral flow of the propane gas from the burners. This ensures turbulent mixing which is a prime requisite for good combustion.

For runs 13 and 14 sighting ports were provided diametrically opposite in line with the entrance to the nozzle at the lower end of the quick cooler to permit an estimation of the gas temperature with a radiation pyrometer or by line reversal spectroscopic technique. These were not very satisfactory because of trouble with water and soot accumulation on the windows and air leakage through the openings in the inner brick lining. These sighting ports were removed for run 15. It is hoped that this facility will be reinstalled with an improved design to provide valuable information on the correlation of temperature measurement by various methods.

Quick Cooler. A diagram of the quick cooler is shown in Figures 1 and 3. The inner tube is a one inch O.D. type 316 stainless steel tube, 0.065 inch thick. A sliding O-ring seal at the end of the water jacket takes care of the thermal expansion of this tube.

The quick cooler is designed to cool very rapidly a gas flow of 0.1 lb./sec. from about 2500°K. to 1350°K. Furnace temperatures greater than 2500°K. were to be handled by adjusting water flow rates to the quick cooler to promote boiling with the resulting high boiling heat transfer coefficient. However, a quick cooler probe (½ inch O.D.) was found to be necessary to provide the additional cooling.

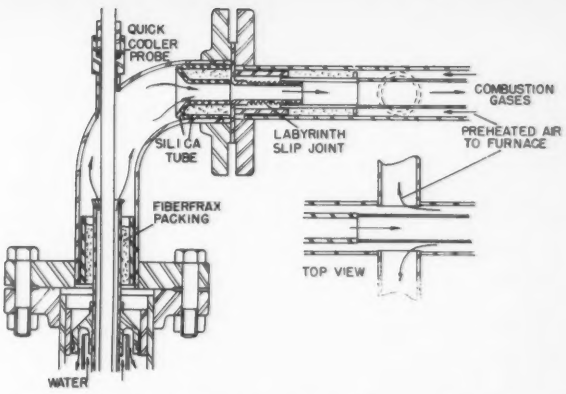

Figure 3—Quick cooler head and labrynth slip joint.

Instrumentation

The instrumentation of this facility consists essentially of thermocouples for the higher gas temperatures; resistance thermometers for the low gas temperatures and for the water temperatures; rotameters for the measurement of flow rates.

Optical and radiation pyrometers are used for those temperatures beyond the range of thermocouples. Pressure regulators are installed in the propane, air, and oxygen lines to ensure steady flow rates and an automatic pressure controlling valve is used to control the pressure in the furnace. Finally, numerous safety devices are used to provide some measure of safety in case of emergency. Details are provided in reference[16].

Modifications to Facility

For runs No. 11 and 12 certain changes were made in the furnace and quenching system in order to test the effectiveness of air quenching, water quenching and kinetic quenching.

Mixing Zone and Quenching Probes

Sketches of the quenching air manifold, the water spray probe, and the mixing zone are shown in Figures 4 and 5.

The purpose of the mixing chamber and the various probes is to determine the effectiveness of quenching the nitric oxide with a jet of cold air or with a spray of water directed into the mixing zone.

Once the effectiveness of air quenching is established, it is proposed to recycle, as the quenching gas, part of the cold exhaust gases containing nitrogen dioxide to prevent dilution of nitrogen dioxide concentration that occurs when quenching with air. The mixing zone is constructed from standard interlocking zirconia bricks held together with zirconia cement. It is roughly

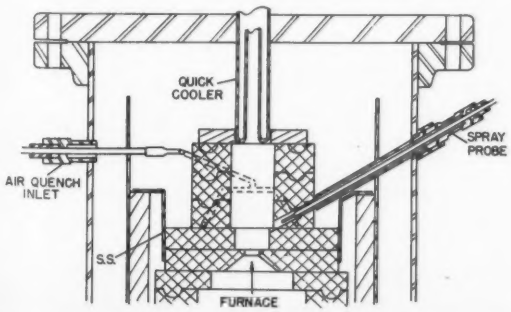

Figure 4—Mixing chamber with water spray probe and air quench manifold (side view).

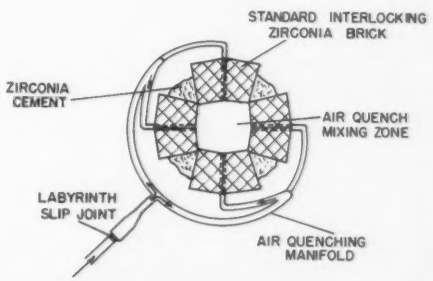

Figure 5—Mixing chamber and air quenching manifold (top view).

2¾ inches square and has a height of 7 inches. Also, the port through which the water spray probe is inserted can be used alternatively as a sight port to measure flame temperature, and radiation and absorption characteristics simply by removing the probe and screwing on the sight glass holder.

Quenching Nozzle

One type of quenching nozzle shown in Figure 6(a) consists of a coil in the shape of a nozzle and is made from a length of ¼" O.D. type 310 stainless steel tube. A machined type is shown in Figure 6(b). The nozzle is expected to cool the combustion gases by the acceleration of the gases through the nozzle. The kinetic energy thus acquired must come from the internal energy of the gases. The directed kinetic energy comes at the expense of the mean random molecular energy and since random molecular motion is responsible for collision, it is reasonable to assume that reaction rate is a function of the static temperature of the gas rather than the total temperature[11].

The relation between the total temperature and static temperature is given as follows:

$$t = T - \frac{V^2}{2Cp}$$

Thus for a gas velocity of 2500 ft./sec. in the nozzle with a length of about 0.1 feet, the temperature drop $(T - t)$ is 280°C. and the cooling rate is 3.5×10^6°C./sec.

Performance of the Facility

(1) Zirconia Brick Furnace

The zirconia brick furnace has been successfully operated with estimated flame temperatures exceeding 3000 °K. The interlocking zirconia bricks have stood up quite well and have retained their original shape after a total running time of almost 100 hours at temperatures of 2200°K. to over 3000°K. However, tiny cracks have begun to appear near the inner surface of the bricks, due probably to the thermal shocks encountered during the relatively rapid heating and cooling of the furnace. The average rate of heating the bricks has been of the order of 300°C./hr. up to Run No. 10. For the following runs the heating rate was reduced to about 100°/hr. with the result that no further damage to the interlocking bricks was evident.

For run 15 further improvements were made (see Figure 7). The air was injected radially close to fuel inlets and hence there was rapid mixing with little or no chance of the fuel jetting or leaking anywhere except up into the furnace. Further improvements were incorporated in the sealing arrangement at the top of the furnace. These included a more positive seal with fibrefrax rope, allowing for expansion; better seals for the air inlet tubes and spring loading of the top of the furnace to improve the sealing of the upper plates. Better sealing was installed to prevent any back diffusion of the propane to the bottom of the furnace.

(2) Mixing Chamber

Considering the severe thermal shocks the zirconia bricks in the mixing zone have stood up fairly well when air alone was injected into the mixing zone. However, inspection after Run No. 12, during which water was sprayed into the mixing zone, revealed the bricks to be in poor condition. Almost all of the bricks were cracked and many had pieces broken completely off.

The mixing of the cold air with the hot combustion gases has been unsatisfactory due probably to the swirling effect that occurred during the mixing with the result that the denser cold air is centrifuged out while the hot gases passed up through the center, hindering a rapid transfer of heat. This centrifuging effect was confirmed in Run no. 12 when gas samples taken near the inside wall of the mixing chamber showed zero concentrations of carbon dioxide. As a result, yields of nitric oxide in the gases for an air quench process are appreciably lower than those for the quick cooler quench process.

(3) Quenching Nozzle

The quenching nozzle has readily withstood the high gas temperatures although a considerable knocking sound was emitted during the run due to the violent formation of steam inside. Actually the kinetic quenching principle has not yet been given a fair test because of the leakage that occurs between the nozzle and the quick cooler entrance and because of another leakage between the coils of the nozzle. In the test on the type shown in Figure 6(b) there were difficulties with unstable combustion and bypass leakage in the furnace and no reliable results have been obtained.

(4) Quick Cooler

The quick cooler, unfortunately, did not have the heat transfer capacity predicted by the design calculations so that the maximum permissible gas temperature was 2350°K. instead of 2500°K. The optimum design gas temperature drop from 2800°K. to 1400°K. was calculated to be obtainable only by means of a boiling water coefficient to provide a greater overall heat transfer coefficient. However, because of the extremely high gas temperatures, it was felt that due to an excessive temperature difference the boiling coefficient was diminished by superheated vapor boiling with the result that the inner quick cooler tube would be overheated. Consequently, the quick cooler by itself is capable of safely cooling the gas from a maximum temperature of only 2350°K. at a quenching rate up to 150,000°C./sec.

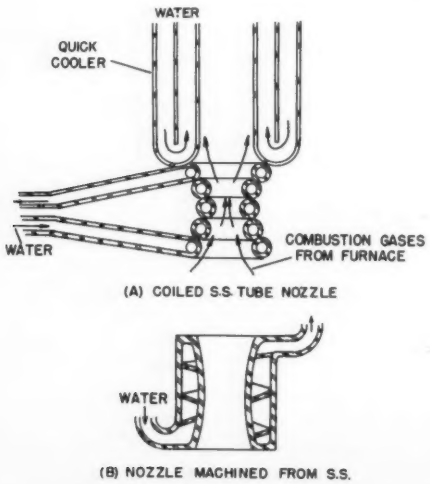

Figure 6—Quenching nozzles.

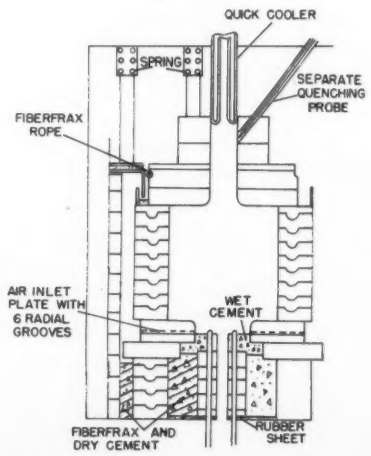

Figure 7—Modified furnace construction for run No. 15.

The experimental overall heat transfer coefficients were found to be lower than the theoretical coefficients as predicted by the equations in McAdams[17]. This discrepancy is probably due to the thin layer of carbon soot that deposited on the quick cooler tube. The amount of fine carbon particles collected after the run from the quick cooler tube was calculated to give a layer thickness of 0.008 inches. Calculations of the theoretical heat transfer coefficients with this layer of soot brought these values down to within 5% of the experimental heat transfer coefficients. The soot deposition is the result of the poor combustion in the relatively cold furnace at the time of the quick cooler insertion. Once the soot collects on the tube surface the water cooling effect keeps the temperature of the carbon particles below the ignition point: — thus preventing the soot from burning off.

(5) **Quick Cooler Probe**

The quick cooler probe was designed and constructed when it was discovered that the quick cooler alone could not handle normal gas flows at temperatures exceeding 2350°K. With this probe gas temperatures exceeding 3000°K. could be permitted in the furnace without any trouble. This probe also lends flexibility in controlling the exhaust gas temperature simply by varying the depth of the probe in the quick cooler. Furthermore, by lowering the probe down to the lower tip of the quick cooler, the quenching rates can be more than doubled from the combined effects of faster gas velocity, higher heat transfer rate, and greater heat transfer surface.

(6) **Air Preheater**

The air preheater has functioned quite successfully. The preheater was designed to provide an air preheat temperature of 1000°K. and experimentally, 1030°K. has been achieved without difficulty. The inside tube is made of type 310 stainless steel which has the highest heat resistance properties among the stainless steels. For the preheater, the theoretical heat transfer coefficients are close to the experimental values since no carbon particles could accumulate in the inner tube due to the tube's high temperature which allows the carbon to burn off.

(7) **Separate Quenching Probe**

Since there were operational problems in run 13 using the water-cooled quenching nozzle welded to the quick cooler it was removed for runs 14 and 15. A separate quenching probe (see Figure 7) was provided to permit a study of the effect of a varied quenching rate which would not influence the overall operation and to provide an independent estimate of gas temperature.

Results

Quick Cooler Quenching

The results of Runs no. 6 to 12 are presented here. Those of the previous runs can be used only as indications since the true temperatures in the furnace could not be calculated due to the lack of by-pass data in the slip-joints.

The results with quick cooler quenching are plotted in Figures 8 and 9 and tabulated in Table 1*. In Figure 8 the oxygen concentration includes the oxygen made available when the carbon dioxide and water vapor dissociate at the high temperatures prevailing in the furnace. Only those results that gave three or more points through which a curve can be drawn are plotted for the sake of simplicity. The points of Figure 9 are obtained from a more detailed set of curves similar to those in Figure 8.

In Table 1, "T_F" is the temperature of the gases leaving the furnace and is calculated by a series of heat balances using published mean values for Cp[18]. The effect of dissociation of carbon dioxide and water vapor is considered in the calculation of "T_F". The absolute value of "T_F" is probably not accurate to more than plus or minus 50°K., but since the factors contributing to this inaccuracy are approximately the same for each temperature determination, the calculated temperatures relative to each other for the purpose of drawing trends should be quite reliable.

The quenching rates for the last three temperatures in Table 1 are not given since they could not be calculated due to the fact that the quick cooler probe was not inserted down to the tip of the quick cooler. For those high gas temperatures, further lowering of the probe into the hot gas stream would have caused violent boiling to take place in the probe with a serious threat of probe failure. The first column of "% O_2" in Table 1 shows the oxygen concentration calculated from the complete combustion of propane going into the furnace. These values have been periodically checked with values obtained from the back calculation from the Orsat analysis of the exhaust gases. The "% O_2" in the second column includes the additional oxygen from the dissociation of part of the carbon dioxide and water vapour into carbon monoxide, hydrogen, and oxygen. The "% NO" in the last column of Table 1 is the nitric oxide concentration actually in the furnace as calculated from the

*Table 1 of this paper has been deposited as Document No. 6437 with the ADI Auxiliary Publications Project, Photoduplication Service, Library of Congress, Washington 25, D.C. A copy may be obtained by citing the Document No. and by remitting $1.25 for photoprints, or $1.25 for 35 mm. microfilm. Advance payment is required. Make cheques or money orders payable to: Chief, Photoduplication Service, Library of Congress.

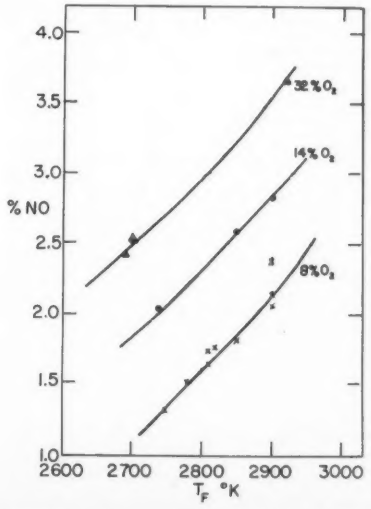

Figure 8—"NO" concentration as function of furnace gas temperature.

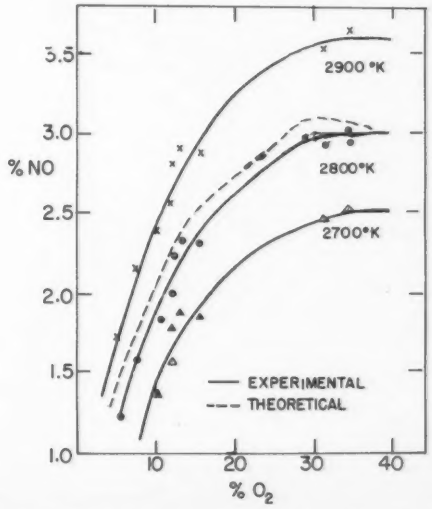

Figure 9 — "NO" concentration as function of oxygen concentration.

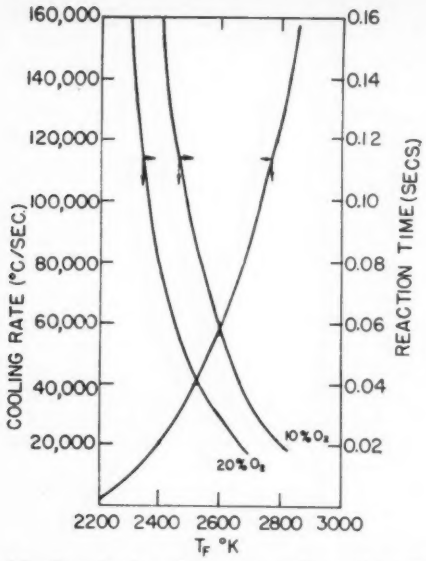

Figure 10—Required cooling rate and reaction time (to form 90% equi. conc.) as a function of furnace gas temperature.

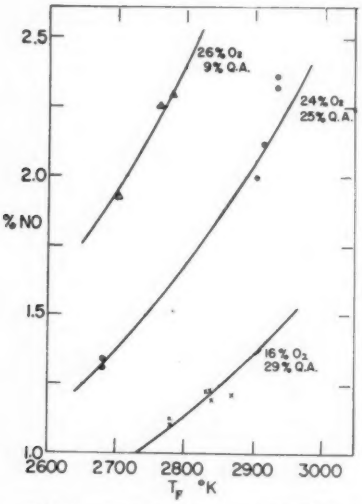

Figure 11—"NO" concentration as function of furnace temperature for air quenching.

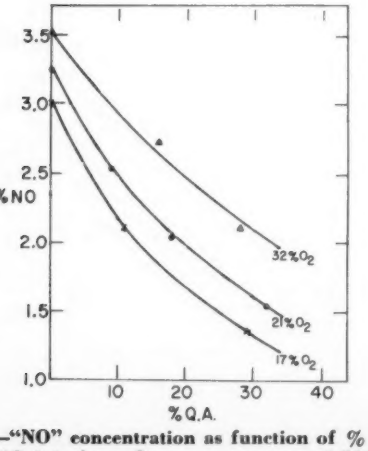

Figure 12—"NO" concentration as function of % quenching air (Q.A.), for a flame temperature of 2900°K.

"NO" analysis of the exhaust gases after most of the water is condensed. The methods of sampling and analysis are described elsewhere[16].

Figure 10 presents the cooling rates and reaction times theoretically required for fixing and forming nitric oxide as a function of furnace gas temperature. The curves are obtained from the extrapolation of data presented in a paper by Gilbert and Daniels[7].

Air Quenching (Q.A.)

The results with air quenching are plotted in Figures 11 and 12. Figure 11 shows the "NO" concentration as a function of furnace gas temperature when quenching with air and Figure 12 shows the NO concentration as a function of percent quenching air. (Q.A.) Here again, the oxygen concentration and the percent quenching air are the average of the individual points on the curves.

Separate Quenching Probe

The values obtained for furnace gas temperatures are not too reliable because of experimental and operating difficulties (e.g., unforeseen problems with water condensation in the lines resulting in inaccurate measurement of the gas flow and the relatively large heating of the probe by the gases flowing on the outside and by radiant heating). However the results as given in Table 2 indicate that in the region of 3000°K. the oxygen concentration appears to have less effect on the NO yield than at lower temperatures.

The quenching rate was about 2×10^6°C./sec. to 1500°K. and 0.62×10^6°C./sec. to 500°K. at the outlet of the 0.125 inch I.D. tube.

Discussion of Results

Figure 9 indicates that the nitric oxide yield increases rapidly with temperature and that concentrations of nitric oxide greater than 4% should be obtained quite readily. Actually for the purpose of nitric oxide recovery the "NO" concentration in the exhaust gases will be about 20% greater than that in the furnace since the water vapor formed from combustion is condensed out with but a minor loss of nitrogen dioxide. As a result, the "NO" concentration for purposes of recovery can be as high as 5%.

The quenching process at the highest temperature is unsatisfactory since the maximum quenching rate of 150,000°C./sec. obtainable without a quick cooler probe is far too low to effectively quench any nitric oxide at temperatures over 3000°K. This fact is clearly indicated in the curve of Figure 11 which shows the relationship between required quenching rates and gas temperatures.

Figure 10 shows that nitric oxide concentration increases with oxygen concentration at a decreasing rate and indicates that for the conditions prevailing in the experimental runs, the maximum yield of nitric oxide will be obtained at about 38%

TABLE 2

SUMMARY OF RESULTS FROM RUN NO. 15

(Using separate quenching probe)

Reaction Time = 0.25 seconds

Furnace Pressure = 75 p.s.i.a.

Test No.	T_F (corrected for dissociation) °K	% O_2 In Furnace	% O_2 + % O_2 from dissociation.	% NO
9	2810	14.5	17.4	3.5
10	2870	14.6	18.2	3.0
11	2860	23.7	26.7	3.3
12	2935	30.3	33.7	3.5
13	2960	35.9	39.3	3.4
14	2980	44.1	47.6	3.7

oxygen concentration. Theoretically, the maximum yield should be obtained when the gases contain equal molar concentration of oxygen and nitrogen. The maximum equal molar concentration of oxygen and nitrogen is a function of the air preheat temperature which determines the amount of fuel required to heat the gases up to reaction temperature. A higher preheat temperature means lower fuel consumption which, in turn, means less carbon dioxide and water vapor. Thus for a given reaction temperature, the point of maximum yield increases with higher preheat temperatures. For the experimental preheat temperatures of about 1000°K., the maximum equal molar concentrations of oxygen and nitrogen are found to be about 35% from the Orsat analysis of the exhaust gases. This is in agreement with the theoretical curve for 2800°K. in Figure 9. This curve which gives the equilibrium concentrations of nitric oxide for a preheat temperature of 850°K. using propane as the fuel, reaches a maximum at approximately 35% oxygen concentration. The discrepancy between the theoretical 35% and the experimental 38% for the point of maximum yield is well within the range of possible errors. Figure 10 also shows that concentrations of nitric oxide close to their theoretical equilibrium concentrations can be achieved with but a small loss during quenching.

Figure 11 reveals that for the air quench process, the nitric oxide yields also increase rapidly with temperature but they are considerably lower than those for the quick cooler quench process. The ineffectiveness of air quenching is more clearly shown in Figure 12 where the NO yield decreases rapidly with increase in the amount of quenching air. The reason for the rather poor results may be that the quenching air is not mixing thoroughly with the hot combustion gases but is kept separated by a centrifugal effect in the mixing zone causing the far denser cold air to centrifuge out and spiral around the core of hot gases. It is quite conceivable that if this centrifugal effect can be eliminated, quenching by air can be as effective as quick cooler quenching.

Although some results were obtained with the quenching nozzle and water spray quenching, these results are too meager to be included in this report. Additional work with more rigid control will have to be performed to obtain more reliable data.

The results with the separate quenching probe are preliminary and serve to point up the great difficulties of accurate temperature control and measurement in the region of 3000°K. and over. The decreased effect of oxygen on the yield of nitric oxide has been predicted by Wise and Baker[15] but the quenching rate may still not be high enough. The yield of 3.5% NO at 3000°K. is about one half the equilibrium concentration of 7.2% calculated by Larsen *et al*[18].

Conclusions

Nitric oxide concentrations up to 3.7% have been obtained with every indication that with higher gas temperatures, nitric oxide yields above 4% should readily be realized.

Extension of the curves to temperatures beyond 3000°K. and to oxygen concentrations beyond 50% would be of considerable interest since in both curves, the points of maximum yield can thus be determined.

Acknowledgements

The authors wish to thank C. B. Purves for his initial assistance and continued interest in the project. J. J. Gravel has been most helpful on instrumentation. S. K. Fang assisted with the project for a period of about one year. Several of the Gas Dynamics Laboratory Shop Staff (most notably B. Takats) have helped in the construction and operation.

The financial assistance of the Canadian Defence Research Board is gratefully acknowledged.

Nomenclature

C_p = specific heat in absolute mechanical units.
t = static temperature of gas.
T = total temperature of gas.
T_F = flame temperature.
V = mean velocity.

References

(1) Mordell, D. L., Purves, C. B., and Thompson, A. L., Gas Dynamics Laboratory, Note N 9, 1955.

(2) Mordell, D. L., Thompson, A. L., Yano, G., and Lin, T., Gas Dynamics Laboratory, Report No. R 39, 1953.

(3) Foster, G. E., and Daniels, F., Ind. and Eng. Chem., **43,** 986-992, 1951.

(4) Foster, G. E., Ph.D., Thesis, University of Wisconsin, 1945.

(5) Nichols, G. S., Ph.D., Thesis, University of Wisconsin, 1952.

(6) Fauser Process, J. Chem. Eng., **238,** Jan., 1952.

(7) Gilbert, N., and Daniels, F., Ind. and Eng. Chem. **40,** 1719-23, 1948.

(8) Henrickson, W. G., and Daniels, F., Ind. and Eng. Chem. **45,** 2613-15, 1953.

(9) The Wisconsin Process for Nitrogen Fixation–Sunflower Project–Wisconsin Alumni Research Foundation.

(10) Moving Pebble Bed Heat Exchanger, Chemical Engineering News, April 5, 1954, **32,** No. 14, p. 1388.

(11) Penner, S. S., Quenching by DeLaval Nozzle, Chemical Reactions in Flow Systems, Butterworth Scientific Publications, 1955.

(12) Weisenberg, I. J., and Winternitz, P. F., [illegible]. Symposium on Combustion, p. 813.

(13) Duvall, G. E., High Temperature–A Tool for the Future; Proceedings of a Symposium at Berkeley in 1956, p. 53.

(14) Sage, B. J., Same book as reference 13, on pages 210-211, questions and in Report on trip to California in June 25-27, 1956, by A. L. Thompson (G.D.L. Note N 27).

(15) Wise, H., and Baker, D. I., Kinetics of Fixation of Atmospheric Nitrogen at Elevated Temperatures, J. Chem. Phys. Vol. 21, No. 10, 1904-05, October 1953.

(16) Yano, G., Thompson, A. L., and Mordell, D. L., Gas Dynamics Laboratory, Report R 44, October, 1955.

(17) McAdams, W. H., Heat Transmission, 3rd Ed., 1954, McGraw-Hill.

(18) Larsen, A. et al, C. A., **50,** 9833 f, 1956 and Kgl Norske Vickvskal Solskabs Forh **27,** 156-62, 1954 (Pub. 1955 in English).

★ ★ ★

The Efficiency of Fibrous Aerosol Filters:

Deposition by Diffusion of Particles of Finite Diameter[1]

RALPH E. PASCERI[2] and S. K. FRIEDLANDER[2]

A brief review is given of the derivation of a semi-theoretical expression for the filtration efficiency of fibrous aerosol filters operated at low velocities. The correlation is compared with new data taken from the literature and is presented in a simplified form for design calculations. The existence of a minimum filtration efficiency is discussed and theory and data are compared.

In a previous paper, one of the authors [1] reviewed the theory and some of the literature of aerosol filtration and proposed a semi-empirical expression for the efficiency of fibrous filters. Using this expression it was possible to correlate the data of a number of investigators with some success. In this paper, the correlation is presented in alternate forms and applied to additional data taken from the literature.

The usual model of the fibrous filter is an array of cylinders placed in the aerosol flow. Since the fibers are most often randomly oriented, an average removal efficiency is defined by the expression:

$$\eta = b/d_F \quad \ldots\ldots (1)$$

For a filter with fraction solids α, in a differential distance, dh, in the flow direction, the total length of fiber per unit cross section normal to the flow is $\alpha dh/(\pi d_F^2/4)$. The fraction of particles removed in the volume represented by dh is:

$$-\frac{dN}{N} = \frac{b\alpha dh}{(\pi d_F^2/4)} \quad \ldots\ldots (2)$$

Rearranging and integrating from $h = 0$ to $h = H$ gives:

$$\eta = \frac{\pi d_F}{4H\alpha} \ln N_1/N_2 \quad \ldots\ldots (3)$$

In an experimental determination of η, the practice is to measure N_1 and N_2, the inlet and outlet concentrations, respectively, of a homogeneous aerosol passed through the filter, and an average fiber diameter, d_F, by microscopic examination. The value of η so determined is a function of time although little information on the relationship is available [2]. Most of the data refer to initial efficiencies of fresh filters and the discussion will be limited to such systems.

The central problem of filtration theory is the prediction of η from the characteristics of the aerosol and filter. It is customary to assume that η depends on five effects, namely, impaction or impingement, diffusion, direct interception, sedimentation, and electrical precipitation. The experimental work of Chen [3,4] and of Wong and Johnstone [5,6] indicated that a range existed in which only diffusion and direct interception were of importance. Friedlander [1] has shown that for these two regions it is possible to derive limiting theoretical laws for the cylindrical geometry. Assuming that efficiencies were additive, he proposed a form for the dependence of the efficiency on the Peclet (or Schmidt) number, the direct interception parameter, and the Reynolds number. The derivation is reviewed in the next section.

Derivation of an Expression for the Efficiency

The usual model chosen for efficiency calculations is the single cylinder placed normal to the aerosol flow. In the region very near the surface of the fiber, it is assumed that the velocity parallel to the surface can be written in the form

$$u = B(N_{Re})\, F(x) y \quad \ldots\ldots (4)$$

The parameters u, x, and y are dimensionless ratios with respect to gas velocity and fiber diameter. Applying boundary layer theory to the thin concentration boundary layer near the cylinder surface gives an expression for the filtration efficiency by diffusion alone of the form [7]:

$$\eta \sim B^{1/3} N_{Pe}^{-2/3} \quad \ldots\ldots (5)$$

Removal by direct interception alone is given by

$$\eta = \int_0^{N_R} u\, dy \quad \ldots\ldots (6)$$

N_R being the direct interception parameter

The integral is evaluated at the value of x at which the particle streamline comes closest to the surface of the cylinder. Substituting Equation (4) for the velocity distribution and integrating gives:

$$\eta \sim B N_R^2 \quad \ldots\ldots (7)$$

Contrary to the statement often found in the literature, the direct interception efficiency does depend on the gas velocity since the shape of the streamlines depends on the Reynolds number.

On a logarithmic plot of $\eta\, N_R\, N_{Pe}$ *vs* $(BN_{Pe}\, N_R^3)^{1/3}$, a slope of unity should be obtained for small values of $(BN_{Pe}\, N_R^3)^{1/3}$ (pure diffusion) while a slope of three would be expected for large values of this parameter. In [1], this was found to be approximately true when it was assumed that

$$B \sim N_{Re}^{1/2} \quad \ldots\ldots (8)$$

Comparison with Experimental Data

The data used in the original correlation were for the most part those of Chen and Wong, Ranz, and Johnstone for liquid aerosols composed of dioctyl phthalate or sulphuric acid. Subsequently, it was found that additional data, taken by Thomas and Yoder [8], using dioctyl phthalate were available and these are included in the correlation shown in Figure 1. For the data shown, droplet diameters ranged from 0.15 to 1.1 microns and glass fibers from 1.5 to 9.57 microns in diameter. In agree-

[1]*Manuscript received March 8; accepted July 12, 1960.*
[2]*Department of Chemical Engineering, The Johns Hopkins University, Baltimore, Maryland.*

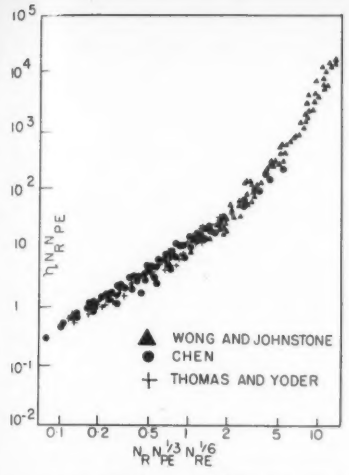

Figure 1—Recalculated data of several investigators showing characteristic slopes of about 3 for large values of the abscissa and 1 for small values.

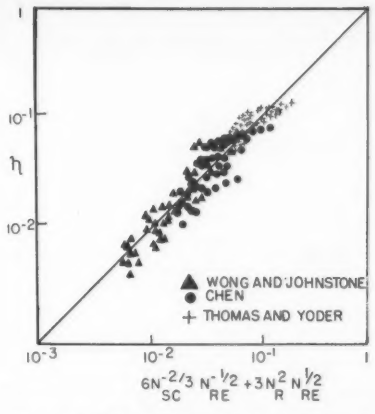

Figure 2—Recalculated data of several investigators compared with empirical equation.

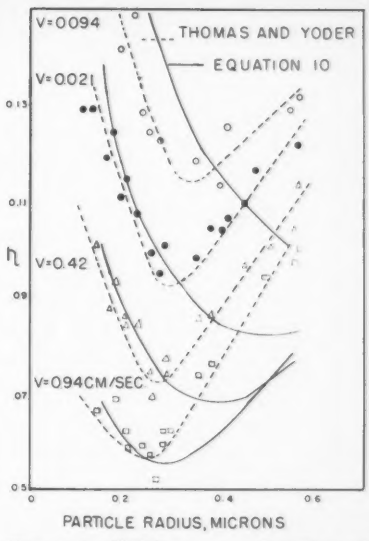

Figure 3—Efficiency as a function of particle diameter compared with empirical equation. Recalculated data of Thomas and Yoder [8].

ment with the theoretical prediction, a single-valued function is obtained with a slope of about three at high values of $N_R N_{Pe}^{1/3} N_{Re}^{1/6}$ and about one for lower values. There seems to be no influence of the impaction parameter which, for the data shown, ranged from $5(10)^{-4}$ to 1. At values of the impaction parameter greater than 1, the scatter became appreciable showing the increased importance of the impaction mechanism. The data in Figure 1 can be represented approximately by the expression:

$$\eta N_R N_{Pe} = 6(N_R N_{Pe}^{1/3} N_{Re}^{1/6}) + 3(N_R N_{Pe}^{1/3} N_R^{1/6})^3 \quad \ldots\ldots\ldots (9)$$

This expression can also be written in a form more useful for design calculations:

$$\eta = 6N_{Sc}^{-2/3} N_{Re}^{-1/2} + 3N_R^2 N_{Re}^{1/2} \quad \ldots\ldots\ldots (10)$$

The data are replotted in Figure 2 with Equation (10) represented by the 45° line. The diffusion and direct interception ranges do not appear as separate regions in this figure.

Sedimentation was of importance in the experiments of Thomas and Yoder who ran at low velocities. They found a clearly defined maximum in their plot of penetration *vs* particle diameter which they ascribed to the interaction between diffusion and sedimentation. Their data are replotted in Figure 3 as efficiency *vs* particle diameter along with the semi-empirical correlation Equation (10). The agreement between data and correlation is seen to be very good indeed along the lower branch of the curve where diffusion alone is of importance. The upper branches agree best at the higher velocities at which sedimentation is least important. Hence our analysis indicates that the minimum was a result of the interaction among diffusion, sedimentation, and direct interception with direct interception more important at the higher velocities and sedimentation controlling at the lower velocities. The deviation of Equation (10) from the data of Thomas and Yoder is reflected in Figure 2 by the scatter below the 45° line at the upper end of the data.

It should be noted that the data upon which the correlation is based are for high porosity fiber beds. The data of Chen and of Wong and Johnstone were both extrapolated to zero fraction solids while those of Thomas and Yoder were taken at $\alpha = 0.005$. The effect of porosity on efficiency is difficult to estimate. In the direct interception region Wong found little variation over a rather limited range. Chen found a linear relationship

$$\eta = \eta_o (1 + 4.5\alpha) \quad \ldots\ldots\ldots (11)$$

In the absence of more complete information, it is suggested that Equation (9) be used with the actual velocity (superficial velocity/$(1 - \alpha)$).

Acknowledgement

This work was supported by U.S. Public Health Service Grant S-85 (C1) and A.E.C. Contract AT (30-1)-2165.

Nomenclature

Roman Symbols

- b = average width corresponding to a region of flow completely cleared of particles, microns
- B = dimensionless function of N_{Re}.
- d_f = average diameter of a fiber, microns
- h = distance along flow direction in filter, cm.
- H = thickness of filter, cm.
- N = particle concentration of a homogeneous aerosol, number/cc.
- N_{Pe} = Peclet number.
- N_R = direct interception parameter.
- N_{Re} = Reynolds number based on fiber diameter.
- N_{Sc} = Schmidt number.
- u = velocity parallel to a surface, dimensionless with respect to mainstream velocity
- x = distance along a surface measured from the forward stagnation point, dimensionless with respect to fiber diameter
- y = distance normal to a surface, dimensionless with respect to fiber diameter

Greek Symbols

- α = fraction of solids, dimensionless
- η = average removal efficiency, dimensionless

References

(1) Friedlander, S. K., Ind. Eng. Chem., **50,** 1161 (1958).
(2) LaMer, V. K., Report No. NY0-512, Columbia University (1951).
(3) Chen, C. Y., Annual Report, Contract DA 18-108-CML-4789, Eng. Exp't. Station, Univ. of Ill. (Jan. 30, 1954).
(4) Chen, C. Y., Chem. Revs. **55,** 595 (1955).
(5) Wong, J. B., and Johnstone, H. F., Tech. Rep't. No. 11, Eng. Exp't. Station, University of Ill., Oct. 31, 1953.
(6) Wong, J. B., Ranz, W. E., and Johnstone, H. F., J. Appl. Phys. **27,** 161 (1956).
(7) Friedlander, S. K., A.I.Ch.E. Jour. **3,** 43 (1957).
(8) Thomas, J. W., and Yoder, R. E., A.M.A. Arch. Ind. Health, **13,** 545 (1956).

★ ★ ★

Design of Steam Tracing Systems for Protection Against Freezing[1]

W. S. COTTON[2]

Process or service pipe lines containing materials which freeze readily must be protected during shutdown periods in cold weather. The desired temperature may be maintained in the pipe by installing a steam-heated tube under the pipe, and enclosing both the pipe and tracer tube with the insulation. A rational thermal design method has been developed which permits the estimation of the heating requirements. The method may also be applied to tracers containing other heating media.

Steam tracing systems are generally installed to prevent the freezing of materials in process or service lines during shutdown periods in cold weather. Also, process liquids having relatively high melting points require protection against freezing throughout the year. In specific cases, vapor lines may require tracing to keep the temperature of the pipe wall above the dew-point in order to avoid condensation; this is particularly necessary in suction lines of compressors and in the vicinity of gas meters if the vapor is at or near its saturation temperature.

The usual method of tracing a pipe is to install a steam-heated tube on the underside of the pipe and to cover both the tracer line and pipe with insulation. The desired temperature is maintained in the pipe by transferring heat from the tracer to the air space between the pipe and insulation and then from the air space to the pipe.

This paper reviews methods of calculating heat losses from insulated pipes. The transfer of heat in the confined space between the pipe and insulation is considered and a rationalized method for the design of tracer systems is presented. Installation techniques for tracing systems are also discussed.

Description of Tracing Systems

Figures 1 and 2 illustrate a method of installing a single tracer tube on a pipe line. The tracer tube is installed underneath the pipe and separated from it by 0.25-in. thick × 1-in. long asbestos rings spaced at approximately 1 ft. centres along the tracer line. The tracer is held securely against the pipe by means of wires twisted around the tube and looped over the pipe.

[1]*Manuscript received June 15, 1959; accepted August 25, 1960.*
[2]*Engineering Department, Du Pont of Canada Limited, Montreal, Que.*
Based on a paper presented at the C.I.C. 42nd Annual Conference, Halifax, N.S., May 25-27, 1959.

The rings provide an air space between the tracer and the pipe. They are effective in restricting the tube wall temperature and are of value when the material contained in the pipe is sensitive to heat so that conduction between the hot tracer and pipe must be avoided. Since the insulation must be at least one size larger than the pipe, the spacers also assist in making the insulation fit tightly over the pipe and tracer assembly. The size of the spacer ring can be chosen to provide a tight fit in any specific case. Alternatively, small blocks of asbestos board can be inserted between the pipe and spacers.

When two tracers are required to provide the necessary heat, they may be installed as shown in Figure 3.

Alternative Methods

Steam jacketting is sometimes employed to prevent freezing of material in a pipe but this method is expensive and would not normally be used unless close temperature control or a high rate of heat input is desired. Another means of obtaining rapid heating is to clamp the tracer directly under the pipe and to join them by continuous welding [1], or with a cement consisting of carbon and sodium silicate. In these cases the transfer of heat is mainly by conduction and the pipe temperature will approach that of the heating medium. Another alternative tracing system is extruded aluminum pipe with an oval-shaped tracer which forms an integral part of the pipe.

Although steam is the most usual medium for maintaining pipe temperatures at the required level, other heat sources may be substituted. When a wax or polymer is to be protected against freezing, Dowtherm vapor may be used in place of steam. In this case particular attention should be given to the transient heating condition that occurs during the start-up period to avoid freezing of the Dowtherm condensate. When dealing with a material which is particularly sensitive to heat, a hot liquid tracing system may be specified. Under these circumstances, the hot water or anti-freeze solution is circulated at a sufficiently high rate so that the temperature drop of the tracing liquid is small and the rate of heat transfer is relatively uniform. The proposed method for determining the heat transfer requirements in tracing systems utilizing spacer rings may be applied to any type of heating medium.

Design Basis

Tracing systems are generally designed to maintain the required pipe temperature during periods of no-flow. Normally no attempt should be made to raise the temperature of the material in the line under flowing conditions because the transfer

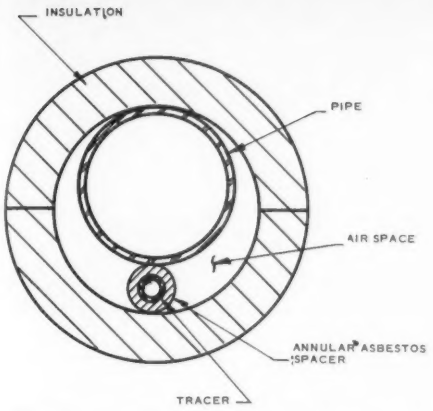

Figure 1—Location of a single tracer under a process pipe.

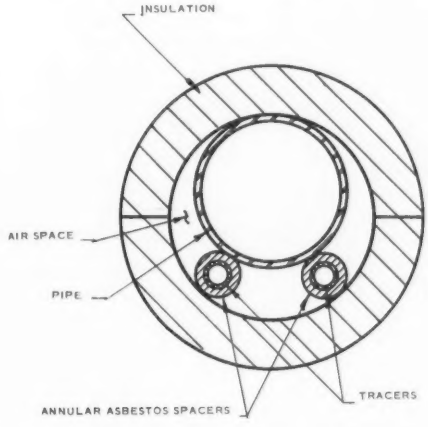

Figure 3—Installation of two tracers under a pipe.

of heat by tracers is extremely inefficient when compared to conventional methods of heating. Owing to lack of specific experimental information on the transfer of heat in enclosed spaces having a variable cross-sectional area, it is necessary to use a rational design method to select the proper size of tracer tube. The method to be described should provide adequate protection against freezing in the absence of a more fundamental approach.

Review of Heat Losses from Pipes

The loss of heat from an insulated cylinder takes place by the mechanism of convection through the fluid film on the inside surface of the pipe, conduction through the pipe wall and insulation and then by convection and radiation from the outer surface of the insulation into the surrounding air. Equation (1) permits the calculation of the heat loss per foot length of cylinder, all resistances except those of the insulation and air film being neglected.[2] The significance and dimensions of the symbols used in the following equations are given in the Nomenclature.

$$q = \frac{\pi (t_p - t_a)}{\frac{2.3}{2k} \log (D_o/D_i) + \frac{1}{h_a D_o}} \quad \ldots\ldots (1)$$

The heat transfer coefficient, h_a, is the combined coefficient of radiation and convection between the outside surface of the insulation and the ambient air. When the heat loss is occurring to still air, the transfer of heat is by natural convection and for

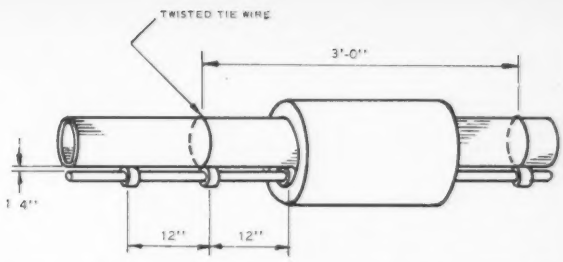

Figure 2 — Method of installing a single tracer using asbestos spacers.

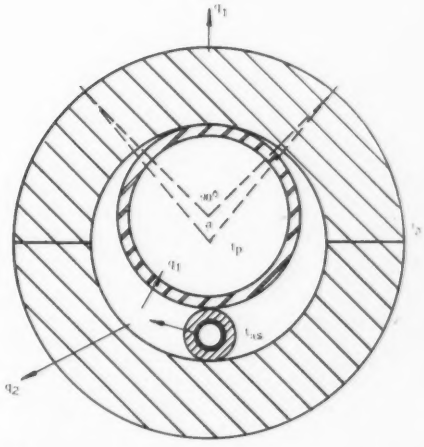

Figure 4—Flow of heat in a tracer system.

a horizontal cylinder may be computed from the following dimensional equation[3].

$$h_{nc} = 0.27 (\Delta t/D_o)^{0.25} \quad \ldots\ldots (2)$$

For cases of forced convection, the heat transfer coefficient for air may be obtained from a dimensional equation which applies for N_{Re} from 1,000 to 50,000 and for a film temperature of 200°F.[3]

$$h_{fc} = 0.11 C_p G^{0.6}/D_o^{0.4} \quad \ldots\ldots (3)$$

The transfer of heat by radiation between two surfaces, separated by a non-absorbing medium, may be computed from Equation (4)[3].

$$q_r = 0.171 \epsilon A F \left[\left(\frac{t_1 + 460}{100}\right)^4 - \left(\frac{t_2 + 460}{100}\right)^4\right] \quad \ldots\ldots (4)$$

The geometric factor, F, depends only on the shape and relative orientation of the emitting and receiving surfaces. In the case of pipes which are radiating heat to the atmosphere the geometric factor is unity. It is convenient to convert Equation (4) to a heat transfer coefficient which can be used directly with the convection coefficient as shown in Equation (5).

$$h_r = 0.171 \epsilon F \left[\left(\frac{t_1 + 460}{100}\right)^4 - \left(\frac{t_2 + 460}{100}\right)^4\right]/(t_1 - t_2) \quad \ldots (5)$$

Since the transfer of heat by convection and radiation takes place simultaneously, the combined coefficient of radiation and convection becomes the sum of the two individual coefficients.

$$h_a = h_r + h_c \quad \ldots\ldots (6)$$

When calculating heat losses for outside conditions with the wind blowing, little accuracy is lost if the outside surface

of the insulation is assumed to be at the ambient air temperature and only conduction through the insulation is considered. Under these conditions, Equation (1) will be approximated by Equation (7).

$$q = \frac{2\pi k (t_p - t_a)}{2.3 \log (D_o/D_i)} \quad \ldots\ldots\ldots\ldots\ldots\ldots (7)$$

Flow of Heat in Tracer Systems

Theoretically there will be a line of contact between the top outside surface of the pipe and the inside surface of the insulation as shown in Figures 1 and 3. Although some types of insulation are quite rigid, in time the weight of the insulation, vibration of the pipe, or the tension of the clamps holding the insulation together may cause a portion of the pipe surface to come in contact with the insulation. When this occurs, heat is lost at a rate q_1 from the pipe by conduction through the top surface of the insulation as shown in Figure 4.

If the pipe is to be maintained at the desired temperature, the heat lost from the top section of the insulation must be replaced by an equal amount transferred from the air space to the pipe. Thus, the rate q_1, due to the driving force $t_p - t_a$ is balanced by the heat supplied by the driving force $t_{as} - t_p$. Heat is also transferred from the remaining section of the insulaton at a rate q_2 under the influence of the driving force $t_{as} - t_a$. It is evident that the tracer must supply the total amount of heat lost from both sections of the insulation.

$$q_t = q_1 + q_2 \quad \ldots\ldots\ldots\ldots\ldots\ldots (8)$$

Heat leaves the tracer by natural convection and radiation. The transfer of heat by the mechanism of natural convection from the tracer to the air space and from the air space to the pipe is complex and will be discussed in more detail in the section which follows. The heat radiated from the tracer will be absorbed by both the inside surface of the insulation and the pipe. It is proposed to neglect the radiation between the tracer and pipe since it can be shown[3] that when the diameter of the tracer is small compared to the diameter of the pipe and located close to it as shown in Figure 4, the geometric factor, F, is such that a relatively small fraction of the heat is transferred directly. In this case, the tracer can see but a small fraction of the pipe area and, in addition, the curvature of the surfaces results in ineffectual transfer of the radiation.

TABLE 1

SELECTED VALUES OF EMISSIVITY AT THE TEMPERATURE RANGE OF TRACER SYSTEMS.

Material	Emissivity
Aluminum	0.055 – 0.20
Brass	0.029 – 0.22
Copper	0.072 – 0.40
Steel	0.66 – 0.80
Stainless Steel	0.44 – 0.80
Cast Iron	0.80 – 0.95
Asbestos	0.95

Since air is a non-absorbing medium, the radiation proceeds from the tracer to the inside surface of the insulation and is almost completely absorbed because of the high absorptivity (or emissivity) of insulating materials. Heat is then radiatep from the insulation surface to the process pipe by virtue of the temperature difference which exists between the surfaces.

Typical values of emissivity are shown in Table 1[3]. Ranges are given for the values as temperature and condition of the surface exert a considerable influence on the emissivity.

Flow of Heat in Confined Air Spaces

A general equation for the transfer of heat by natural convection from surfaces of various shapes and positions is shown below.

$$N_{Nu} = C (N_{Gr} + N_{Pr})^n \quad \ldots\ldots\ldots\ldots\ldots\ldots (9)$$

In the laminar flow region, characteristic of steam tracing systems, 0.53 and 0.25 have been reported as values for C and n respectively for horizontal cylinders[3]. Simplified equations for the heat transfer coefficients from heated surfaces to air at ordinary temperatures and atmospheric pressure may be derived by substituting values for the physical properties of air in the general equation. This is the manner in which Equation (2) has been obtained.

When a heated horizontal cylinder is placed in still air, eddy currents are set in motion by the buoyancy of the air as it becomes heated. It has been found[4,5,7] that air within 0.4 in. of the sides and bottom of the cylinder becomes warmer than the ambient air and flows upward, while from the top surface of the cylinder it rises without restriction.

However, in the restricted air spaces of tracing systems there is a limitation imposed on the movement of the air currents and it would not be expected that heat would be transferred at the rate predicted by Equation (2).

The effect of restricting the air currents on the transfer of heat between concentric horizontal cylinders has been investigated by Beckman[6,7]. His correlation accounts for the fact that when the clearance between the cylinders is small, heat is transferred mainly by conduction. As the gap is increased the flow of heat is by the mechanism of natural convection. When the diameter of the outside cylinder becomes large the rate of heat transfer approaches that given by Equation (2).

The data of Beckman have been transposed into the form of Equation (9) and values of the constant C have been determined in order to establish the effect of restricting the eddy currents. It will be seen from Figure (5) that depending on the magnitude of the Grashof Number when the diameter ratios lie in the range 1.5 to 2.5, the rate of heat transfer is reduced to 55-65% of the rate obtained on a single horizontal cylinder. The correction to the heat flow rate owing to the nearness of the tracer and the other components of the tracing system has been termed the "proximity factor". For calculating the rate of heat transfer in tracing systems, a value of 50% is suggested.

Performance of Tracing Systems

Details of tracing systems which have operated for at least two winters are given in Table 2. Their performance from a

TABLE 2

DESIGN INFORMATION ON EXISTING TRACER SYSTEMS

Line Designation	Pipe Diam. in. IPS	Pipe Metal	Tracer Outside Diam. in.	No. of Tracers	Tracer Metal	Nominal Insulation Size in. IPS	Nominal Insulation Thickness in.
A	3	Aluminum	$\frac{5}{8}$	1	Aluminum	4	2
B	3	Carbon Steel	$\frac{1}{2}$	1	Copper	4	2
C	2	Carbon Steel	1	2	Copper	4	2
D	$1\frac{1}{2}$	Carbon Steel	$\frac{1}{2}$	1	Copper	$2\frac{1}{2}$	2

TABLE 3

THERMAL CONDITIONS OF EXISTING TRACER SYSTEMS

Line Designation	Average Temp. of Heating Medium, °F.	Freezing Point of Process Material, °F.	Calculated Temp. of Process Material °F.	Ambient Air** Temperature °F.	Heat loss B.t.u./(hr.) (ft.)
A	150*	32	43	−10	15
B	274	32	85	−40	35
C	250	125	136	−40	49
D	274	64	92	−40	27

* Antifreeze solution, 25 wt.% methanol in water
** Wind velocity taken as 20 miles/hr.

thermal stand point has been satisfactory. The design conditions along with the heat losses and estimated pipe temperatures are shown in Table 3. The calculated values were obtained by the procedure outlined below in which the numerical constant of Equation (2) has been reduced by multiplying it by a 0.5 proximity factor. In addition to compensating for the restricted air movement in the confined spaces of the tracing system, it also allows for imperfections in the insulation after it has been in service for some time as well as any weakness in the design method. It can only be inferred from the data that the proximity factor does not have to be smaller than 0.5. Conversely, the upper limit of the proximity factor is approximated by values shown in Figure 5.

Design Procedure

General

The designer must decide on a reasonable minimum process temperature based on the freezing point of the material under consideration. It is suggested that a value between 10 and 25°F. above the freezing point will provide a good basis for design. When the ambient temperature increases to the freezing point of the process material, the pipe temperature will rise if the tracer system is in operation. Using a trial and error procedure, the maximum temperature of the pipe can be calculated. Should this temperature be unacceptable, a hot circulating solution can be substituted as a heating medium. Sufficient flexibility can be incorporated into the design of the liquid heater to permit adjustment of the temperature of the liquid to suit the ambient condition.

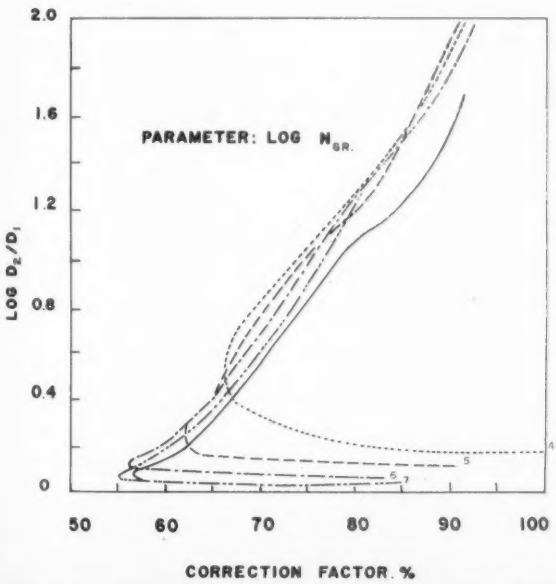

Figure 5 — Effect of diameter ratio on the rate of heat transfer between horizontal concentric cylinders.

Detailed Design Procedure

The design of tracing systems is readily carried out by the following procedure: -

1. Select a trial diameter for the tracer and a suitable spacer size to fit into a standard diameter of pipe insulation.
2. The angle α, as shown in Figure 4, is the angle subtended from the centre line of the insulation to the points where a 90° angle from the centre line of the pipe intersects the outside surface of the insulation. This may be determined by making an accurate layout. However, little accuracy is lost if it is assumed to be 75°. The normal variation is between 70 and 80°, and the calculation is not particularly sensitive to such changes in α.
3. After choosing the thickness of insulation to be used and obtaining its thermal conductivity, calculate the heat loss, q_1, from Equations (1) or (7) corrected for the angle of contact.
4. Assume a temperature difference of 10°F. between the air space and pipe. Using the diameter of the pipe, calculate the convection coefficient from Equation (2) and multiply the result by 0.5. Calculate the radiation coefficient from Equation (5). The value for the emissivity is taken as the product of the emissivities of the insulation and pipe. The sum of the two coefficients calculated above is the heat transfer coefficient for the air space, h_a.
5. Estimate the area of the pipe exposed to the air space as approximately 75% of the total area, and from the value of q_1 and h_a obtain the temperature difference $t_a - t_p$. If this is significantly different from the assumed value, recalculate items 4 and 5 for the new value of Δt.
6. Using the air space temperature, calculate the heat lost from the lower section of the insulation as in item 3, correcting it for the angle of contact, $(360 - \alpha)$.
7. Obtain the rate of heat flow to be supplied by the tracer from Equation (8).
8. Calculate the heat transfer coefficient of the trial tracer size. Using the tracer diameter, calculate the convection coefficient from Equation (2) and multiply the result by a proximity factor of 0.5. Calculate the radiation coefficient from Equation (5). The value for the emissivity is taken as the product of the emissivites of the insulation and the tracer. The sum of the heat transfer coefficients of radiation and convection is the heat transfer coefficient of the tracer, h_t.
9. Estimate the heat given off by the tracer. If it equals the amount required or exceeds it by a reasonable margin, the trial tracer diameter is satisfactory.

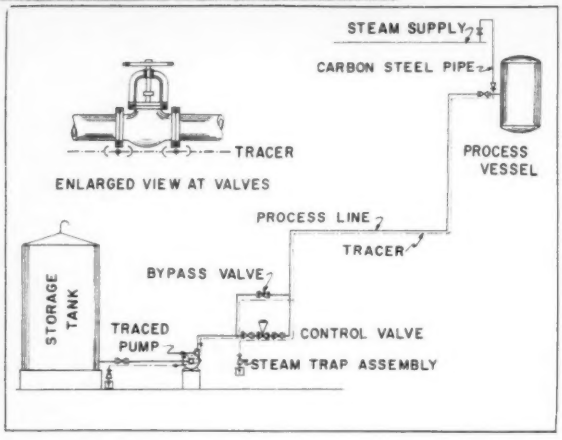

Figure 6—Typical steam tracing system.

10. Should a revision be necessary, a new spacer arrangement and tracer size should be selected to fit into a standard insulation diameter. Alternatively two tracers could be considered.

The above procedure is illustrated by the following example.

Example

Problem

Design a steam tracing system for a 3-in. IPS horizontal line to maintain its contents at a minimum temperature of 60°F. The line is to be operated out-of-doors where the ambient air temperature is −20°F. minimum. Steam at 25 lb./sq. in. ga. is to be used to heat a copper tracer. The insulation thickness is 1½ in.

Solution

Assume a trial tracer diameter and spacers to fit into a standard insulation.

O.D. of process pipe	3.500 in.
trial tracer diameter	0.500 "
	4.000 "
I.D. of insulation	4.500 "
Total thickness of spacers	0.500 "

From Figure 4, $\alpha = 80°$; $k = 0.30/12$ B.t.u./(hr.)(sq.ft.)(°F./ft.)

$$q = \frac{2\pi k\,\Delta t}{2.3 \log D_o/D_i} = \frac{2\pi\,0.30 \times \Delta t}{2.3 \times 12 \times \log(7.50/4.500)} = 0.309\,\Delta t \quad (7)$$

heat loss from pipe, q_1

$$q_1 = 0.309\,(t_p - t_a)\,(\alpha/360) = 0.309\,(60 + 20)\,(80/360) = 5.5 \text{ B.t.u./(hr.)(ft.)}$$

Estimate $t_{as} - t_p = 10°F.$ $\quad D_o = 3.5/12$ ft.

$$h_{ac} = 0.27(\Delta t/D_o)^{0.25} = 0.65 \text{ B.t.u./(hr.)(sq.ft.)(°F.)} \quad (2)$$

From Equation (5) the radiation coefficient for a black body using $t_p = 60°F.$ and

$t_{as} = 70°F.$ is 1.00 B.t.u./(hr.)(sq. ft.)(°F.)
$h_r = 1.00\,\epsilon_i\epsilon_p = 1.00 \times 0.95 \times 0.66 = 0.628$
$h_{as} = (0.5 \times 0.65) + 0.628 = 0.953$ B.t.u./(hr.)(sq.ft.)(°F.) . . . (6)
$A_p = 0.75 \times 3.50 \times \pi/12 = 0.686$ sq. ft./ft.
$\Delta t = t_{as} - t_p = q_1/(A_p \times h_{as}) = 5.5/(0.686 \times 0.953) = 8.4°F.$ (Close enough)

Heat loss from air space, q_2

$q_2 = 0.309\,(t_{as} - t_a)\,(360 - \alpha)/360$
$= 0.309\,(68 + 20)\,(360 - 80)/360 = 21.2$ B.t.u./(hr.)(ft.)

Heat required from tracer = $q_1 + q_2 = 5.5 + 21.2 = 26.7$ B.t.u./(hr.)(ft.)

Tracer coefficient, h_t

$\Delta t = t_t - t_{as} = 266 - 68 = 198°F.$ $\quad D_i = 0.5/12 = 0.0416$ ft.
$h_c = 0.27(\Delta t/D_i)^{0.25} = 0.27(198/0.0416)^{0.25} = 2.21$ B.t.u./(hr.)(sq.ft.)(°F.)
$h_r = 1.75\,\epsilon_i\,\epsilon_i = 1.75 \times 0.95 \times 0.072 = 0.12$
$h_t = (0.5 \times 2.21) + 0.12 = 1.22$
$A_t = 0.5 \times \pi/12 = 0.131$ sq.ft./ft.

Heat available from tracer = $h_t\,A_t\,\Delta t$
$= 1.22 \times 0.131 \times 198 = 31.7$ B.t.u./(hr.)(ft.)

The 0.500-in. diameter tracer is satisfactory since it provides more heat than required.

Installation Techniques

Steam Supply

Steam pressures between 50 and 100 lb./sq. in. ga. are generally preferred for tracing systems because they preclude difficulties in transporting the condensate along the tracer line towards the steam trap. With pressures in this range, the maximum length of tracer line is about 200 ft. Any steam pressure over 15 lb./sq. in. ga. may be utilized, however, if the length of the tracer line is carefully selected so that the pressure drop is reasonable.

Arrangement

The flow in a tracer line should start at the high point in the system and flow towards the lowest point where the trap is installed. It is important to slope the lines and to avoid low points between the steam supply and the trap as freezing may result when the tracer system is shut down. When low points cannot be eliminated from a piping system, an auxiliary trap may be installed. Figure 6 shows a typical arrangement.

The steam is taken from the top of the supply line say with ½-in. black iron pipe and connected to the tracer at the high point of the system. Joints in the tracer tube should be provided at each flange so that if a section of pipe is removed for maintenance purposes, the tracer can be easily disconnected and later reinstalled without damage. It should be noted that the tracer line is kept horizontal when it goes around flanges or valves.

It is obvious that the connections must be tight if leaks are to be avoided and the insulation is to retain its efficiency.

Insulation Covering

Normal installation techniques for insulation and covering are followed for enclosing the tracer system. The two halves of preformed pipe insulation may be secured by steel bands to provide a tight assembly. It has been found that if the top and bottom sections of the insulation are staggered, more rigidity is obtained.

To ensure a good fit between the insulation and tracer system, there should be no greater than ⅛-in. difference between the inside diameter of the insulation and the sum of the diameters of spacer ring and pipe. It is not undesirable for the inside diameter of the insulation to be up to ¼-in. smaller than the sum of the pipe and ring diameters because a tight fit can be obtained by scoring the insulation with a linoleum knife in the vicinity of each spacer ring.

Selection of Tracer Materials

Tracers may be constructed of standard weight pipe or tubing. The latter is preferred since it is cheaper to install, particularly around valves, pumps, etc. and problems arising from thermal expansion are avoided. When uncoiled and installed under a pipe, tubing is seldom perfectly straight thus allowing it to flex between the spacers when the heat is turned on.

Owing to the stiffness of the larger sizes of tubing it is better to limit the diameter to ¾-in.; because of pressure drop limitations, the minimum recommended diameter is ⅜-in.

Conclusions

A method of designing tracing systems has been described which has given satisfactory service in a variety of applications at Company plants. The method offers an advantage where heat sensitive materials are to be protected against freezing. If moderate overheating of a process material is not a consideration, the method provides a satisfactory alternative to bonding the tracer to the pipe and transferring heat by conduction.

Nomenclature

A = Area of heat transfer, sq. ft.
C = Constant, dimensionless
C_p = Specific heat at constant pressure, B.t.u./(lb.) (°F.)
D = Diameter, ft.
F = Geometric factor, dimensionless
G = Mass velocity, lb./(hr.) (sq. ft.)
g = Acceleration due to gravity, 4.18×10^8 (ft./hr.)/hr.
h = Heat transfer film coefficient, B.t.u./(hr.) (sq. ft.) (°F.)
k = Thermal conductivity, B.t.u./(hr.) (sq. ft.) (°F./ft.)
n = Exponent, dimensionless
L = Length, ft.
N_{Gr} = $D^3\rho^2 g\beta\,\Delta t/\mu^2$, Grashof Number, dimensionless
N_{Nu} = hD/k, Nusselt Number, dimensionless
N_{Pr} = $C_p\mu/k$, Prandtl Number, dimensionless
N_{Re} = DG/μ, Reynolds Number, dimensionless
q = Heat flow, B.t.u./hr.
t = Temperature at any point, °F.
α = Angle, degrees
β = Coefficient of expansion, $1/t$
ϵ = Emissivity of surface, dimensionless
Δt = Temperature difference, °F.
ρ = Density, lb./cu. ft.
μ = Absolute viscosity, lb./(hr.) (ft.)

Subscripts

a = Ambient air
as = Air space
c = Convection, forced or natural
fc = Forced convection
i = Inside, insulation
nc = Natural convection
o = Outside
p = Pipe
r = Radiation
t = Tracer
1, 2 = Position 1, 2

References

(1) Barton, E., and Williams, E. V., British Chemical Engineering, **2,** 598 (1957).

(2) Kern, D. Q., "Process Heat Transfer", McGraw-Hill Book Company, New York (1950).

(3) McAdams, W. H., "Heat Transmission", 3rd ed., McGraw-Hill Book Company, New York (1954).

(4) Ray, B. B., Proc. Ind. Assoc. Cultivation Sci., **5,** 95 (1920).

(5) Kennard, R. B., J. Research Nat. Bur. Standards, **8,** 787 (1932).

(6) Beckman, W., Forschung Bd., **2,** 165 (1931).

(7) Jakob, M., "Heat Transfer", John Wiley & Sons, Inc., New York (1953).

★ ★ ★

The Development of the Alum-Amine Process for the Recovery of Alumina from Shale[1]

G. THOMAS[2] and T. R. INGRAHAM[2]

Based on a review of the extensive published literature on the recovery of alumina from clays and shale, sufficient experimental work was done on a bench scale to establish a flow sheet whereby these materials might be treated for the recovery of cell-grade alumina. The significant step in the processing is the recovery of potassium alum, and its purification by either recrystallization or liquid-liquid extraction.

In Canada, aluminum metal is produced from alumina recovered from bauxite. Since bauxite is found principally in tropical regions, it follows that the aluminum industry in Canada is totally dependent upon imported bauxite or alumina.

To decrease this dependence upon foreign materials, many attempts[1-20] have been made to utilize the resources of clays and shales on this continent. None of the processes devised to date have succeeded in displacing the Bayer alumina process, but several of the processes have features which are of interest when assessed against the background of hydrometallurgical techniques developed in the last 15 years.

At the Mines Branch of the Department of Mines and Technical Surveys, various processes for producing alumina have been reviewed, and some of the better features from several have been combined with liquid-liquid extraction techniques into an integrated process for the production of cell-grade alumina. The chemical feasibility of the scheme has been investigated on a laboratory scale by the treatment of a Canadian shale.

The experimental work was done on a typical shale from a large eastern Canadian deposit. The chemical analysis of the raw shale is: 58.2% SiO_2, 23.0% Al_2O_3, 6.1% Fe_2O_3, 3.5% K_2O, 1.7% MgO, 1.3% Na_2O, 1.3% C, 0.9% TiO_2, 0.8% CaO, 0.1% S, 0.09% P_2O_5, and the remainder L.O.I. Based on the mineralogical and chemical analyses, the estimated composition of the raw shale is as follows: quartz, 35%; muscovite, 32%; clay minerals, 12%; chlorite, 11%; andalusite, 6%; magnetite, 2%; iron sulphides, 1%; and carbonaceous matter, 1%.

Preliminary Experiments

When the shale was baked with an equal weight of concentrated H_2SO_4, a sulphated product was obtained from which 93% of the aluminum was extractable in 0.5% *v/v* H_2SO_4. The other constituents (except silica) of the sulphated shale are also soluble, e.g., 95% of the iron and 86% of the potassium.

When sulphated shale was leached with a small amount of 0.5% *v/v* H_2SO_4 and then filtered, a hot concentrated leach liquor was obtained. On cooling the liquor, a viscous crystalline mass of aluminum sulphate, with minor amounts of potassium alum, was obtained which was difficult to filter. Washing of this mass to remove the large amount of entrained iron-bearing mother liquor from the crystals was unsatisfactory.

In contrast, by the addition of sufficient potassium sulphate to the hot concentrated leach liquor for the complete conversion of aluminum sulphate to potassium alum prior to cooling, well-defined, readily-filterable, octahedral crystals of potassium alum were formed which contained only 0.12% Fe. By recrystallizing and washing the impure crystals with equal weights of water, potassium alum crystals containing 0.003% Fe were obtained. Calculations show that alum crystals of this purity would give, after decomposition and leaching, an alumina product that would meet cell-grade specifications for iron.

It seemed worthwhile, therefore, to investigate the alum approach more fully by experiments designed to determine whether it could be applied to the shale sample under study.

Leaching of Sulphated Shale

The first stage of the alum process to be investigated was the leaching of sulphated shale. For this purpose, a 2000 g. sample of sulphated shale, to which 430 g. K_2SO_4 was added for alum formation, was leached with 3300 ml. H_2O for 30 min. at 95°C. The slurry was filtered, and the hot filtered leach liquor was cooled and centrifuged to separate the alum crystals from the mother liquor. The filter residue was repulped twice with boiling water, filtered, and washed again with boiling water. The results are shown in Table 1.

From Table 1, it is evident that about 77% of the soluble aluminum was extracted from the sulphated shale in the initial leaching. In this stage, the Al:Fe ratio was changed from 3:1 in the sulphated shale to 45:1 in the alum crystals which contained 0.12% Fe. An over-all extraction of about 95% of the soluble aluminum was obtained when the residue was repulped and washed. These wash solutions would be suitable for use, instead of fresh water, in the leaching of sulphated shale.

TABLE 1

RECOVERY OF ALUM BY LEACHING SULPHATED SHALE WITH WATER

Sample	Wt (g)	Vol (ml)	Al (g)	Fe (g)	Cum. % Extn.*	
					Al	Fe
Head	2000		133.4*	50.4*		
Alum crystals	1640		91.1	2.0	68.3	4.0
Mother liquor		1560	11.2	29.8	76.7	63.1
1st wash		2850	19.2	1.1	91.1	65.3
2nd wash		6820	4.7	0.3	94.6	65.9
Residue	700		11.5			

*Based on % sol Al and sol Fe in 0.5% *v/v* H_2SO_4.

[1]*Manuscript received January 30; accepted June 27, 1960.*
[2]*Extraction Metallurgy Division, Mines Branch, Department of Mines and Technical Surveys, Ottawa, Ont.*
Contribution from the Extraction Metallurgy Division, Mines Branch, Department of Mines and Technical Surveys, Ottawa, Ont.

Removal of Iron from Mother Liquor

To investigate the removal of iron from mother liquor, synthetic solutions were prepared which were saturated at room temperature with alum and contained 10-20 g. Fe/1. Lime (CaO) was added to these solutions to raise the pH to 2.5. The mixtures were heated for 2.5 hr. at 95°C., to assist in the precipitation of iron by hydrolysis, and then the iron precipitates were removed by filtration. Under these conditions of neutralization and hydrolysis, it was possible to remove about 80% of the iron, and about 20% of the aluminum, from synthetic mother liquors. Since mother liquors contain about 10% of the aluminum extracted from sulphated shale (see Table 1), a precipitation of 20% of the aluminum from mother liquor corresponds to an over-all aluminum loss of only 2%. When the iron precipitates, which contained hydrated iron oxides and jarosite, $K_2SO_4 . Fe_2(SO_4)_3 . 4\ Fe\ (OH)_3$, were thermally decomposed and leached, potassium sulphate and an iron product were recovered.

To determine whether the iron removal treatment of mother liquors could be simplified by combining the separate stages of leaching and hydrolysis, several samples of sulphated shale were heated at 95°C. for various periods of time, with synthetic mother liquors containing 10 and 20 g. Fe/1. It was found that by leaching sulphated shale for about 10 minutes with mother liquor, a 15% extraction of iron from the shale was obtained. By using longer leaching periods, 1 to 8 hr. to facilitate hydrolysis, there was no net extraction of iron from the shale but there was a decrease of from 14 to 76% of iron in the liquors. At the same time, all of the aluminum in the recycled mother liquor was recovered, together with 86 to 90% of the aluminum from the sulphated shale. Hence, a combination leaching-hydrolysis stage for sulphated shale is possible for the extraction of aluminum into the liquor and the rejection of iron, by hydrolysis, into the shale residue.

Purification of Alum Crystals

Impure alum crystals, obtained from the leaching of sulphated shale and containing 0.12% Fe, were used in the purification experiments. Slurries of 1:1 mixtures of alum and water by weight were heated to about 90°C. to dissolve the impure alum, and then cooled to crystallize the purified alum. After filtration, the crystals and wash liquors were moved countercurrently in a 4-stage countercurrent crystallization circuit. These tests were continued until steady-state conditions were obtained, and in the four successive stages the alum was found to contain, respectively, 0.01% Fe, 0.002% Fe, 0.0005% Fe, and 0.0003% Fe.

As an alternative to recrystallization, it was found possible to use liquid-liquid extraction to remove iron. Experimentally, an aqueous slurry of 25 g. of moist, freshly prepared impure alum crystals (0.12% Fe) in 25 ml. of water was shaken with 100 ml. of a 5% *v/v* Primene JM* solution in kerosene. The organic phase was decanted from the aqueous slurry, and the purified crystals which were separated from the aqueous solution by filtration contained 0.004% Fe. The purified alum crystals, after a second treatment with fresh water and fresh organic solution contained 0.0005% Fe. The Primene solution, therefore, effected an almost complete removal of iron from the alum.

As shown by countercurrent liquid-liquid extraction tests, Primene solution removes mainly iron and only traces of aluminum. Under the steady-state conditions of one experiment, the aqueous phase was found to contain 0.002 g. Fe/1 and 50 g. Al/1, whereas the organic phase contained 3.2 g. Fe/1 and 0.04 g. Al/1. Other preliminary results from the countercurrent tests indicate a consumption of 3 to 4 lb. CaO and 0.1 to 0.2 lb. Primene, per lb. iron removed from Primene, during the regeneration of Primene for recycling. These results indicate that reagent costs should be low when Primene is used to remove the relatively small amounts of iron in the alum crystals.

*Primene JM is a primary amine from the Rohm and Haas Company, Philadelphia 5, Penn., U.S.A.

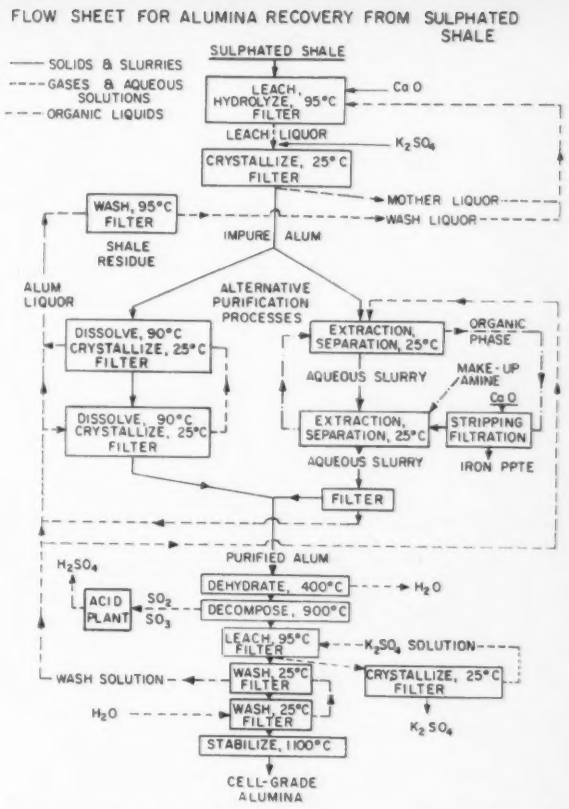

Figure 1—Flow sheet for alumina recovery from sulphated shale.

Recovery of Alumina from Alum

The feasibility of preparing alumina from alum has already been established in a pilot plant investigation in the United States[9]. In a few experiments at the Mines Branch laboratories at Ottawa, pure chemical grade alum was dehydrated in an oven at 400°C. and, after pulverization of the fragile porous mass, the powder was decomposed at about 900°C., at a shallow bed depth of 0.5 cm. in a muffle furnace. In other tests, alum was decomposed in a fluidizer, which consisted of a vertical 1 in. diameter silica tube, fitted at its base with a silica cloth for supporting the charge over the gas inlet. Alum was added slowly to the fluidizer at 900°C. for flash decomposition and brief fluidization. All calcines were then leached with water for the removal of potassium sulphate from the alumina. The results from these tests show that, under suitable conditions, the alum can be treated by decomposition and leaching to yield an alumina containing only small amounts of potassium, e.g., 0.08 — 0.13% K.

Recovery of Alumina from Shale

Having prepared a suitable alumina from pure alum, experiments were done to determine whether cell-grade alumina could be obtained from shale, by the foregoing process. For this purpose, three samples of sulphated shale, to which the requisite amount of potassium sulphate had been added, were leached at 95°C. with hot water. The hot filtered leach liquors were cooled, and the resultant alum crystals were separated from the mother liquor by a basket centrifuge or by a sintered glass filter. The alum was recrystallized and washed several times for the removal of iron, and the purified alum was decomposed at 900°C. By leaching the calcine with water for the removal of potassium sulphate, an alumina product was obtained. The purity of the alumina from these tests is given in Table 2.

TABLE 2
PARTIAL ANALYSIS OF ALUMINA RECOVERED FROM SULPHATED SHALE

Sample	Fe (%)	K (%)	Na (%)	Si (%)	Cu (%)	Ti (%)	V (%)	Pb (%)	Mg (%)	Ni (%)	Ca (%)	Cr (%)	B (%)
1	0.09*	0.04*	nd*	0.05	0.03	0.001	<0.01	0.005	0.015	nd	0.03	0.003	0.001
2	0.015*	0.14*	nd*	0.08	0.04	0.001	<0.01	0.02	0.01	0.004	nd	nd	0.001
3	0.005*	0.18*	nd*	na	0.002*	0.04*	<0.01*	0.02	0.01	nd	nd	nd	na

*Chemical analysis. The others are by semi-quantitative spectrographic analysis.
nd None detected.
na Not available.

The purity of these alumina products compares favorably with Kalunite alumina from which commercially acceptable aluminum metal has been prepared[7]. The impurity level is slightly in excess of that obtained by the Bayer process, but some improvement might be expected if specific precautions were taken to keep the impurity level low.

A flow sheet for connecting the various steps suggested by these experiments has been sketched and is shown in Figure 1. The flow sheet was investigated by operating the process on a small-scale cyclic basis. In these cyclic tests, 100 g. samples of sulphated shale were leached at 95°C. for 1 hr. with 200 ml. of mother liquor and then with 200 ml. of wash liquor. By filtration, the leach solution was separated from the shale residue, which was washed first with 150 ml. of alum liquor and then with 50 ml. of fresh water. The hot filtered leach liquor, to which was added about 20 g. K_2SO_4, was cooled at 25°C. to form impure alum crystals and mother liquor.

In the cyclic tests, about 94% of the soluble aluminum from the sulphated shale was recovered in the form of impure alum crystals. These alum crystals contained about 0.2% Fe. In subsequent cycles, the accumulation of sulphuric acid from the hydrolysis of ferric sulphate gradually decreased the extent of hydrolysis so that the recycle mother liquor and the alum crystals contained increasing amounts of iron. However, by the addition of CaO to the leaching stage, for neutralizing the acid and thereby permitting continued hydrolysis of iron from the liquor, alum crystals of low iron content were again obtained. The impure alum crystals were purified by the use of equal weights of water in a 5-stage countercurrent crystallization circuit. A spectrographic analysis of products indicated the removal, from the crude alum crystals, of not only iron but also sodium, magnesium, calcium, titanium, and smaller amounts of other contaminants.

The purified alum crystals were dehydrated in silica trays at 400°C. and decomposed at 900°C. with the off-gases being vented to the atmosphere. The decomposed alum was leached at 95°C. and washed at 25°C. for the removal of potassium sulphate from the alumina. The cold wash solution was used in the crystallization circuit for the purification of crude alum. The hot leach solution from the leaching of decomposed alum, after cooling and filtering to remove K_2SO_4 crystals, was reheated and recycled for leaching additional K_2SO_4. The K_2SO_4 crystals were recycled to the head of the circuit to form alum. Alumina from the cyclic tests was of a purity comparable to that in Table 2. Additional experimental investigations based on the flow sheet are now in progress, to determine whether large-scale pilot plant work is warranted. Any final judgment as to the relative merits of this method of producing alumina will have to await an economic assessment based on pilot plant data.

References

(1) J. D. Edwards, F. C. Frary and Z. Jeffries, The Aluminum Industry; Vol. 1, Aluminum and its Production, 358 pp. McGraw-Hill Book Co. Inc., New York, 1930.

(2) G. S. Tilley, R. W. Millar and O. C. Ralston, Acid Processes for the Extraction of Alumina. U.S. Bureau of Mines, Bull. **267,** 1-82 (1927).

(3) J. H. Walthall, P. Miller and M. M. Striplin, Jr., Development of a Sulphuric Acid Process for Production of Alumina from Clay. Trans. Am. Inst. Chem. Engrs. **41,** 53-140 (1945).

(4) T. G. Pearson, The Chemical Background of the Aluminium Industry. Roy. Inst. Chem. Lectures, Monographs and Repts. No. **3,** 103 pp. (1955).

(5) S. Weeks and H. B. McCoy, Materials Survey, Aluminum Office of Defence Mobilization, U.S. Dept. of Commerce (1956).

(6) A. Fleischer, The Kalunite Process. Trans. Am. Inst. Mining Met. Engrs. **159,** 267-79 (1944).

(7) A. Fleischer and J. Glasser, Production of Aluminum from Kalunite Alumina. J. Metals **3,** (Trans. 191), 634-6 (1951).

(8) H. Pedersen, Production of Pure Alumina from Clay. Tids. Kemi Bergvaesen, **3,** 161-4, 175-8 (1923); **4,** 11-7, 55-6 (1924); Chemical Abstracts **18,** 1882 (1924).

(9) C. T. Baroch, A. W. Hackwood and P. G. Knickerbocker, Pilot Plant Investigations—Preparation of Alumina from Potassium Alum. U.S. Bureau of Mines, Rept. Invest. **3845,** 1-26 (1946).

(10) C. C. Popoff, Cowlitz Clay Deposits near Castle Rock, Washington. U.S. Bureau of Mines, Rept. Invest. **5157,** 1-60 (1955).

(11) W. R. Seyfried, The Ammonium Sulphate Process for the Extraction of Alumina from Clay and its Application in a Plant at Salem, Oregon. Am. Inst. Mining Met. Engrs., Mining Technology **12,** Tech. Pub. 2473, 12 pp. (1948).

(12) C. C. March, Investigations into Methods of Producing Pure Alumina from Kaolin by Sulphate Leaching. State College of Washington, Bull. E-4, 1-40 (1943).

(13) R. C. Haff, Method of Recovering Alumina from Alumina-Bearing Ores. U.S. Pat. 2, 551, 944, Apr. 19, 1947.

(14) O. Redlich, C. C. March, M. F. Adams, F. H. Sharp, E. Holt and J. Taylor, Extraction of Alumina from Clay. Ind. Eng. Chem. **38,** 1181-7 (1946).

(15) J. I. Hoffman, R. T. Leslie, H. J. Caul, L. J. Clark and J. D. Hoffman, Development of a Hydrochloric Acid Process for the Production of Alumina from Clay. J. Research Natl. Bur. Standards **37,** 409-28 (1946). (Research Paper 1756).

(16) W. Fulda and H. Ginsberg, Tonerde und Aluminum, Vol. i. W. DeGruyter and Co., Berlin, 1951.

(17) H. W. St. Clair, S. F. Ravitz, A. T. Sweet and C. E. Plummer, The Ammonium Sulphate Process for Production of Alumina from Western Clays. Trans. Am. Inst. Mining Met. Engrs. **159,** 255-66 (1944).

(18) K. K. Kershner, C. W. Funk and W. A. Calhoun, Low Grade Bauxites and Clays as Potential Aluminum Resources. J. Metals **3,** (Trans. AIME, **191,**) 1138-42 (1951).

(19) T. P. Hignett, Production of Alumina from Clay by a Modified Pedersen Process. Ind. Eng. Chem. **39,** No. 8, 1052-60 (1947).

(20) F. R. Archibald and C. F. Jackson, Alumina from Clay by the Lime Sinter Method. Trans. Am. Inst. Mining Met. Engrs. **159,** 227-38 (1944).

★ ★ ★

Contents of Volume 38

The Canadian Journal of Chemical Engineering

INDEX OF AUTHORS

Bancroft, A. R.
"The Incorporation of Fission Products into Glass for Disposal" ..... Feb. 19
Blanchet, J., Cloutier, Leonce, and Cholette, A.
"Performance of Flow Reactors at Various Levels of Mixing" ..... Feb. 1
Brown, R. A. S., Sullivan, G. A., and Govier, G. W.
"The Upward Vertical Flow of Air-Water Mixtures. III. Effect of Gas Phase Density on Flow Pattern, Holdup and Pressure Drop" ..... Apr. 62
Buthod, A. P., and Tien, Chi
"Critical Velocity of Gas" ..... June 74
Cavers, S. D., Eager, R. L., and Hudson, J. H.
"Solvent Extraction of Saskatchewan Lignites. II. Note on the Properties of the Extract" ..... June 88
Cholette, A. See Blanchet, J. ..... Feb. 1
Cloutier, Leonce. See Blanchet, J. ..... Feb. 1
Cotton, W. S.
"Design of Steam Tracing Systems for Protection Against Freezing" ..... Dec. 214
Cox, K. E. and Scott, D. S.
"Temperature Dependence of the Binary Diffusion Coefficient of Gases" ..... Dec. 201
Davies, Geoffrey, and Robinson, Donald B.
"A Study of Aggregative Fluidization" ..... Dec. 175
Dlouhy, J., and Gauvin, W. H.
"Evaporation Rates in Spray Drying" ..... Aug. 113
Downie, J., Graydon, W. F., and Shelstad, K. A.
"Kinetics of the Vapor-Phase Oxidation of Napthalene over a Vanadium Catalyst" ..... Aug. 102
Dunlop, R. G., Sheffer, H., Wheat, J. A., and MacLeod, D.A.
"Preparation of Aluminum Octanoate and Aluminum Isooctanoate" ..... Apr. 55
Eager, R. L. See Cavers, S. D. ..... June 88
Echigoya, E., and Osberg, G. L.
"The Effect of Temperature on the Fluidization of Silver Powders" ..... Apr. 43
Echigoya, E., and Osberg, G. L.
"Oxidation of Ethylene Using Silver Catalyst Coated Strips in an Inert Fluidized Bed" ..... Aug. 108
Fan, Liang-tseng
"Pressure Drop of Single Phase Flow Through Raschig Ring Type Tower Packings: Effect of Hole Size" ... Oct. 138
Friedlander, S. K. and Pasceri, Ralph E.
"The Efficiency of Fibrous Aerosol Filters: Deposition by Diffusion of Particles of Finite Diameter" ..... Dec. 212
Furter, W. F., and Johnson, A. I.
"Salt Effect in Vapor-Liquid Equilibrium, Part II" .. June 78
Gauvin, W. H., and Pasternak, I. S.
"Turbulent Heat and Mass Transfer from Stationary Particles" ..... Apr. 35
Gauvin, W. H. See Dlouhy, J. ..... Aug. 113
Gauvin, W. H., and Hoffman, T. W.
"Evaporation of Stationary Droplets in High Temperature Surroundings" ..... Oct. 129
Gauvin, W. H., and Torobin, L. B.
"Fundamentals Aspects of Solids-Gas Flow. Part IV: The Effects of Particle Rotation, Roughness and Shape" ..... Oct. 142
Gauvin, W. H. and Torobin, L. B.
"Fundamental Aspects of Solids-Gas Flow. Part V: The Effects of Fluid Turbulence on the Particle Drag Coefficient" ..... Dec. 189
Godard, Hugh P.
"The Corrosion Behavior of Aluminum in Natural Waters" ..... Oct. 167
Govier, G. W. See Brown, R. A. S. ..... Apr. 62
Graydon, W. F. See Downie, J. ..... Aug. 102
Hall, Raymond C.
"Graphical-Numerical Determination of Variable Diffusion Coefficient in Solids" ..... Oct. 154
Hanratty, Thomas J., Scheele, George F., and Rosen, Edward M.
"Effect of Natural Convection on Transition to Turbulence in Vertical Pipes" ..... June 67
Heric, E. L., and Rutledge, Ronald M.
"A Method for the Determination of Tie-Lines in Ternary Liquid Systems" ..... Apr. 46
Hoffman, T. W. See Gauvin, W. H. ..... Oct. 129
Hudson, J. H. See Cavers, S. D. ..... June 88
Hueston, F. H.
"Nuclear Grade Uranium Tetrafluoride by the Moving Bed Process" ..... Feb. 29
Ingraham, T. R. and Thomas, G.
"The Development of the Alum-Amine Process for the Recovery of Alumina from Shale" ..... Dec. 220
Jegier, Z., Katz, Morris, and Rennie, R. P.
"Effect of Diesel Locomotive Operation on Atmospheric Conditions in a Railway Tunnel" ..... Aug. 123
Johnson, A. I., and Yesberg, D.
"Machine Computations for Transient Stagewise Processes" ..... Apr. 49
Johnson, A. I. See Furter, W. F. ..... June 78
Johnson, A. I., and Poutanen, A. A.
"Studies of Bubble Formation and Rise" ..... Aug. 93
Katz, Morris. See Jegier, Z. ..... Aug. 123
Kilgallon, J. D., and Streight, H. R. L.
"Polymeric Self-Sealing Distillation and Extractor Trays" ..... June 89
Lu, Benjamin C.-Y.
"Note on the Evaluation of Antoine Constants" .... Feb. 33
MacLeod, D. A. See Dunlop, R. G. ..... Apr. 55
Mordell, D. L., Thompson, A. L. and Yano, G.
"Formation and Quenching of Nitric Oxide in a Continuous Flow Furnace" ..... Dec. 206
Osberg, G. L. See Echigoya, E. ..... Apr. 43
Osberg, G. L. See Echigoya, E. ..... Aug. 108
Pasceri, Ralph E. See Friedlander, S. K. ..... Dec. 212
Pasternak, I. S. See Gauvin, W. H. ..... Apr. 35
Poutanen, A. A. See Johnson, A. I. ..... Aug. 93
Regalbuto, J. A., and Soo, S. L.
"Concentration Distribution in Two-Phase Pipe Flow" ..... Oct. 160
Rennie, R. P. See Jegier, Z. ..... Aug. 123
Robinson, Donald B. See Davies, Geoffrey ..... Dec. 175
Rosen, Edward M. See Hanratty, Thomas J. ..... June 67
Rothenberg, Ronald E. and Smith, J. M.
"Heat Transfer to a Surface Reacting Fluid in Turbulent Flow" ..... Dec. 184
Rutledge, Ronald M. See Heric, E. L. ..... Apr. 46
Scheele, George F. See Hanratty, Thomas J. ..... June 67
Scott, D. S. See Cox, K. E. ..... Dec. 201
Sheffer, H. See Dunlop, R. G. ..... Apr. 55
Shelstad, K. A. See Downie, J. ..... Aug. 102
Smith, J. M. See Rothenberg, Ronald E. ..... Dec. 184
Soo, S. L. See Regalbuto, J. A. ..... Oct. 160
Streight, H. R. L. See Kilgallon, J. D. ..... June 89
Sullivan, G. A. See Brown, R. A. S. ..... Apr. 62
Tien, Chi
"A Simplified Method for Determination of Solid Diffusion Coefficient with Non-Linear Adsorption Isotherm" ..... Feb. 25
Tien, Chi. See Buthod, A. P. ..... June 74
Thomas, G. See Ingraham, T. R. ..... Dec. 220
Thompson, A. L. See Mordell, D. L. ..... Dec. 206
Torobin, L. B. See Gauvin, W. H. ..... Oct. 142
Torobin, L. B. See Gauvin, W. H. ..... Dec. 189
Wheat, J. A. See Dunlop, R. G. ..... Apr. 55
Yano, G. See Mordell, D. L. ..... Dec. 206
Yesberg, D. See Johnson, A. I. ..... Apr. 49

INDEX OF PAPERS

Concentration Distribution in Two-Phase Pipe Flow...Oct. 160
Corrosion Behavior of Aluminum in Natural Waters, The....Oct. 167
Critical Velocity of Gas....June 74
Design of Steam Tracing Systems for Protection Against Freezing....Dec. 214
Development of the Alum-Amine Process for the Recovery of Alumina from Shale, The....Dec. 220
Effect of Diesel Locomotive Operation on Atmospheric Conditions in a Railway Tunnel....Aug. 123
Effect of Natural Convection on Transition to Turbulence in Vertical Pipes....June 67
Effect of Temperature on the Fluidization of Silver Powders, The....Apr. 43
Efficiency of Fibrous Aerosol Filters: Deposition by Diffusion of Particles of Finite Diameter, The....Dec. 212
Evaluation of Antoine Constants, Note on the....Feb. 33
Evaporation Rates in Spray Drying....Aug. 113
Evaporation of Stationary Droplets in High Temperature Surroundings....Oct. 129
Formation and Quenching of Nitric Oxide in a Continuous Flow Furnace....Dec. 206
Fundamental Aspects of Solids-Gas Flow. Part IV: The Effects of Particle Rotation, Roughness and Shape....Oct. 142
Fundamental Aspects of Solids-Gas Flow. Part V: The Effects of Fluid Turbulence on the Particle Drag Coefficient....Dec. 189
Graphical-Numerical Determination of Variable Diffusion Coefficient in Solids....Oct. 154
Heat Transfer to a Surface Reacting Fluid in Turbulent Flow....Dec. 184
Incorporation of Fission Products into Glass for Disposal, The....Feb. 19
Kinetics of the Vapor-Phase Oxidation of Naphthalene over a Vanadium Catalyst....Aug. 102
Machine Computations for Transient Stagewise Processes....Apr. 49
Method for the Determination of Tie-Lines in Ternary Liquid Systems, A....Apr. 46
Nuclear Grade Uranium Tetrafluoride by the Moving Bed Process....Feb. 29
Oxidation of Ethylene Using Silver Catalyst Coated Strips in an Inert Fluidized Bed....Aug. 108
Performance of Flow Reactors at Various Levels of Mixing....Feb. 1
Polymeric Self-Sealing Distillation and Extractor Trays. June 89
Preparation of Aluminum Octanoate and Aluminum Isooctanoate....Apr. 55
Pressure Drop of Single Phase Flow Through Raschig Ring Type Tower Packings: Effect of Hole Size....Oct. 138
Salt Effect in Vapor-Liquid Equilibrium, Part II....June 78
Simplified Method for Determination of Solid Diffusion Coefficient with Non-Linear Adsorption Isotherm, A. Feb. 25
Solvent Extraction of Saskatchewan Lignites. II. Note on the Properties of the Extract....June 88
Study of Aggregative Fluidization, A....Dec. 175
Studies of Bubble Formation and Rise....Aug. 93
Temperature Dependence of the Binary Diffusion Coefficient of Gases....Dec. 201
Turbulent Heat and Mass Transfer from Stationary Particles....Apr. 35
Upward Vertical Flow of Air-Water Mixtures, The. III. Effect of Gas Phase Density on Flow Pattern, Holdup and Pressure Drop....Apr. 62

★ ★ ★